COMMISSIONING A DYNAMIC MULTILEAF COLLIMATOR ON A LINEAR ACCELERATOR

by

Dominic Gélinas
Department of Medical Physics
McGill University, Montréal
April 1999

A Thesis submitted to the
Faculty of Graduate Studies and Research
in partial fulfillment of the requirements for the degree of
Master of science

0-612-50775-0

ABSTRACT

The present generation of medical linear accelerators is computer controlled providing great precision in dose delivery in addition to other options, such as conformal radiotherapy which involves intensity modulated fields. These fields are produced with multileaf collimators (MLCs) capable of delivering a radiation beam with a pre-determined modulated intensity using the dynamic capabilities of the MLC leaves. Two dynamic beam delivery methods are currently used: the step and shoot method and the continuous motion method. The first consists of several static subfields with the motion of the leaves occurring without the presence of radiation, while in the other the leaves may move with the beam on.

The work presented here intends to prove that dynamically enabled linear accelerators can be used with confidence by verifying the accuracy and the stability of motions of the movable axes for the two dynamic beam delivery methods. Prior to clinical use, the integrity of the entire beam delivery system must be tested and the dosimetry related to the MLC must be examined. The purpose of this thesis is to develop, analyze and perform tests for the commissioning of the dynamic beam delivery capabilities of a medical linear accelerator and to catalogue these tests to facilitate their implementation in a routine quality assurance program.

RÉSUMÉ

La présente génération d'accélérateurs linéaires médicaux est contrôlée par ordinateurs ce qui permet une grande précision dans l'application des doses de radiation en plus d'autres possibilités telle la radiothérapie conforme qui est constituée de champs à intensité modulée. Ces champs sont produits en utilisant un collimateur multilame qui, par le mouvement dynamique de ses lames, peut produire un champ d'intensité modulée pré-déterminé. Deux méthodes de traitements dynamiques pour obtenir un champ à intensité modulée sont présentement utilisées. La première méthode est constituée de plusieurs sous-champs statiques et les lames sont déplacées seulement en l'absence de radiation. Avec la deuxième méthode, les lames peuvent se déplacer en présence de radiation.

Ce travail a l'intention de prouver que les accélérateurs linéaires permettant des traitements dynamiques sont fiables si l'exactitude et la stabilité des déplacements des composantes de l'accélérateur linéaire qui peuvent être contrôlées par ordinateurs pour les deux méthodes de traitement dynamique mentionnées sont vérifiées. Avant d'être utilisé en clinique, l'intégrité de tout le système de déposition de dose doit être testée et la dosimétrie du collimateur multilame doit être vérifiée. Le but de ce mémoire est de développer, d'analyser et d'effectuer des tests pour l'acceptation d'un accélérateur linéaire médical permettant des traitements dynamiques et de cataloguer ces tests pour faciliter leurs intégrations à un programme de contrôle de qualité de routine.

ACKNOWLEDGEMENTS

I would like to sincerely thank my supervisor, Michael D.C. Evans, and Dr. Ervin B. Podgorsak for their understanding of my particular situation and for the judicious guidance in the choice of my thesis subject. Many thanks to Michael D.C. Evans whom has patiently corrected all my grammar mistakes over the other corrections. I could probably not have worked on this project without the financial support from the Centre hospitalier régional de Trois-Rivières, whom I also thank for their trust.

Many thanks to Joe Larkin and Paul Lefebvre for all the time they took to explain the complexity of the Clinac 2300 C/D and the cobalt unit at the Montreal General Hospital and their kindness the many times I called late to report a malfunction of the linac.

I have to thank François Deblois for his energetic implication in the dose non-linearity problem of the linac and the ionization chamber. Without his help, my resource would have been very limited, compromising the understanding of the phenomenon. Finally, I have to thank Tony Falco who offered his time and his computer when I needed it.

TABLE OF CONTENTS

CHAPTER 3: DOSIMETERS

CHAPTER 4: PHYSICAL CHARACTERISTICS OF THE MULTILEAF COLLIMATOR (MLC)

CHAPTER 5: EVALUATION OF THE STATIC MLC

CHAPTER 7: DISCUSSION AND RESULTS

CHAPTER 8: CONCLUSIONS

APPENDICES

AN INTRODUCTION TO MODERN RADIOTHERAPY

1.1 Basic aspects of conformal radiotherapy.

The current approach to cancer treatment utilizes several treatment modalities. Surgery, chemotherapy and radiotherapy are widely used, and two treatment modalities may be used together. The primary approach is often to surgically remove the tumor wherever possible, however this is not always an option, and other treatment modalities must be considered. The functionality of the affected organ as well as the cosmetic appearance of the patient should be conserved. A patient cured of cancer but disfunctional in society is not necessarily a healed patient.

External beam radiotherapy is used to treat about half of all patients with cancer. Most medical centers providing radiotherapy treatments use linear accelerators (linacs) that are able to produce x-ray and electron beams in the megavoltage range, and computer control has been extended to most linacs. This new generation of computer controlled linacs has opened the door to efficient conformal radiotherapy with the goal of increasing the dose to the tumor while sparing surrounding healthy tissue. The objective is to increase tumor control without increasing morbidity.

Computer controlled linacs can deliver dose dynamically, thus leading to intensity modulated beams necessary for conformal radiotherapy. Dynamic dose delivery refers to the computer controlled motion of one of the components of the linear accelerator in the presence of radiation. For example, the appropriate automatic motion of one secondary collimator in the presence of the x-ray beam can create the classical wedged dose distribution produced by a static wedge.

The purpose of this project was to develop, analyze and perform quality assurance tests for the dynamic beam delivery capabilities of the Clinac 2300 C\D (Varian, Palo Alto, CA). Because the precision required in the delivery of radiation to treat disease is on the order of 5%, uncertainties in each of the many steps involved in delivering radiation treatment to a patient have to be minimized. Quality assurance programs must ensure that standards of precision in the delivery of dose are met at all times. Computer control of the motion of one or many parts of the linear accelerator during a treatment requires a rigorous quality assurance program so that dynamic treatments may be administered with confidence.

1.2 Thesis organization.

Chapter 2 reviews the basic concepts of medical physics used for this project. Factors used to characterize the megavoltage x-ray beam are introduced. Standard methods used to analyze an x-ray beam are explained, and the production of radiation with a linear accelerator is briefly mentioned.

Chapter 3 provides explanations of the dosimeters used for this project. Other equipment involved in the measurement of dose deposited by a megavoltage x-ray beam are also introduced.

In *chapter 4*, the multileaf collimator (MLC) is described. The shape of the leaves and the manner in which the linac's computer exercises control over the movement of the leaves is explained, together with other special features related to the MLC.

Chapter 5 describes the series of tests performed to verify the quality of the MLC system when used in the static mode. This chapter establishes a basis upon which analysis of the dynamic MLC mode will be examined.

In *chapter 6*, the tests conducted to test the dynamic multileaf collimator and to verify the possibilities of the dynamic toolbox are explained. In brief, the positional reproducibility, the speed constancy, the effect of acceleration, and positional accuracy are verified for all axes that can be moved in the presence of the radiation beam.

Chapter 7 reports and discusses the results obtained for the tests introduced in chapter 5 and 6.

The conclusion of the work done for this project is explained in *chapter 8* with possible future work.

Finally, a precise description of the tests explained in chapter 5 and 6 is presented in the *appendices*. This compact collection of tests was implemented for easier reference to implement a quality assurance program for the dynamic beam delivery possibilities as applied to linacs generically.

INTRODUCTION TO MEDICAL PHYSICS

Before delivering therapeutic radiation treatment with high energy radiation, it is important to be able to predict the dose distribution that will be delivered to the patient. In order to calculate and analyze the dose deposition anywhere in a patient, pertinent photon beam parameters must be known, such as beam quality, percentage depth dose, tissue maximum ratio, off-axis ratio, and absolute machine output.

2.1 Beam quality.

The quality of a radiation beam is related to its ability to penetrate materials of known composition[1,2,3]. The best method for describing the quality of an x-ray beam would be to specify its spectral distribution which provides a plot of the relative number of photons per unit energy interval contained in a photon beam. Spectral distributions are difficult to measure in practice and, moreover, such a complete description of the photon beam is not necessary in most clinical situations. A simpler and widely used method for describing the quality of photon beams is through half-value layer (HVL) measurements. HVL is defined as the thickness of an absorber of a specified composition required to attenuate the intensity of the photon beam to half its original value. The intensity of a beam is usually stated as its energy fluence per unit time. The material used to measure the HVL depends on the quality of the beam examined. For the lower energy beams, the HVL is expressed in millimeters of aluminum while for higher energy beams copper or lead is used. Mathematically, when a monoenergetic photon beam travels through an attenuator it will be attenuated exponentially according to the following relationship:

$$I(x) = I_0 \cdot e^{-\mu(E) \cdot x}, \tag{2.1}$$

where I(x) is the intensity of the photon beam passing through a thickness x of the attenuator material, μ is the linear attenuation coefficient of the attenuator material for photon energy E, and I_0 is the incident beam intensity. As a result, when $I(x) = 0.5\ I_0$, the expression for the HVL is found to be:

$$HVL = \frac{0.693}{\mu(E)}. \tag{2.2}$$

Hence, the linear attenuation coefficient obtained from the measurement of HVL can be used to derive the effective beam energy from tables relating attenuation coefficient and photon energy[2].

It is interesting to note that for a monoenergetic photon beam, the first half-value layer (HVL1) is the same as the second half-value layer (HVL2), where HVL2 is the additional thickness of material required to reduce the beam intensity from (0.5 I_0) to (0.25 I_0). On the other hand, for a polyenergetic beam from a linear accelerator, the first and second HVL will not be equal. For lower energy photon beams where photoelectric and Compton interactions dominate, HVL2 will be larger than HVL1, illustrating that low energy photons are preferentially attenuated by the absorbing material resulting in a more penetrating, or harder beam as the thickness of attenuator material is increased. For higher energy photon beams, above 10 MV, pair production becomes more predominant, and HVL2 will be less than HVL1 illustrating that high energy photons are preferentially attenuated by the absorbing material resulting in a softer beam. The HVL for megavoltage x-ray beam is not usually employed to qualify the photon beam. Since the linear attenuation coefficient does not change rapidly with energy in the Compton region, a small change in the value of the attenuation coefficient will give a large change in the effective beam energy. Hence, for megavoltage x-ray beams, if the quality is to be specified by a single parameter, the peak energy rather than HVL may be used, and the average energy of such beams is approximately one-third of the nominal accelerating potential.

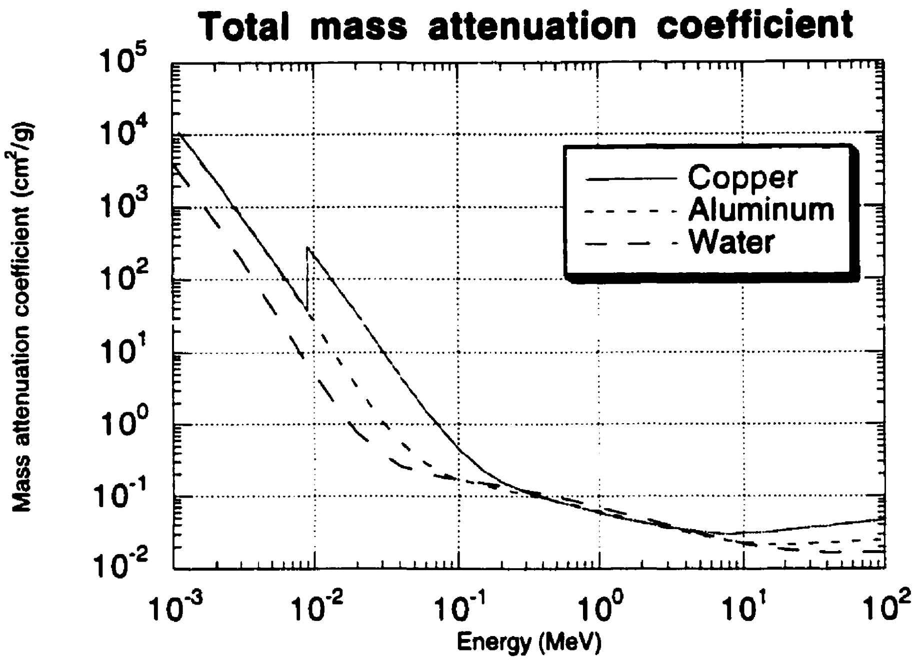

Figure 2.1. Total mass attenuation coefficient for copper, aluminum and water as a function of energy.

In figure 2.1 which gives the mass attenuation coefficient as a function of photon beam energy for copper, aluminum, and water, three distinct regions can be seen. The first region, from low energies up to around 0.1 MeV is dominated by the photoelectric effect with much higher attenuation coefficients at lower energies. The middle region, from around 0.1 MeV to 10 MeV, is dominated by the Compton interactions. The Compton interaction is the most important interaction in radiotherapy as it is the dominant effect for the range of energies normally used in clinical applications. One important feature that is illustrated in figure 2.1 is the mass attenuation coefficient being approximately independent of the attenuator material in the Compton region. The third region for photon energies above10 MeV, shows the beginning of pair production interactions. As opposed to the photoelectric and Compton interactions, the attenuation coefficient for pair production increases with increasing energy.

2.2 Percentage depth dose.

A practical way of characterizing a radiotherapy beam is to measure the percentage depth dose (PDD) on the central axis. The PDD consists of the relative dose on the central axis at a given depth in phantom divided by the maximum dose at depth d_{max} on the same axis[1]. It can be expressed mathematically as follows:

$$PDD(d, FS, SSD, E) = 100 \times \frac{D(d, FS, SSD, E)}{D(d_{max}, FS, SSD, E)} = 100 \times \frac{D_Q}{D_P}, \qquad (2.3)$$

where d is the depth below the phantom surface, d_{max} is the depth of maximum dose, *SSD* is the source-to-surface distance, *FS* is the field size at SSD, and *E* is the energy of the incident photon beam. This expression puts in evidence all the parameters that influence the dose at a given point in medium and demonstrates that the only parameter changing when measuring PDD is the depth of measurement. To simplify, the PDD can be expressed with D_P and D_Q representing the dose at depths d_{max} and d in phantom, respectively, as illustrated in figure 2.2.

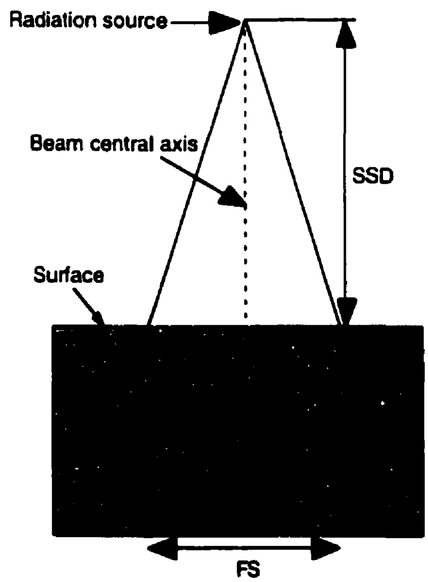

Figure 2.2 Diagram showing the setup characterizing the PDD. D_P is the dose at point P that is at d_{max} and D_Q is the dose at point Q, at an arbitrary depth. Both points are on the beam central axis with a fixed source-surface distance (SSD). FS is the field size at SSD.

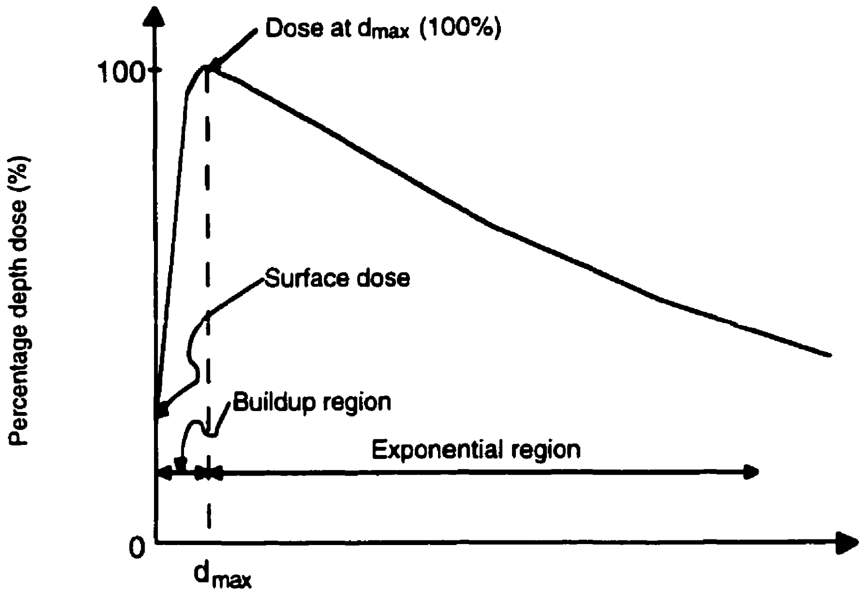

Figure 2.3. Diagram of a typical percentage depth dose (PDD).

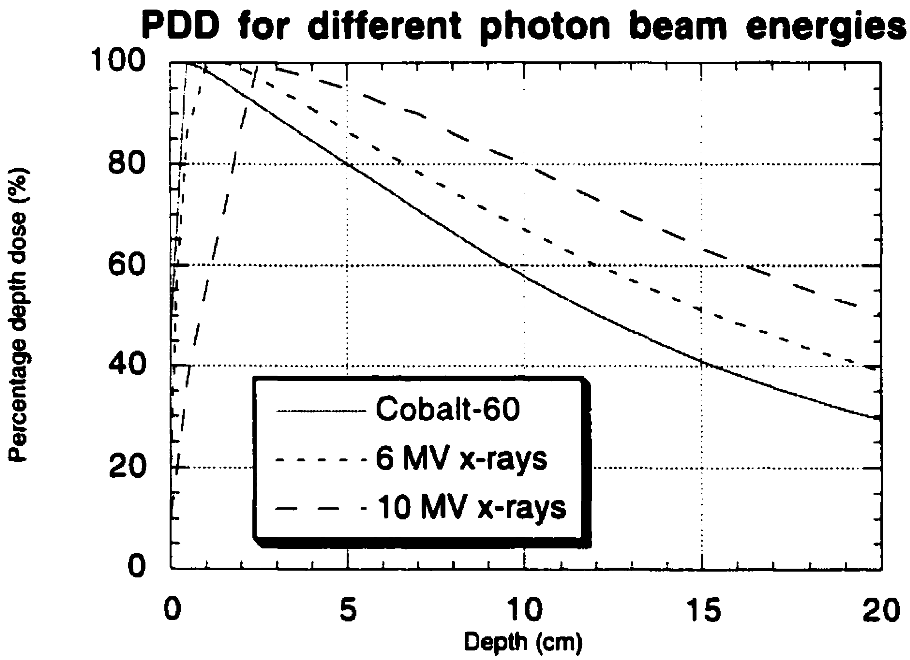

Figure 2.4 PDD for different beam energies illustrating that higher energy beams have more penetrating power.

In figure 2.3, a diagram of the characteristic behavior of a PDD curve is shown for a typical beam in the megavoltage energy range. For a given point at a depth beyond the depth of dose maximum, the percentage depth dose will increase with beam energy because higher energy beams have more penetrating power in the Compton region, as seen in figures 2.1 and 2.4.

The PDD illustrated in figure 2.3 is split into two regions, the buildup region and the exponential attenuation region. The exponential region can be explained by the exponential attenuation, expressed by equation 2.1, dominating the inverse square law and scattering effects. The buildup region has the very important characteristic that the dose increases with depth such that the dose at the surface is significantly less than at d_{max}. This is often referred to as the skin-sparing effect which is more pronounced as the energy of the beam is increased. The significance of this feature lies in the ability to deliver higher doses to deep seated tumors without exceeding the limiting skin tolerance dose levels, unlike orthovoltage beams which have their depth of dose maximum on the surface, eliminating the skin-sparing effect.

The dose buildup region is produced when the photon beam enters the phantom and sets in motion secondary electrons from the surface and successive layers. These electrons deposit their energy as they travel downstream. As a result, the absorbed dose in the medium, which is proportional to the electron fluence, will increase with depth. However, the photon energy fluence because of beam attenuation continuously decreases with depth such that the production of electrons also decreases. The result is that the absorbed dose will increase with depth from the surface to a depth of maximum dose from which point the PDD decreases approximately exponentially. The surface dose shown in figure 2.3 should be zero, however it becomes significant because of electrons produced before the beam reaches the phantom surface. These electrons result from the interaction of photons with the collimators of the accelerator, the flattening filter, and the column of air between the source and the phantom surface.

2.3 Collimator factor.

The collimator factor (CF), often called the relative-exposure factor, is defined as the ratio of the dose rate to a small mass of tissue in air for a given field size to that for a reference field size, usually 10x10 cm^2. This factor accounts for the dependence of the beam output in free space on the field size. As the field size is increased, the collimator scatter increases and is added to the primary beam. CF is measured with an ion chamber with a buildup cap of a size just large enough to provide maximum dose buildup for the given energy beam with the chamber placed at the isocenter.

2.4 Relative dose factor.

The relative dose factor (RDF) is defined as the dose at a reference depth in phantom, normally the depth of dose maximum, for a given field size divided by the dose at the same point and depth for the reference field size, usually 10x10 cm^2. Thus RDF contains both the collimator and the phantom scatter. The CF and RDF for a given field size A can be related to give the scatter factor (SF(A)) by the following relationship:

$$RDF(A) = CF(A) \times SF(A). \quad (2.4)$$

The SF may be defined as the ratio of the dose rate for a given field size at a reference depth, or d_{max}, to the dose rate at the same depth for the reference field size, with the same collimator opening. SF takes into account the change in scatter radiation originating in the phantom at a reference depth as the volume of irradiated phantom is changed for a fixed collimator opening.

2.5 Equivalent field size.

The dosimetric factors described above are usually tabulated with respect to square or circular field sizes. However, in practice fields are often rectangular or of an irregular shape due to the presence of field blocks. Hence, two methods to predict the equivalent field size are presented: the area over perimeter approach[4] and the Clarkson method[2].

2.5.1 Area over perimeter method.

This approach relates rectangular fields to square fields if they have the same area over perimeter (A/P) ratio. Mathematically,

$$S_{eq} = \frac{2a \times b}{a+b}, \tag{2.5}$$

where S_{eq} is the size of the equivalent square field, a is the rectangle field long axis and b is the rectangle field short axis. Even though this expression is not based on physical principles, it has been shown to be a good approximation for rectangular field with an a/b ratio not greater than 2 or 3. On the other hand, equation 2.5 cannot be used for circular irregular fields. However the radii of equivalent circles can be derived by assuming that the equivalent circle is the one that has the same area as the equivalent square. Hence,

$$r_{eq} = \frac{a}{\sqrt{\pi}}, \tag{2.6}$$

where r_{eq} is the equivalent radius of the square field with side a.

2.5.2 Clarkson method.

The basic principle of this method is that the scattered component of the depth dose is independent of the primary component. The scatter-air ratio (SAR) is used to calculate the scatter component of the dose. SAR is defined as the ratio of the scattered dose at a given point in the phantom to the dose in free space at the same point.

In order to calculate the dose to an arbitrary point for an irregular field, radii are drawn for this point to divide the field in sectors of 5° or 10°. If only one sector is considered, the SAR for that part of the field is the SAR with the average radius of the sector scaled by the angle of the sector divided by 360°. The scaled SARs for each sector are summed to give the total SAR of the irregular field so that the dose at the point of interest may be calculated, and an equivalent field size deduced.

2.6 Dose profile.

The dose profile or off-axis ratio shows the variation of dose in the irradiated medium perpendicular to the beam central axis, at a constant depth in the medium. Dose values off center are usually normalized to the dose value on the central axis at d_{max}. For a cobalt-60 beam, the dose is greatest on the central axis and decreases toward the edges of the beam. Linac x-ray beams may exhibit "horns" in the periphery of the field at shallow depths. These horns are created by the flattening filter which is designed to flatten the beam at a depth beyond d_{max} (typically 10 cm). The flattening filter is nearly conical in shape and it is made of iron, tungsten, or copper. It is thickest along the central axis of the photon beam so that more low energy photons are attenuated on the central axis. As a result, the edges of the field have a greater number of low energy photons that are easily attenuated, causing a rounding of the dose profile at the edges, gaining importance with depth. As in the case of PDD, the dose profile is a function of beam energy, field size, depth in phantom, and SSD.

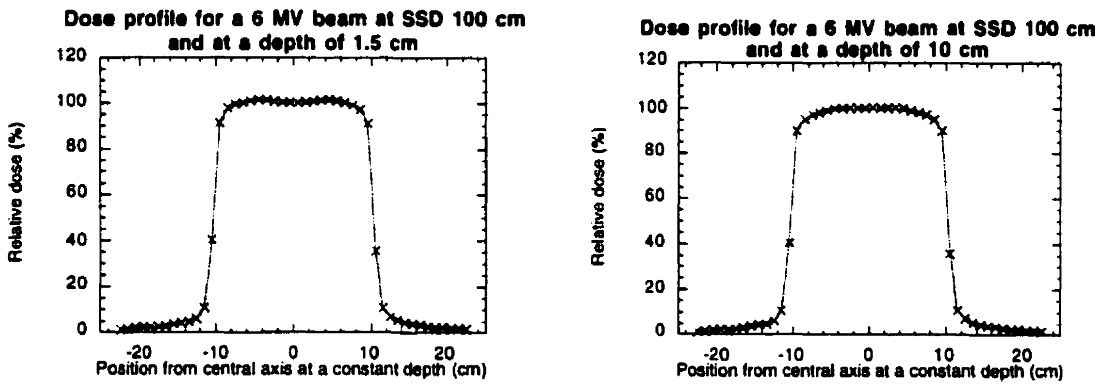

(a) (b)

Figure 2.5. Dose profiles at a constant depth for a flat phantom (a) at a shallow depth showing the "horns" and (b) at 10 cm depth giving a relatively flat profile.

2.7 Penumbra.

The penumbra refers to the region at the edge of a radiation beam over which the dose rate changes rapidly as a function of lateral distance from the beam central axis. It can be separated into two components, the geometric penumbra and the transmitted penumbra. The geometric penumbra, illustrated in figure

2.6, is due to the finite dimension of the radiation source. At the edge of the field, the radiation source becomes obscured, proportionally decreasing the dose given to these points. Mathematically, from similar triangles, the width of the geometric penumbra is given by:

$$p = {}^{s(f - f_c)}\!\Big/_{f_c}\,, \tag{2.7}$$

where p is the width of the geometrical penumbra, s is the diameter of the "source", f_C is the distance from the source to the end of the collimator, and f is the distance from the source to the point of interest as indicated in figure 2.6.

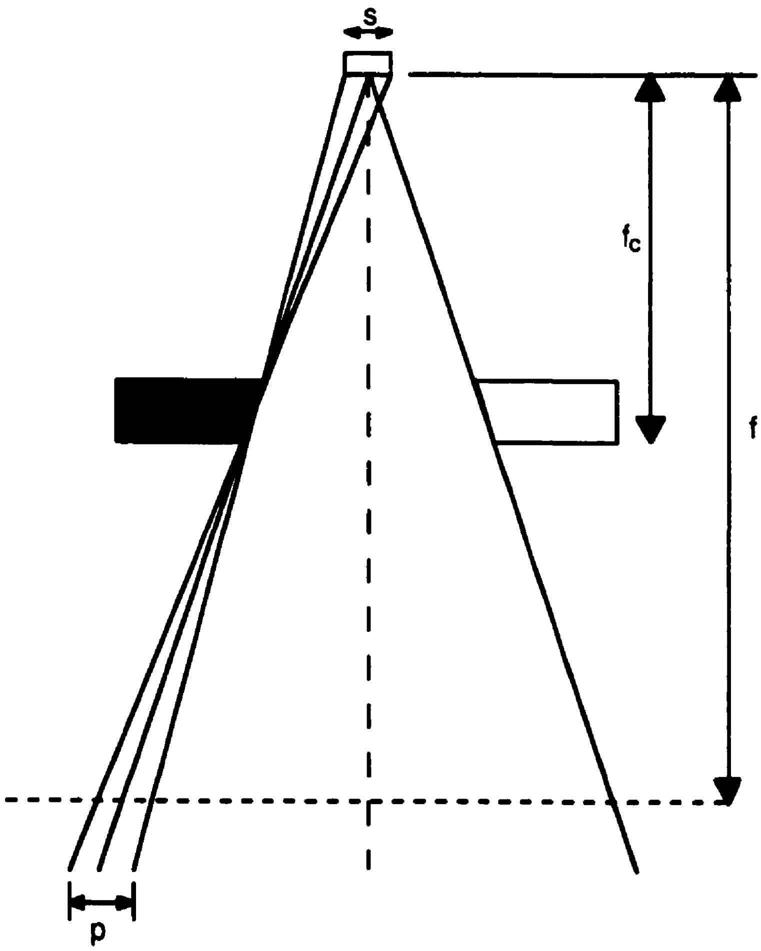

Figure 2.6. Illustration of the origin of the geometric penumbra resulting from the finite size of the source of radiation.

The transmission penumbra refers to the falloff of the beam due to the reduced side scatter. The most representative description of penumbra is the physical penumbra which is defined as the lateral distance between two specified isodose curves at a specified depth. Typically the lateral distance between the 90% to 10% isodose lines at d_{max} or the distance between the 80% to 20% isodoses are used. By extension, the definition of the field size is somewhat arbitrary and is often defined as the distance between the 50% isodose lines on each side of the beam profile.

2.8 Clinac 2300 C/D electron linear accelerator.

The high energy linear accelerator installed at the Montreal General Hospital is a Clinac from Varian, model 2300 C/D[5,6]. It is able to produce a 6 MV and a 18 MV photon beam as well as a selection of electron beams with energies of 6, 9, 12, 15, 18 and 22 MeV. Photon beams can be delivered with a dose rate ranging from 100 monitor unit (MU) per minute to 600 MU per minute in steps of 100 MU per minute. The unit is isocentrically mounted with a source-axis distance (SAD) of 100 cm. At the isocenter, the field size can vary from 0.5x0.5 cm^2 to 40x40 cm^2, with a precision within 0.1 cm.

The Clinac 2300 C/D is computer controlled, offering a wide variety of treatment possibilities with a monitored quality of operation. If the machine detects an operation beyond a tight tolerance, an interlock is enabled that terminates the beam production or prevents the beam from turning on.

A brief description of the functional components of a linear accelerator, based on the Varian Clinac 2300 C/D, is presented. The important components and their interrelationships are included in a block diagram below.

The megavoltage x-ray beam delivered by a linac is produced through a process that can be subdivided into three parts: the generation of the proper radio frequency (R.F.) waves, the acceleration of electrons, and the shaping of the photon beam.

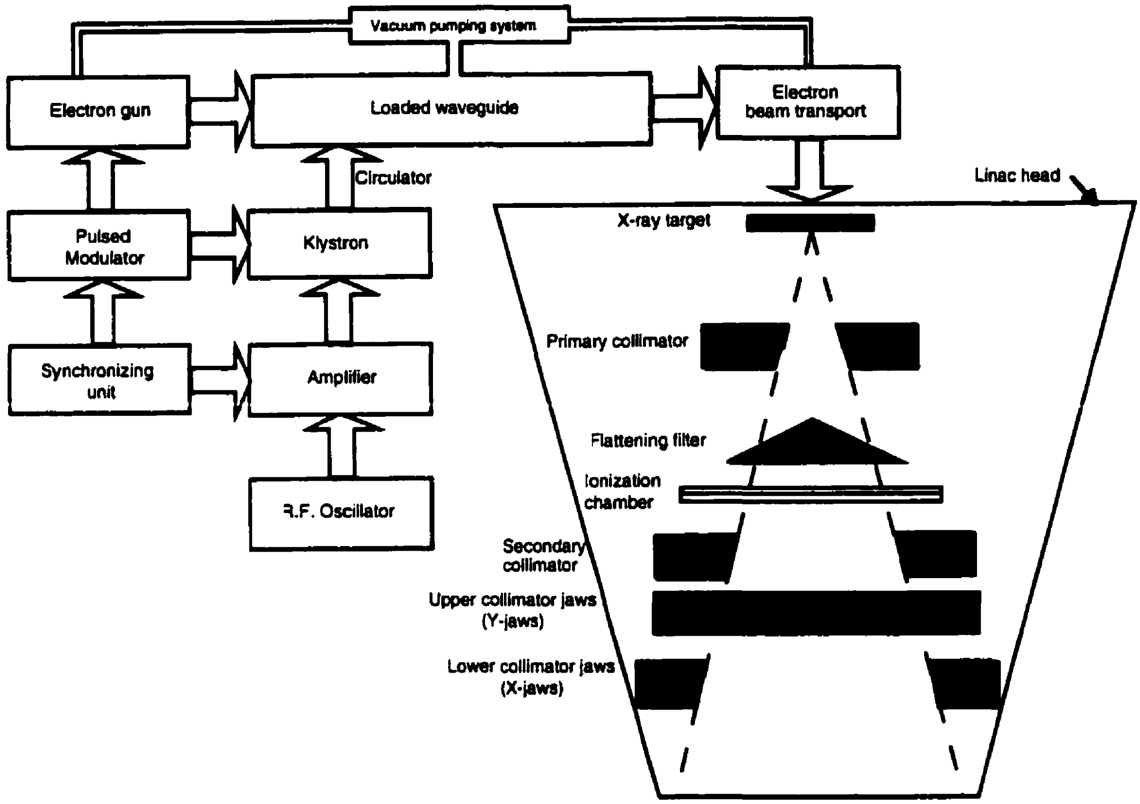

Figure 2.7. Basic block diagram of the linear accelerator (Clinac 2300 C/D) with the principal interactions between each component.

2.8.1 Synchronizing unit.

For the appropriate acceleration of the electron to take place, a precise series of events must occur. For this reason, the control processor is responsible for timing signals, known as triggers, that synchronize the actions taken by several components. These pulses are about 5 ms wide and occur at specific time intervals after the system clock pulse which has a frequency of 360 Hz.

2.8.2 Pulse modulator.

The pulse modulator generates a pulsed high voltage waveform that is sent to the klystron and to the electron gun. This waveform is produced by a pulse forming network that is charged by a high voltage DC voltage supply.

2.8.3 Radio frequency oscillator.

As shown in figure 2.7, the oscillator is used to produce RF pulses injected to the klystron. The RF driver is activated by the synchronizing unit, upstream from the klystron, to ensure that the pulses fed into the klystron are stable. These pulses are injected at almost the same time as the high voltage (HV) klystron transformer pulse is received at its cathode. The pulses are 12 ms in duration with a central frequency of 2856 MHz, which is the resonant frequency of the accelerator waveguide. In the case that a shift of the resonant frequency occurs (e.g. due to a temperature change) the frequency is adjusted by the automatic frequency control (AFC) to within 1 MHz.

2.8.4 Klystron.

The klystron is a microwave amplifier rather than a generator, explaining why RF has to be injected to the klystron from an RF oscillation. This device consists of three parts: the electron gun, RF section, and the collector. The electron gun of the klystron is similar to the Clinac 2300 C/D electron gun explained later in section 2.8.6. The RF section refers to cavities, known as bunchers, separated by drift tubes. The stream of electrons introduced in the cavities is accelerated by the RF waves by creating an alternative electric field across the cavity. As a result, some electrons are sped up while others are slowed down forming tight groups of electrons referred to as bunches. This process is called velocity modulation. When the electron bunches arrive at the collector, they induce charges on the ends of the cavity and thereby generate a retarding electric field. Consequently, the electrons are decelerated producing high-power microwaves with the same frequency than the inputted RF.

The RF produced by the klystron is directed to the accelerator waveguide through a circulator which allows the RF to go only one way. The role of the circulator is to protect the klystron against reflected RF that could potentially damage it.

2.8.5 Electron gun.

A schematic diagram of the electron gun of the Clinac 2300 C/D is shown in figure 2.8. Electrons are emitted from the heated cathode surface and then accelerated by a potential difference between the anode and the cathode. The cathode is maintained at a high negative DC voltage while the accelerator guide is kept at ground potential and serves as the anode. Because the electrons experience electrostatic repulsion, there is a focusing electrode to compensate for the divergence of the electron beam. In order to regulate the emission of electrons, a control grid is placed between the cathode and the anode with a voltage which is more negative than the cathode by 100 V. When the control grid is triggered, it becomes positive relative to the cathode for a 3.5 ms pulse which produces a bust of electrons. The potential of the control grid ranges in magnitude in order to vary the gun current required.

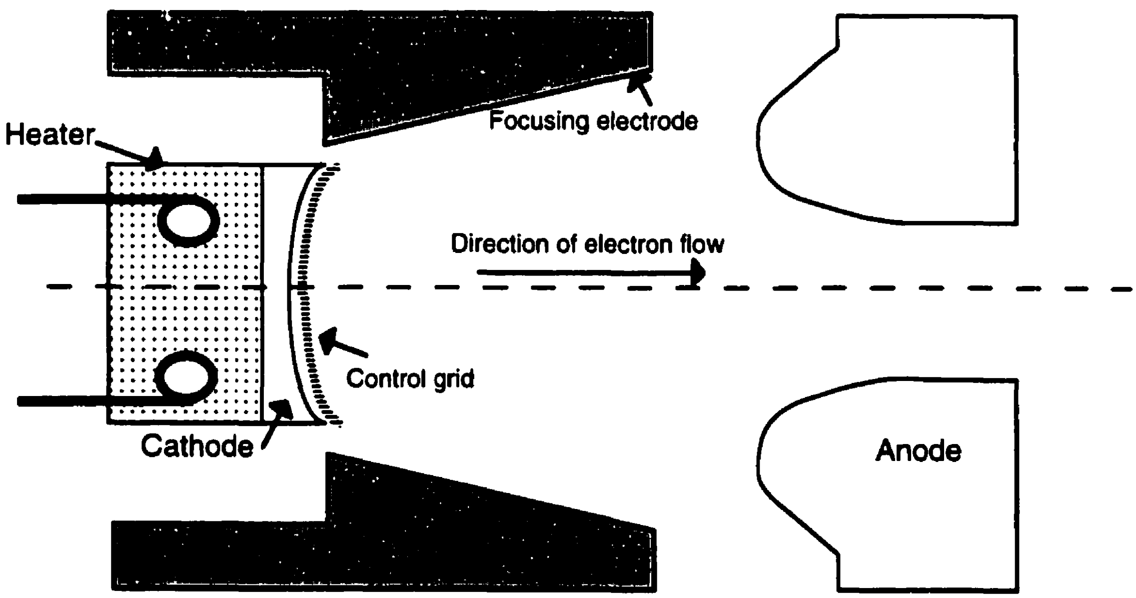

Figure 2.8. Schematic diagram of the electron gun of the Clinac 2300 C/D.

2.8.6 Loaded waveguide.

The accelerating waveguide is where the acceleration of the electrons occurs. There are two designs of linear accelerator used for radiotherapy: the traveling and the standing wave structure. The traveling wave accelerator consists of an electromagnetic wave accelerating the electrons through a wave-like analogy. This wave is injected in the high vacuum waveguide on the electron gun side and is absorbed by a dummy load at the other end of the structure, preventing the wave from reflecting back. On the other hand, the standing wave structure, as used in the Clinac 2300 C/D, reflects the wave at both ends of the waveguide which leads to the creation of a stationary wave from the forward and backward traveling waves. Both structures are using the loaded waveguide design that is necessary to have the accelerating electric field phase velocity slowed to the velocity of the electrons. It consists of annular disks inserted in the waveguide which modify the electric field pattern. Without the disks in the waveguide, the phase velocity of the accelerating rf field would exceed the speed of light, and the electrons would not be able to follow during the acceleration process.

A unique component of the standing wave structure is its coupling cavities. They are sections of the waveguide in which the net electric field, the addition of the forward and backward moving waves, is always zero. As a result, these cavities do not participate in the acceleration process, and may be placed on the side of the acceleration axis and serve only to couple the microwave power between the cavities accelerating the electrons. This forms the side coupled standing wave accelerator structure and has the advantage of shortening the length of the structure.

2.8.7 Electron beam transport.

Because of the accelerator length, the x-ray target is placed perpendicularly to the waveguide. Hence the electron beam must be redirected in order to strike the target. This is accomplished through passing the electron beam through a series of bending magnets that make the beam to turn 270 . The redirected beam is also confined by energy slits in the process to produce a well focused beam with a narrow energy spectrum. The principle is that electrons with different energy will curve more or less in a magnetic field such that confining the beam in a magnetic field results in constraining the energy spectrum.

2.8.8 Linac head.

The desired x-ray beam is produced by impinging the electron beam on a copper target. X rays are produced by the rapid deceleration of the electrons in the target material and are referred to as bremsstrahlung radiation. Bremsstrahlung has a continuous energy spectrum with a maximum given by the maximum kinetic energy of the incoming electrons. The radiation produced by this process is mainly directed in the forward direction at the energies used clinically. The higher the energy, the more forward peaked is the photon distribution.

The x-ray beam is defined by a series of primary collimators. It is further modified by passing through a flattening filter which attenuates the x-ray beam preferentially along the central axis, where it is thickest. The purpose of the flattening filter is to produce a dose profile with a ±3% flatness at 80% of the field at a depth of 10 cm in phantom.

After passing through the flattening filter the beam passes through two transmission ionization chambers which monitor the output of the beam. The chamber readings are used to stop the linac when the appropriate dose has been delivered. In addition, the two ion chambers are sandwiched together with their collection plates at 90 from each other, allowing for the detection of beam displacement. Before leaving the linac, the beam is shaped with movable rectangular collimators. The collimators of the Clinac 2300 C/D can be used to produce asymmetric field, as well as intensity modulated beams through dynamic beam sequences.

2.9 Summary.

In this chapter, a brief overview of the basic principles of medical physics used for the work discussed in this document has been presented. The terms and methods of characterizing the quality and penetrability of a x-ray beam was given. Several factors used to describe the dose given to a point have been introduced as well as basic features of vertical and horizontal dose profiles. Finally, a simplified description of the operation of a linear accelerator was introduced.

2.10 References.

1. F. M. Khan, The Physics of Radiation Therapy, 2nd edition, Williams & Wilkins, Maryland, U.S.A. (1994).

2. H. E. Johns, J. R. Cunningham, The Physics of Radiology, 4th edition, Charles C. Thomas, Springfield, Illinois, U.S.A. (1983).

3. F. H. Attix, Introduction to Radiological Physics and Radiation Dosimetry, John Wiley & Sons, Inc., New York, U.S.A. (1986).

4. M. J. Day and E. G. A. Aird, "Central axis depth dose data for use in radiotherapy: 1996," Br. J. Radiol. **25**, 138–151 (1996).

5. D. P. Barry, *Dynamic Wedge Dosimetry on a Dual Energy Linear Accelerator*, M. Sc. Thesis, McGill University, Montreal, Canada, 1997 .

6. Clinac 2300 C/D maintenance manual, Varian Associates, Palo Alto, California (1992).

DOSIMETERS

Several tools have been developed to measure the dose delivered to a medium. There are two categories of radiation detectors: absolute and relative. Absolute dosimeters include the calorimeter, the chemical dosimeter and the standard free air ionization chamber. Relative dosimeters include film and solid state dosimeters such as thermoluminescent dosimeters, diode dosimeters, optically stimulated luminescence detectors, and radioelectrets. Relative dosimeters require calibration in a known radiation field before being used for the determination of absorbed dose. Each dosimeter has advantages and disadvantages that dictate which one will be used to measure the radiation dose given to a medium in a particular situation.

3.1 Ionization chamber.

The ionization chamber is the most widely used dosimeter[1,2,3]. The Farmer-type chamber used in our experiments can give dose to the medium following calibration with respect to a standards laboratory. Typically, a Farmer-type chamber, also called a thimble chamber, is made of a thin wall of graphite, coated with a conductive material to form the outer electrode surrounding a small volume of air. A voltage is applied between this electrode and a central electrode often made of aluminum. The combination of the two materials of the electrodes yields an air-equivalent chamber which is important for determining the exposure in air, in the following manner. In the presence of a voltage difference in the chamber, the positive charges produced in the volume of air will migrate toward the negative electrode while the negative charges will go toward the positive electrode. The charges collected are produced by the x-ray beam that sets electrons in motion (mainly by Compton effect, photoelectric effect, and pair production) with sufficient energy to produce ion pairs. The inner electrode of the chamber is connected to an electrometer by the central conductor of a grounded triaxial cable. The high voltage between the two electrodes of the chamber is applied via the outer braid of the triaxial cable connected to the wall of the chamber. The cable has its central conductor surrounded by an insulator with a grounded inner braid which in turn is separated by an insulator from the outer braid at high potential. As a result, the central or measuring electrode of the chamber is surrounded by ground potential at all places except in the sensitive volume where the potential difference is applied. The chamber is guarded in close proximity to the sensitive volume, resulting in a low natural leakage current and in reduced irradiation-induced stem effects. One of the biggest advantages of the ionization chamber over other dosimeters is its relatively flat energy response.

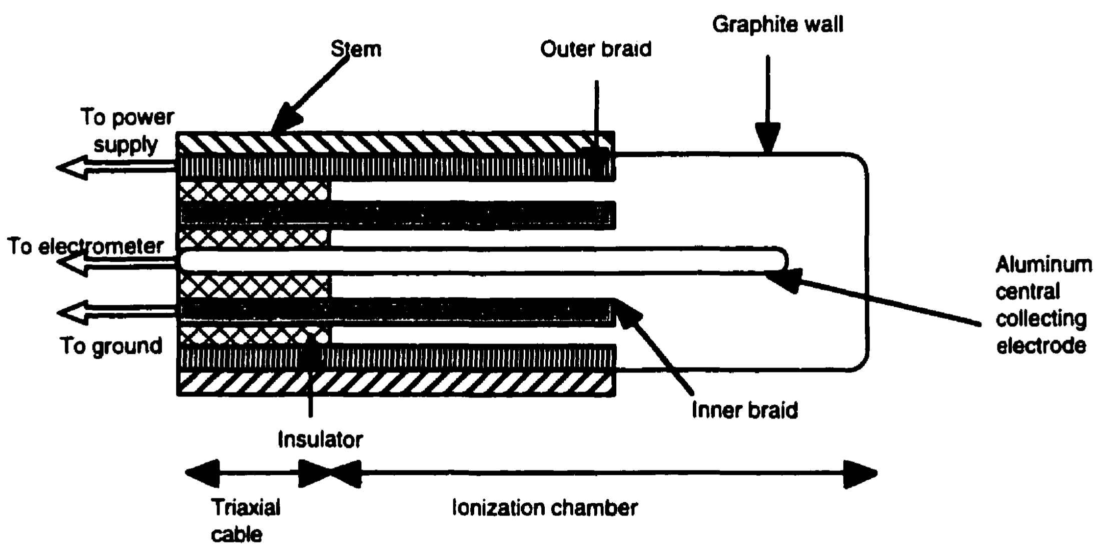

Figure 3.1 Schematic diagram of a Farmer-type ionization chamber.

3.2 Electrometer.

Due to the small current or charge measured at the collecting electrode of an ionization chamber, in the range of 10^{-6} to10^{-14}A, it is impossible to use an ammeter, thus special electrometer circuits have been designed[1,3,4]. The most widely used is the negative-feedback operational amplifier that can be thought of simply as an ultrahigh-impedance voltmeter. In figure 3.2, the triangle represents the operational amplifier and the positive and negative input designations refer to the inverting and non-inverting inputs, respectively.

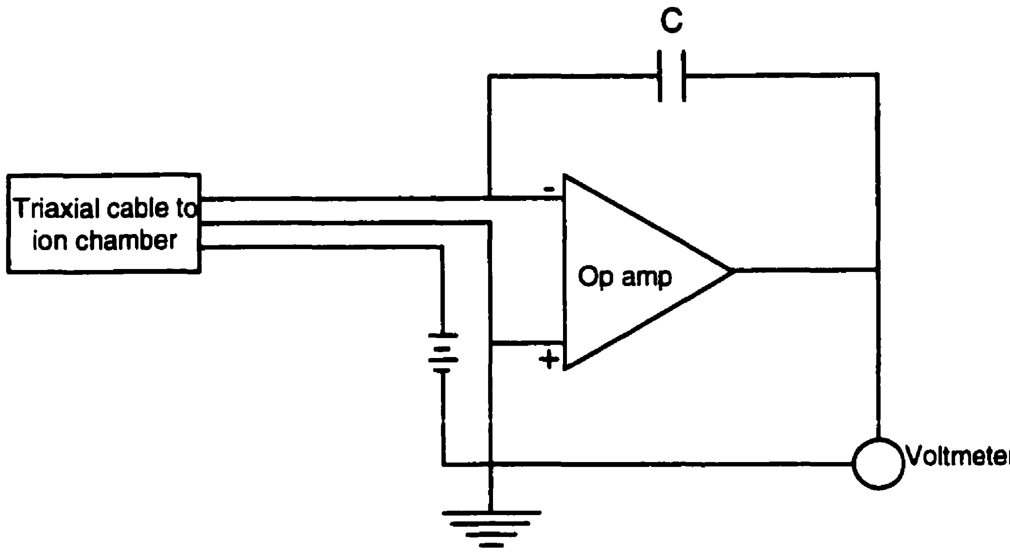

Figure 3.2 Operational-amplifier (Op amp) electrometer circuit for charge measurement. For current measurement, the capacitor is replaced by a resistor.

For example, when a negative charge Q flows from the ionization chamber, the input circuit is driven to a negative potential V_i. At the same time, the output potential rises to a 105 times greater positive potential V_o which is applied to the capacitor C. Hence the total potential across C is V_i+V_o which implies a charge of:

$$C(V_i+V_o) = Q - C_iV_i, \tag{3.1}$$

where C_i is the distributed capacitance of the input circuit to ground. The input impedance of the operational amplifier may be assumed to be too high (greater than 1012 ohm) to allow the passage of any significant charge. Hence, the voltage V across the capacitor can be measured with a voltmeter and if the capacitance C is known, then the charge collected Q is given by:

$$Q = C \times V. \tag{3.2}$$

3.3 Three-dimensional water scanner.

Ionization chambers in conjunction with a 3-D scanner were used to measure the beam parameters of the Clinac 2300 C/D. The scanner is able to place the ionization chamber precisely to any location within the water tank of dimension 50x50x50 cm^3. Since the output of the linear accelerator may vary with time, a stationary reference ionization chamber is also used so that the relative signal between the field and reference detector is stored. This system has been used to perform linear scans so as to obtain depth doses and beam profiles. The software can be used to further analyze, process, and store the measured data. For example, penumbra analysis and comparison of profiles can be done quickly and precisely using these tools.

3.4 Diodes.

Even though the ionization chamber is used to measure the radiation intensity in most applications, other types of dosimeters may also be used. Diodes have the advantages of a small measuring sensitive volume, a fast response, and are many times (around 20 000 times) more sensitive than an ion chamber[3,5,6,7]. The diode is used without a bias voltage so that it is operated in the photo-voltaic mode. This design has the advantage of reducing the leakage current. Radiation will induce a current in the diode which will create a voltage difference between the electrodes. The current induced is usually measured with an electrometer in a similar manner as for the ionization chamber.

The main disadvantages of the diode as a radiation detector is its energy dependent response as well as its radiation induced damage altering its sensitivity. However, a high-Z filter surrounding the silicon detector has been designed that flattens the energy dependence of the diode. Also, diodes are often pre-irradiated by manufacturers thus reducing the radiation damage induced variation of the diode response.

3.5 Linear diode array.

A linear diode array[8,9,10] (Profiler, model 1170, Sun Nuclear Corporation, Melbourne, Florida) consisting of an array of 46 diodes, 23 on each side of the central axis, placed 5 mm apart for a total length of 22.5 cm was used in our experiments. The top of the detector has a template indicating the location of each diode and the limits of 10x10, 15x15 and 20x20 cm^2 field sizes. The diodes are sandwiched between two acrylic plates, the top plate being 0.7 cm and the bottom plate 2.3 cm thick. The total build-up is 0.9 g/cm^2. Shielding against radiofrequency from the treatment room is achieved by a conductive surface placed between the acrylic and the circuit board. The active area of a diode is a square of 3.9 mm^2 parallel to the surface of the detector.

The p-type diodes are able to measure each pulse of radiation liberated by the linear accelerator with a maximum rate of measurement of 1000 pulses/sec. Pulses are detected by a separate circuit with a trigger-detector placed 2.2 cm away from each detector and an instantaneous dose rate of at least 500 cGy/s is necessary. The charge is integrated for 1 second and then transmitted to a personal computer which is running the manufacturers software. This software displays either dose rate over one second or the dose accumulated for one second. Data can be saved as ASCII files. The software also has several processing functions. For example, it is possible to compare profiles and analyze the flatness of the beam. Hence, the linear diode array is a very easy and fast way to measure the profiles of the radiation output of a linear accelerator, and is especially designed for dynamic-type beam measurements.

3.6 Film densitometry.

Film consists of a transparent base usually made of cellulose acetate or polyster resin coated with an emulsion containing very small crystals of silver bromide. The darkening of the film results when ionizing radiation interacting with the crystal to yield chemical changes that form the latent image. When film is developed, the crystals having undergone chemical changes are reduced to small grains of metallic silver. Crystals unaffected by the radiation are washed away by the fixing solution, leaving the clear transparent base in their place. Hence, the degree of darkening on the film depends on the amount of free silver deposited which in turn depends on the radiation energy absorbed.

Film is a well established relative dosimeter. It has the ability to record two dimensional distributions of dose with a single irradiation. Film has the highest spatial resolution of all dosimeters[1]. On the other hand, film response is highly energy dependent and corrections must be applied as it does not have the same effective atomic number as air or tissue. Moreover, the degree of response of a film is affected by processing conditions, such as developer temperature and development time. The amount of darkening of the film is related to the dose delivered to it and it is expressed as the optical density (OD), which is a function of the amount of light transmitted through a specific portion of the film. Mathematically,

$$OD = \log\left(\frac{I_o}{I_t}\right), \tag{3.3}$$

where I_o is the incident light intensity upon the film and I_t is the transmitted light intensity through the film. There are two main reasons for representing optical density on a logarithmic scale. First, large differences in numerical values can be accurately represented on a small scale. Secondly, the physiological response of the human eye to differences in light intensity is essentially logarithmic in nature.

In order to relate the optical density to the dose, the sensitometric curve, or the H-D curve[11], has to be measured. This curve is obtained by plotting optical density as a function of dose when irradiating films to a known dose. To keep the precision of the measurement as good as possible, film from the same batch should be used and processed at the same time. In the present work, film has been used only for relative dose measurements thus the sensitometric curve has not been required.

A commercial film densitometer system (Wellhöfer) has been used to analyze irradiated films. In general, a densitometer consists of a light source, a tiny aperture through which the light is directed and a light detector, such as a photocell, to measure the light intensity transmitted through the film. The system used has an infrared densitometer mounted on a track system which can be positioned precisely in a plane. The film is placed on a glass support and the limits of the scans are entered in the controlling system. When the preparation of measurement is done, this system can automatically scan the film and profiles can be stored in the computer for future analysis.

3.7 Summary.

Several classes of radiation detectors are available for measurement of radiation beam parameters and in this section the detectors used in our measurements are described. They include the ionization chamber, with the electrometer and a three dimensional scanner, the diode and the linear diode array, and the film and densitometer. Other dosimeters are also available but were not used. For example, the linac used in our experiments has an electronic portal imaging device (EPID) that can be used as a relative dosimeter. Also, thermoluminescent dosimeters were a possible option not used in our experiments.

3.8 References.

1. F. M. Khan, The Physics of Radiation Therapy, 2nd edition, Williams & Wilkins, Maryland, U.S.A. (1994).

2. H. E. Johns, J. R. Cunningham, The Physics of Radiology, 4th edition, Charles C. Thomas, Springfield, Illinois, U.S.A. (1983).

3. F. H. Attix, Introduction to Radiological Physics and Radiation Dosimetry, John Wiley & Sons, Inc., New York, U.S.A. (1986).

4. D. P. Barry, *Dynamic Wedge Dosimetry on a Dual Energy Linear Accelerator*, M. Sc. Thesis, McGill University, Montreal, Canada, 1997.

5. L.D. Gager, A.E. Wright, P.R. Almond, "Silicon diode detectors used in radiological physics measurements. Part I: Development of an energy compensating shield", Med. Phys. 4(6), 494-498 (1977).

6. A.E. Wright, L.D. Gager, "Silicon diode detectors used in radiological physics measurements. Part II: Measurement of dosimetry data for high-energy photons", Med. Phys. 4(6), 499-502 (1977).

7. D. Wilkins, X.A. Li, J. Cygler, L. Gerig, "The effect of dose rate dependence of p-type silicon detectors on linac relative dosimetry", Med. Phys. 24(6), 879-881 (1997).

8. T.C. Zhu, L. Ding. C.R. Liu, J.R. Palta, "Performance evaluation of a diode array for enhanced dynamic wedge dosimetry", Med. Phys. **24**(7) 1173-1180 (1997).

9. Profiler Model 1170 Operating Instructions, Oct. 1996, Sun Nuclear Corp., Melbourne, FL.

10. R. Watts, "Evaluation of a diode detector array for use as a linear accelerator QC device", Med. Phys. **25**(2), 247-250 (1998).

11. In honor of Hunter and Driffield, who in 1890 used such curves to characterize the response of photographic film to light.

PHYSICAL CHARACTERISTICS OF THE MULTILEAF COLLIMATOR

The major limitation of radiotherapy is the complication induced by the irradiation of healthy tissue in the treatment of tumors. Usually, x-ray beams from linear accelerators are shaped by secondary collimators, often called jaws, that are able to produce rectangular treatment areas. From this limited set of field shapes, beams that conform more closely to the tumor and avoid the irradiation of surrounding healthy tissue are created by the addition of specially shaped metal blocks below the jaws which shield the patient. Typically these blocks are made of a low melting point lead alloy, called cerrobend, and are custom made for a particular field for a given patient. These blocks have several disadvantages[1,2]. First, their fabrication is time consuming, and involves the handling of potentially toxic materials. In addition, blocks are mounted on a tray and must be attached and removed from the accelerator by the radiation therapist for each treatment. Since these blocks are heavy, they might be at the origin of an injury to therapists or the patients.

On modern accelerators, cerrobend blocks may be replaced by multileaf collimators (MLC) to shield part of the rectangular field defined by the jaws. The MLC comprises independently movable leaves that can block a portion of the radiation beam. Using a computer, individual leaves can be moved to delineate an arbitrarily-shaped field.

In this chapter, the physical characteristics of MLCs are described, with particular attention to the multileaf collimator found on the Clinac 2300 C/D used for this project. The composition and the shape of the MLC is specified as well as a description of how the position of the leaves is controlled.

4.1 MLC configuration.

There is as yet no unique configuration among manufacturers for the multileaf collimator[1,3]. Some MLCs replace one set of secondary jaws (x-jaws or y-jaws). For example, the Philips MLC replaces the upper jaws, or y-jaws, and the leaves move parallel to the axis of rotation of the gantry. This design also has a back-up collimator inserted between the MLC and the lower jaws. On the other hand, the Siemens MLC corresponds to the lower jaws which are split into a set of leaves.

The MLC used during this project (Varian 2300 C/D) uses another design. It is a tertiary collimator system attached under the lower set of jaws. The advantage of this design is that the linac can be used with jaws and blocks in the case of a MLC malfunction. On the other hand, the linac head is heavier and bigger such that there is less clearance between the isocenter and the gantry. This design is potentially limiting for treatments where the support tray must be used since it is attached under the MLC system, closer to the patient.

4.2 Shape of the leaves.

An MLC must attenuate the x-ray beam at least to the same degree as custom cerrobend blocks. Each leaf has to be precisely machined with an optimal shape that will limit to an acceptable level the transmission of radiation between adjacent and opposing leaves. The material of choice for the leaf construction is tungsten alloy due to its very high density and hardness. Pure tungsten is brittle, but alloys can be made that retain a high density and are readily machinable. The Varian MLC used in these experiments has 26 pairs of tungsten leaves, 5.4 cm thick, that project to a 1.0 cm width at the isocenter. The length of the leaf is 16.0 cm when projected at the isocenter. The maximum positional variation for leaves on the same carriage is 14.5 cm and the appropriate jaw is always placed so as to shield the end of the leaves attached to the carriage in order to avoid radiation exposure outside the main field.

The cross-sectional shape of the leaves is complex[1,4,5,6,7]. In order to limit the interleaf transmission, a leaf has to overlap its neighbors. In addition, the MLC is focused in the plane orthogonal to their direction of travel to account for divergence of the beam[6]. The Varian leaves are overlapped by stepping out and back again in the middle of the thickness of the leaves as illustrated in figure 4.1a, giving a "tongue and groove" design. As a result, no photon ray can pass through the MLC without being attenuated since the MLC never offers a straight path to the x-ray. For the MLC studied, the leaves travel in a plane perpendicular to the beam central axis and do not follow beam divergence. Normally, the collimators move along an arced path to maintain alignment with divergent beam geometry. In order to produce a constant penumbra as the leaf end position is changing on a plane, the tip of the leaves is curved. However the end of the leaves was designed with two flat segments as illustrated in figure 4.1b and it has been shown[3] to result in little change in penumbra width as a function of leaf position across the field.

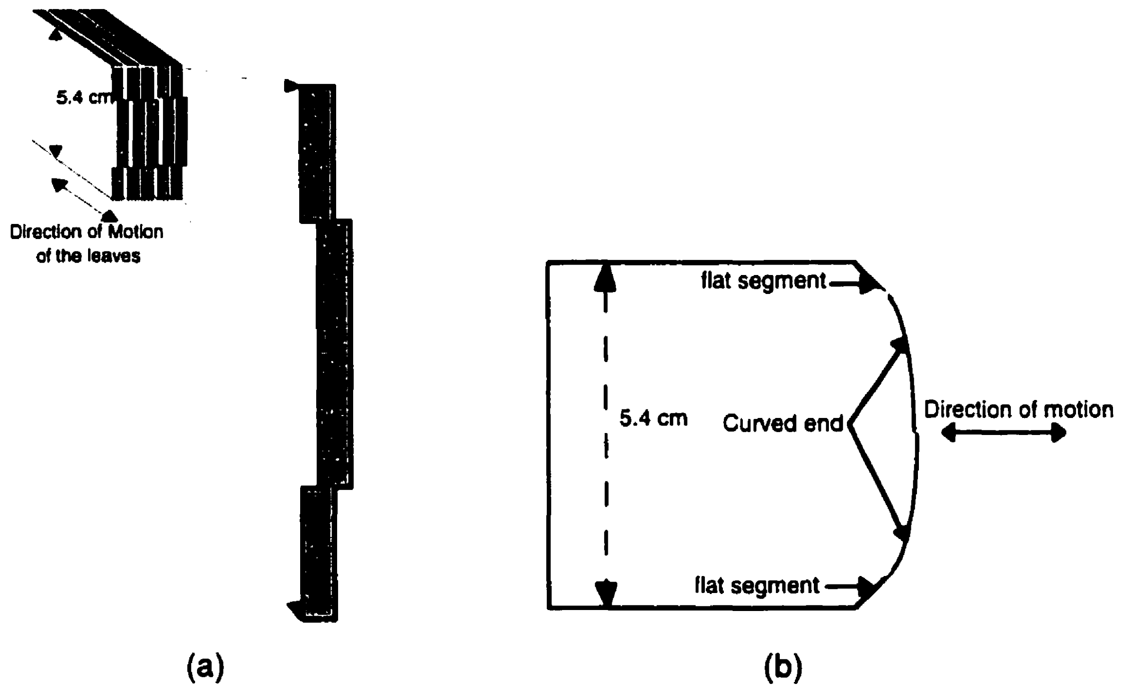

Figure 4.1 MLC shape. In (a), the "tongue and groove" shape of the leaf is illustrated as seen when looking directly at the front of the leaf. In (b), the curved end of the leaf is shown as seen when looking directly from the side of the leaf.

4.3 Control of the motion of the MLC.

Apart from a robust leaf design, the accurate and reproducible motion of the leaves is critical in the clinical use of the MLC. A motor for each leaf permits the independent motion of the leaves with a maximum speed of 1.5 cm/sec and for the MLC used, the position of each leaf is measured by its own potentiometer[1]. The calibration of the leaf position must be done regularly to ensure the integrity of the controlling system. The Varian MLC system uses a narrow infrared beam permanently placed in the collimator assembly to automatically calibrate the leaf position each time the computer controlled operating system is initialized. The calibration is done by having each leaf intercept the infrared beam one at the time, recording the value of the position encoders in a look-up table used by the control system.

The MLC system consists of a computer interfacing with an MLC controller board placed in the linac head. The MLC controller board controls the carriages and the leaves. The MLC computer is an independent computer which monitors the position of the collimator and the presence of an electron applicator by communicating with the linac controlling computer. The linac system will not allow the electron beam to be turned on if the MLC system is engaged during routine clinical mode.

4.4 Light field position correction.

Normally, the field edge is defined as the position of the 50% dose level through the penumbra. The position of the radiation field edge usually coincides with the position of the light field edge such that are both easily understood to correspond to the ray starting from the center of the x-ray source and passing along the focused collimator. However, the leaves have a curved end such that the position of the tip of the leaf has been shown to neither correspond to the light shadow position at SAD nor the radiation field edge position[8]. Considering figure 4.2, the distance traveled by the physical tip of the leaf W' is not the same as the distance W traveled at SAD by the leaf light shadow. In fact, the distance at SAD traveled by the leaf (W) is related to the
actual motion of the leaf (W') by:

$$W = W' \times \frac{SAD}{SCD}, \tag{4.1}$$

where SCD is the distance from the x-ray source to the center of the leaf depth. However, equation 4.1 is considering the tip of the curved end leaf such that it does not describe the position of the light field edge at SAD leading to an overestimate that has been shown[8] to be up to 5 mm. Instead of using the tip of the leaf, the tangent of the curved end that passes through the center of the x-ray source should be used for all leaf positions in the field. In figure 4.2, these tangents correspond to line ending at A and D instead of points B and E when the tip of the leaf describes a field halfwidth of H as opposed to W. Mathematically, the light field position was derived to be approximately:

$$H = \frac{W \times SCD \pm \left\{ R \times SAD \times \left(1 - \frac{SAD}{\sqrt{SAD^2 + W^2}} \right) \right\}}{SCD \pm \frac{R \times W}{\sqrt{SAD^2 + W^2}}}, \tag{4.2}$$

where *R* is the radius of curvature of the leaf curved end. As a result of using this expression, the deviation between the leaf position and the light field projection of any leaf is found to have a maximum of about 1 mm. In fact, equation 4.2 is used by the Varian MLC controller to compensate this non-linearity of the light shadow of the leaf.

Unfortunately, equation 4.2 does not give agreement between the radiation leaf edge and light field. The reason for this is that the radiation edge is defined as the 50% dose point which implies that the radiation passed roughly though one HVL of material. The derived expression is for a ray tangent to the curved leaf. As a result, the x-ray field is wider than the light field by a small value that was shown[8] to be almost constant from calculations with an expression similar to equation 4.2 but considering a 1 HVL chord. This small discrepancy, to a maximum of 1 mm, is usually considered clinically insignificant.

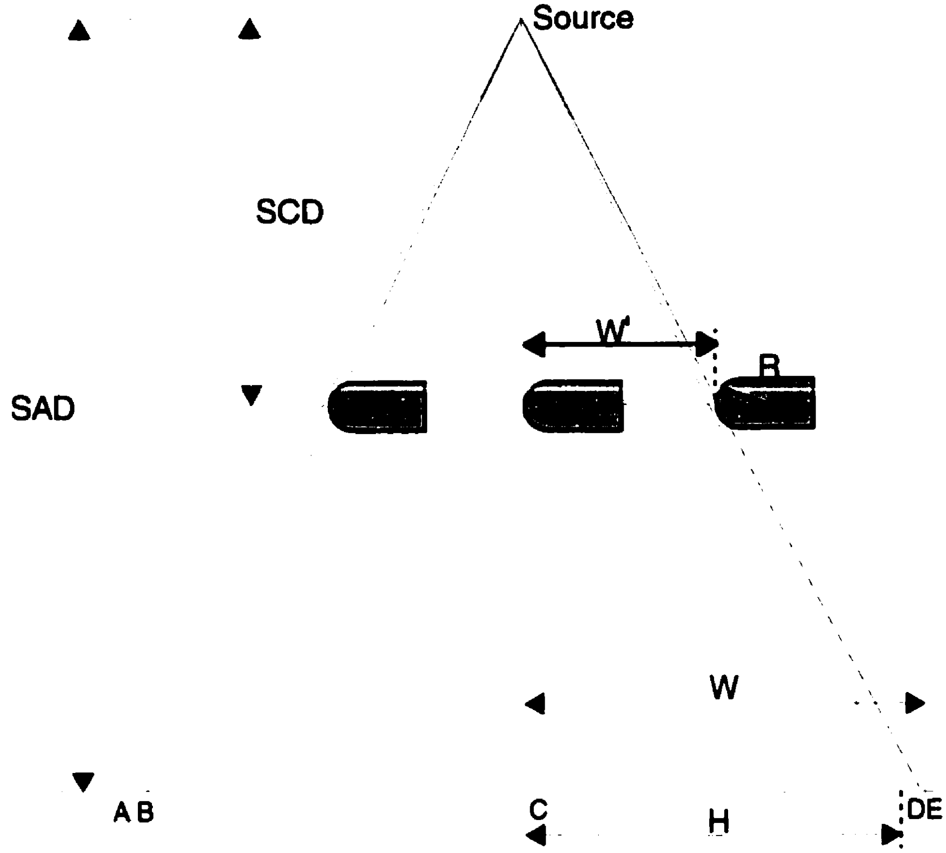

Figure 4.2 Diagram illustrating the difference between the light field resulting from considering the tip of the curved end leaf versus the tangent of the curved surface passing through the middle of the x-ray source.

4.5 Configuration of the MLC field.

The MLC controller reads the position of each leaf from a text file. For the present work, the MLC text files were created in two ways: with a regular text editor on a personal computer and with proprietary software that has an intuitive graphical interface.

4.5.1 Text file.

The structure of the MLC text file[1], shown in figure 4.3, must be strictly followed. The "*keyword = value*" sequence has to appear in the exact order shown in figure 4.3 with the same capitalization. However almost any text editor can be used since the MLC controller is expecting a standard ASCII text file. Due to the strict formatting requirements, the position of each leaf for both carriages must be entered in centimeters. The position is given relative to the central axis which correspond to the position 0.00 cm. When the leaf end travels past the central axis, the position of the leaf is negative while a positive leaf position indicates that the leaf end is placed between its carriage and the central axis.

Even though the MLC file can be produced with a regular text editor, the file should be opened and saved with the proprietary program since this software performs a check of the validity of each value. For example, it verifies that the position of any two leaves of the same carriage do not differ by more than 14.5 cm and also checks for leaf collisions. Also the software calculates a cyclic redundancy check (CRC) to ensure that no error was introduced during the file handling processes.

4.5.2 Shaper.

A dedicated software package known as the "shaper" is used to create MLC fields. It presents a simple and intuitive graphical interface illustrating each leaf. The position of the leaves can be simply changed by selecting the appropriate leaf with the computer mouse and dragging the leaf to the required position as indicated in centimeters at the top of the screen. Each leaf of the field can be positioned and the final leaf arrangement saved on the computer hard drive.

"Shaper" can also be used when interfaced with a digitizing tablet. The contours of the desired portal are entered using a spark pen stylus and localization hardware that has been previously calibrated. The position of each leaf can be adjusted, and the position of the collimator can be changed, along with a variety of other parameters listed in figure 4.3.

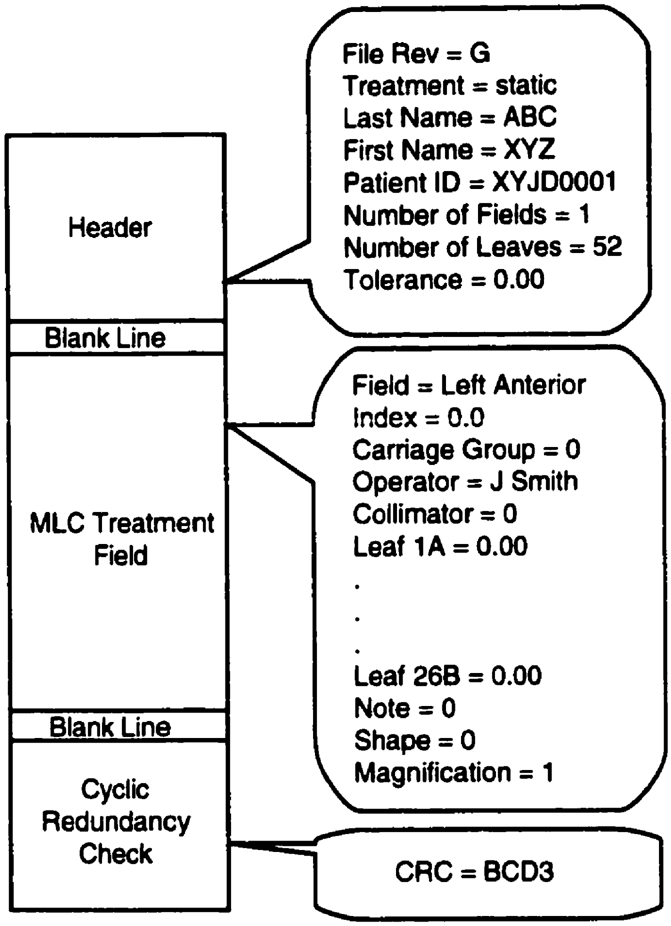

Figure 4.3 Static MLC text file structure including the simplified form of the file to the left and an example of the value for every mandatory keyword to the right.

4.5.3 Dynamic MLC files.

When the MLC is used to produce intensity modulated fields or dynamic compensators, MLC subfields are created in the same manner that the static MLC fields are: either with text files or using a proprietary software. However an additional parameter, the dose fraction, most be specified for each subfield[9]. The dose fraction is normalized to 1 at the end of the treatment such that it will always be between 0 and 1. This dose fraction specifies the normalized dose at which this particular subfield applies. Hence when the MLCs are used in the dynamic or constantly moving mode, the MLC system will linearly interpolate the position of all leaves for all dose fractions between these two subfields enabling the leaves to move in the presence of radiation. On the other hand, for the step and shoot method, the same dose fraction will appear for two consecutive subfields, instructing the MLC and linac systems to produce no radiation when the leaves are moving. As a consequence, the same MLC pattern will be used for two consecutive subfields with the dose fraction increased, instructing the MLC system not to move the leaves in the presence of radiation.

When the MLC system supports dynamic MLC, two modes of operation are available, the static and the dose dynamic mode, and the two are mutually exclusive.

4.6 Summary.

In this section, the physical properties of the multileaf collimator used for this project were explained. The configuration of the MLC assembly was indicated. The thickness of the leaves, their shape and the method of motion was described, and the correction of the leaf position due to the curved end design was explained. Finally, the means used to create the MLC fields were briefly discussed.

4.7 References.

1. A.L. Boyer, "Basic Application of a Multileaf Collimator", in Teletherapy Present and Future, Proceedings of the 1996 Summer School of the American Association of Physicists in Medicine, edited by J. Palta and R. Mackie (Medical Physics Publishing, Madison, WI (1996).

2. A.L. Boyer, T.G. Ochran, C.E. Nyerick, T.J. Waldron, C.J. Huntzinger, "Clinical dosimetry for implementation of a multileaf collimator", Med. Phys. **19**(5), 1255-1261 (1992).

3. I.J. Das, G.E. Desobry, S.W. McNeeley, E.C. Cheng, T.E. Schultheiss, "Beam characteristics of a retrofitted double-focused multileaf collimator", Med. Phys. **25** (9) (1998).

4. E.E. Klein, W.B. Harms, D.A. Low, V. Willcut, J.A. Purdy, "Clinical implementation of a commercial multileaf collimator: dosimetry, networking, simulation, and quality assurance", International Journal of Radiation Oncology, Biology, Physics. **33**(5), 1195-1208 (1995).

5. J.P.C. van Santvoort, B.J.M. Heijmen, "Dynamic multileaf collimator without 'tongue-and-groove' underdosage effects", Med. Biol. **41**, 2091-2105 (1996).

6. J.M. Galvin, A.R. Smith, B. Larry, "Characterization of a Multileaf Collimator System", Int. J. Radiation Oncology Biol. Phys., Vol. **25**, 181-192 (1993).

7. J.M. Galvin, A.R. Smith, R.D. Moeller, R.L. Goodman, W.D. Powlis, J. Rubenstein, L.J. Solin, B. Michael, M. Needham, C.J. Huntzinger, M.M. Kligerman, "Evaluation of Multileaf Collimator Design for a Photon Beam", Int. J. Radiation Oncology Biol. Phys., Vol **23**, 789-801 (1992).

8. A.L. Boyer, S. Li, "Geometric analysis of light-field position of a multileaf collimator with curved ends", Med. Phys. **24**(5), 757-762 (1997).

9. DMLC Implementation Guide, Varian Associates, Palo Alto, California (1997).

EVALUATION OF THE STATIC MLC

As stated in chapter 4, the multileaf collimator has been implemented to overcome the disadvantages of custom made, poured blocks. However it also has some inherent limitations, such as the discrete nature of the field definition due to the fixed width of the leaves. The relatively large leaves may not offer sufficient discrimination between the healthy tissue and the tumor[1]. In order to use the MLC clinically some physical factors, including the output factor and the percentage depth dose, must be well established. In this chapter, only the MLC used in static mode is considered, but the basic parameters tested here are also important when the MLC is used in the dynamic mode.

All the measurements described in this chapter have been performed with the gantry and the collimator at 0° if not otherwise stated. The surface of the phantom was placed at 100 cm from the source except for the measurements done in air or where otherwise explicitly stated.

5.1 Output factor.

Ordinarily, when custom made blocks are placed in the x-ray beam, a simple dosimetric approach to the beam output using two different equivalent fields is used to calculate the output factor. The field defined by the jaws is used to find the appropriate tabulated component of scatter radiation in air, called collimator factor (CF). For the component of scatter radiation in phantom, the scatter factor (SF), the equivalent field given by the blocked field is used. From the literature, it is well established that the Varian MLC used can be considered as a tertiary custom block in the determination of the output factor[1,2,3]. Hence the relative dose factor is given by:

$$RDF = CF(FS_j) \times SF(FS_{MLC}), \tag{5.1}$$

where FS_j is the equivalent square field defined by the jaws and FS_{MLC} is the equivalent square field defined by the MLC or the blocked field. On the other hand, for other configurations of the MLC which consist of the replacement of one pair of jaws, the output factor is determined by the irregular field formed by the MLC and the traditional method of calculating the output factors may not be applicable. Tests have been conducted to establish that the RDF is given by equation 5.1 for the MLC system investigated.

5.1.1 CF and RDF for field defined by the jaws.

As a first step, the CF was measured for square fields centered on the beam central axis defined by the regular secondary collimators, or jaws, ranging from 5x5 cm^2 to 40x40 cm^2. These measurements were done for the 6 MV photon beam of the Clinac 2300 C/D. The CF is measured in air such that a buildup cap must be added to the ion chamber in order to get sufficient dose buildup, or electronic equilibrium. For a 6 MV beam, a buildup cap of thickness equivalent to 1.5 cm of water was installed on the ion chamber which was positioned at the isocenter (SAD 100 cm). Two sets of buildup caps were used, one of acrylic with a density very similar to water and the other of aluminum, which is significantly smaller due to its higher density. Care was taken to have the radiation field fully covering the buildup cap, especially with the large acrylic mini phantom. For the smaller field sizes, the ion chamber was placed at an extended distance from the source and the collected charge was adjusted with the inverse square law to correct the reading as if it was measured at the isocenter. For the field sizes in the middle range, the CF was measured at both the isocenter and the extended distance with both buildup caps. Using these data, a curve of CF as a function of field size defined by the jaws for the 6 MV beam of the Clinac 2300 C/D was constructed.

5.1.2 RDF for field defined by the MLC.

The second step was to measure the RDF for radiation fields defined by the MLC inside a square field defined by the jaws. The goal is to verify that the RDF can be calculated using equation 5.1. The chosen method was to use the multileaf collimator to define a square with its axis rotated 45° inside the square field given by the jaws to create a diamond shaped field as illustrated in figure 5.11. This configuration of the MLC was chosen for two reasons. First, the effective shape of the radiation field is still a square, which is convenient. Also, it presents the worst case scenario for the MLC relative to the inherent limitation of its discrete resolution. Using a constant jaw position, the RDF was measured for the 6 MV beam for a range of rotated MLC square fields by incrementing the field size defined by the MLC from 4x4 cm^2 to the maximum square fitting in the jaws setting. The measurements were repeated for a range of jaws settings. For each fixed jaw setting, the RDF was measured with all the possible MLC diamond fields fitting in the square field given by the jaws. The RDF was calculated by dividing the collected charge with a setup illustrated in figure 5.1 by the charge collected for a 10x10 cm^2 field defined by the jaws only.

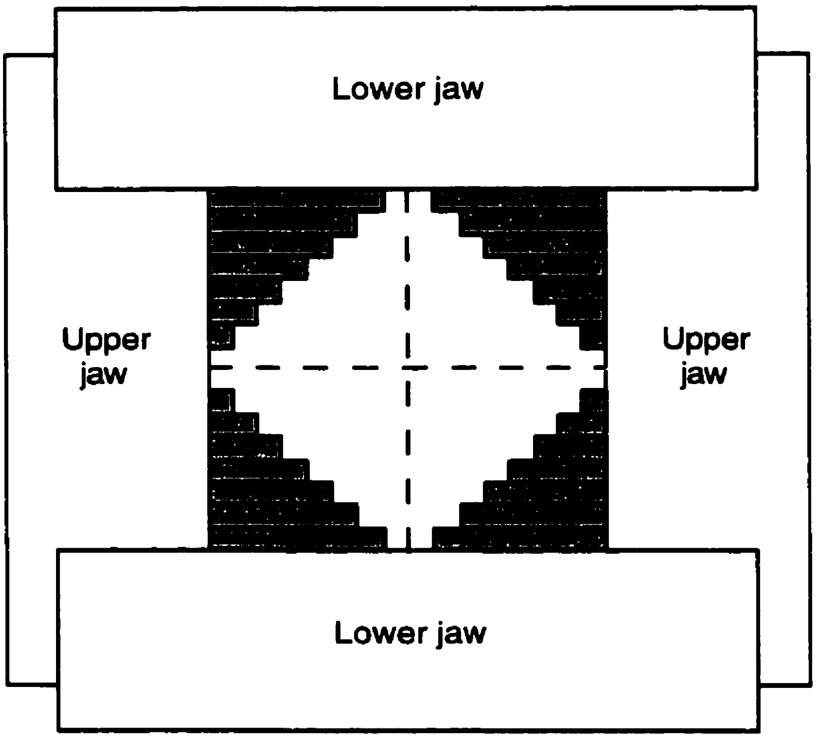

Figure 5.1 Diagram illustrating an example of the MLC square field setting inside the fixed jaw square field. The MLC square field is rotated to give a diamond shaped area.

5.1.3 SF given by the MLC setting.

Finally, if equation 5.1 applies to the MLC studied, the calculated SF as a function of MLC field size should be independent of the position of the jaws. The SF curves are obtained by dividing the RDF obtained with the MLC in section 5.1.2 by the CF for the appropriate jaw setting measured in section 5.1.1. In practice, a distinct SF curve will be found for every jaw setting, and the variation of points on this curve should be within ±1%.

5.2 Percentage depth dose.

The PDD was first measured with the regular secondary collimators outlining square fields ranging from 4x4 cm^2 to 25x25 cm^2. The 3D water tank was used to measure the PDD for both available photon energies, 6 and 18 MV, on the Clinac 2300 C/D with the water surface placed at 100 cm from the x-ray source. The scanning speed was made faster at greater depths and slower near the depth of dose maximum and shallow depths due to the rapid change of relative dose in this area. The data collected were analyzed using the software which permits both smoothing of the data and automatic normalization of each data point relative to the maximum dose measured.

The same measurements of the PDD were repeated by using the MLC to define the square fields identical to the fields given by the jaws. The jaws were placed to give a 25x30 cm^2 field, shielding the back of the leaves, near their carriages. The PDD obtained with the MLC were compared with the PDD acquired with the jaws by overlaying the PDD's for the same square field size and photon energy[1,3].

5.3 Penumbra.

The penumbra of fields defined by the MLC is of particular interest due to the curved nature of the tip of the leaves as compared with the jaws that are focused with the x-ray beam divergence[1,3,4,5]. Measurements of the penumbra were obtained using the 3D water scanner. Profiles parallel to the water surface were measured in the direction of motion of the leaves and perpendicular to this direction. The profiles were measured near the central axis for fields defined by the MLC and compared to those defined by the regular secondary collimators. Care was taken to ensure that the profiles were not passing between two leaves where leakage of radiation is important. The scans were acquired at depth of dose maximum (1.5 and 3.0 cm for 6 and 18 MV beams respectively) and at 10 cm for a range of field sizes from 4x4 to 24x24 cm^2.

The collected data were analyzed with the appropriate software. Once the profiles were smoothed, the penumbra was calculated to be the lateral distance in millimeters from the 80% to the 20% dose position relative to 100% dose on the central axis.

In addition, the penumbra width was evaluated for the MLC as a function of the leaf end position. This was accomplished by having the center of a small MLC square field of 4x4 cm^2 displaced from the bottom left to the upper right corner of the possible range of the MLC, as illustrated in figure 5.2, keeping the jaws at a fixed position. Apart from the small square open field, the remainder of the area inside the jaws was blocked by the MLC. For each MLC square field position, two perpendicular profiles near the center of the square, but not passing between two leaves, were taken. The penumbra as a function of the position of the center of the square MLC field was analyzed.

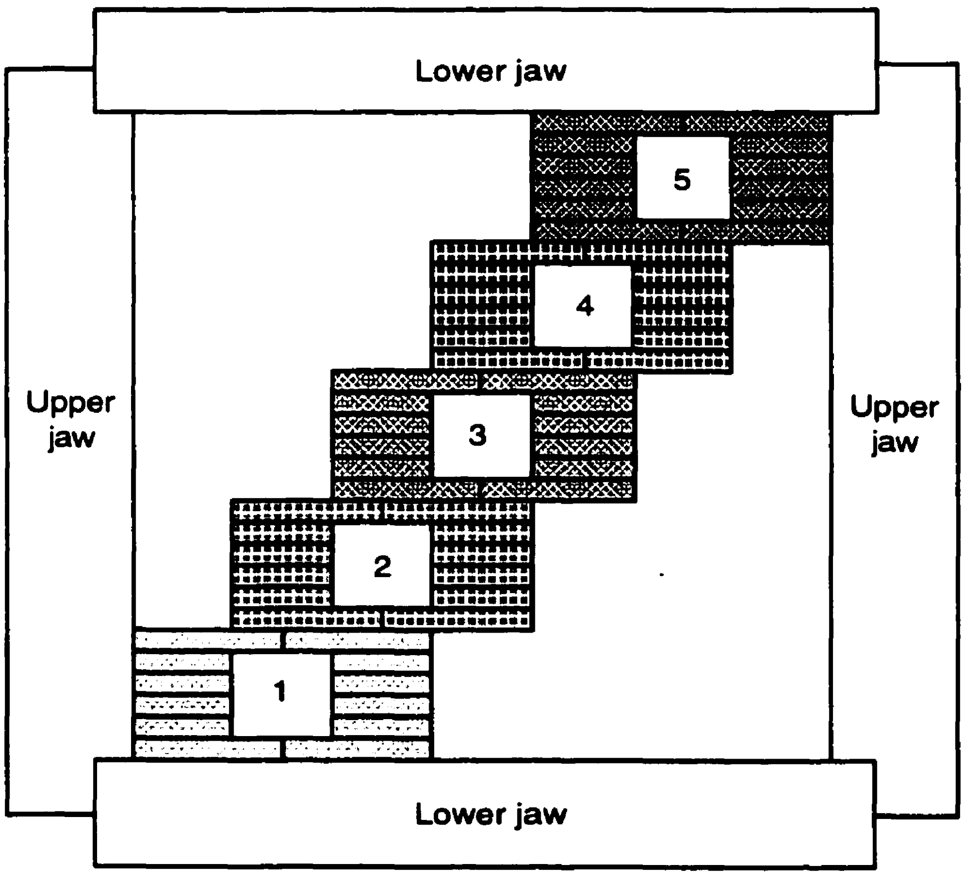

Figure 5.2 Diagram illustrating the successive position of the small square fields given by the MLC inside the fixed large field defined by the secondary collimator. Not shown is the rest of the field blocked by the MLC around the small square field.

5.4 Radiation transmission.

The transmission of radiation through the MLC was evaluated with two different methods using the 3D water scanner. While the two methods proposed to measure the transmission of radiation through the MLC are both simple and practical measurements, they are not an exhaustive study of the transmission of the MLC. The first experiment involves having an increasing number of pairs of leaves inserted around the beam central axis as illustrated in figure 5.3. In a converse manner, the second test consists of taking out of a completely closed field an increasing number of pairs of leaves around the central axis as in figure 5.4[1,6,7].

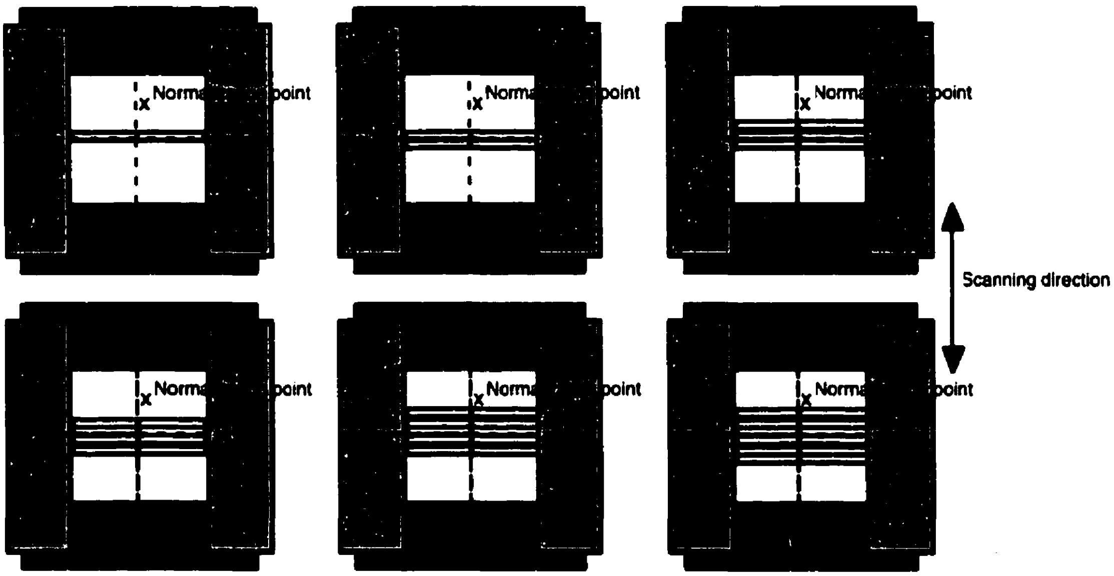

Figure 5.3 Illustration of the manner in which pairs of leaves were added around the central axis in order to test the radiation transmission through the MLC.

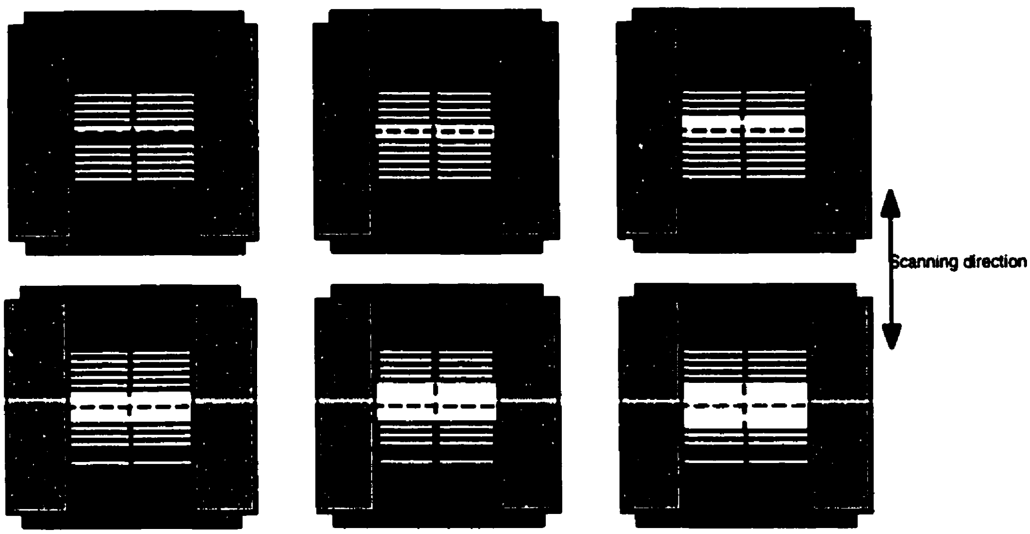

Figure 5.4 Illustration of the manner in which pairs of leaves were taken out of the field to compare with the same field defined by the jaws.

5.4.1 Pairs of leaves in the radiation field.

First, profiles under a limited number of adjacent leaves in an open beam were acquired perpendicular to the leaf motion direction measuring only radiation passing through the MLC. The number of leaves in the beam ranged from 1 to 10 pairs around the beam central axis. The jaws were fixed, defining a 25x30 cm^2 field symmetrical with respect to the isocenter. For each MLC setting, a profile was obtained for both photon energies (6 and 18 MV) at the depth of dose maximum and at a depth of 10 cm. The scanning position was verified not to pass under the junction of the pairs of leaves where radiation leakage is significant. Profiles were smoothed and normalized to be 100% at a point in the open beam portion of the field with 10 pairs of leaves in the beam. Hence each profile was normalized at a point about 6 cm from the isocenter.

Another set of profiles has been measured in the direction of the width of only one pair of leaves in an opened beam for all possible positions of the pair of leaves so that the minimum dose achieved under only one leaf pair as a function of their position in an opened beam is determined. The experiment was conducted for the 6 and 18 MV beams at both the depth of dose maximum and a depth of 10 cm.

5.4.2 Pairs of leaves out of the radiation field.

The radiation field was completely closed by the MLC except for few pairs of leaves, and a profile perpendicular to the leaf motion direction was compared with a profile with the same field but defined by the secondary collimators measuring both the transmission of radiation and the scatter radiation. The number of pairs of leaves out of the beam ranged from 1 to 4. Due to the arrangement of the MLC, it is not possible to have an odd number of pairs of leaves defining a symmetric field with respect to the isocenter since the two middle pairs of leaves have their junction on the beam central axis as seen in figure 5.4. For this reason, the field defined by the jaws was placed asymmetrically in order to get the exact same field as with the MLC. Again the profiles were acquired with the 6 and 18 MV beam at a constant depth of 10 cm and at the depths of dose maximum. The profiles were smoothed and normalized to 100% at the center of the field in order to be able to compare the profile measured with a field defined by the MLC with the same field defined by the jaws.

5.5 Mechanical alignment of the MLC.

Six tests are described in appendix A.1, and they are designed to check the mechanical accuracy of the MLC system[8]. The first two tests verify that the leaves can be placed with a high precision to predetermined points across their range of travel. Even though the MLC system will not allow a treatment to take place if the leaves are not within a tight tolerance of the prescribe leaf position, it is important to have independent tests verifying the integrity of the system. The tolerance of the leaf position can be changed by the user to be from 0.01 to 0.50 cm and the beam will not be turned on until all the leaves are within the tolerance of the prescribed position.

Test 3 and 4 examine the skew of the MLC carriages relative to both sets of secondary collimators. The precise construction of the leaves does not guaranty that the MLC assembly is well aligned with the jaws. Considering the range of travel of the leaves, a small skew of the MLC relative to the jaws can quickly lead to a significant leaf position error, showing the importance of these two tests. The leaves should be parallel to the lower secondary collimators and perpendicular to the upper jaws.

The last two tests were designed to assure that the center of the tertiary MLC assembly is stable with both collimator and gantry angle. Even though the mechanical stability of the MLC assembly with the position of the collimator or the gantry is necessary, achieving this is difficult due to the significant weight of the collimator system. The collimator including the MLC must present a stable radiation center at all gantry angles even though the gravity is pulling so as to induce a sag into the system. The construction of the collimator system must be strong enough to resist this force as verified by test 5 and 6 of appendix A.1.

These six tests are important when the MLC is used to replace custom blocks, as they ensure the accurate placement of the leaves. They are even more critical when the MLC is used for dynamic beam delivery due to the possibility of error propagation with the movement of the leaves.

5.6 Summary.

In this chapter, a series of tests has been described that verify the accurate operation of the MLC system when used to replace custom cerrobend blocks. Measurements of dosimetric factors have been explained in order to check that the traditional method of monitor unit calculations can still be employed. Tests that measure the penumbra and the transmission of the MLC as compared with the regular secondary collimator were described. Finally, a series of experiments to verify the mechanical alignment of the MLC have been introduced.

5.7 References.

1. A.L. Boyer, T.G. Ochran, C.E. Nyerick, T.J. Waldron, C.J. Huntzinger, "Clinical dosimetry for implementation of a multileaf collimator", Med. Phys. **19**(5), 1255-61 (1992).

2. A.L. Boyer, "Basic Application of a Multileaf Collimator", in Teletherapy Present and Future, Proceedings of the 1996 Summer School of the American Association of Physicists in Medicine, edited by J. Palta and R. Mackie (Medical Physics Publishing, Madison, WI (1996).

3. J.R. Palta, D.K. Yeung, V. Frouhar, "Dosimetric considerations for a multileaf collimator system", Med. Phys. **23**(7), 1219-24 (1996).

4. J.M. Galvin, A.R. Smith, B. Larry, "Characterization of a Multileaf Collimator System", Int. J. Radiat. Oncol. Biol. Phys., **25**, 181-192 (1993).

5. J. Sun, Y. Zhu, "Study of dosimetric penumbra due to multileaf collimation on a medical linear accelerator", Int. J. Radiat. Oncol., Biol., Phys. **32**(5),1409-1417 (1995).

6. E.E. Klein, W.B. Harms, D.A. Low, V. Willcut, J.A. Purdy, "Clinical implementation of a commercial multileaf collimator: dosimetry, networking, simulation, and quality assurance", Int. J. Radiat. Oncol., Biol., Phys. **33**(5),1195-208 (1995).

7. M.S. Huq, Y. Yu, Z.P. Chen, N. Suntharalingam, "Dosimetric characteristics of a commercial multileaf collimator", Med. Phys. **22**(2):241-7 (1995).

8. C.D. Mubata, P. Childs, A.M. Bidmead, "A quality assurance procedure for the Varian multi-leaf collimator", Physics in Medicine & Biology. **42**(2), 423-31, (1997).

EVALUATION OF DYNAMIC MLC AND THE DYNAMIC BEAM DELIVERY TOOLBOX

It has been shown that intensity modulated fields can be delivered with a multileaf collimator (MLC)[1-12]. There are two main methods to create intensity modulated fields with a MLC; the step and shoot method and the continuous motion method. This section is meant to explain separately the verification of the MLC when used to create intensity modulated fields using these two methods. The step and shoot technique consists of moving the leaves without the beam on to create the appropriate subfields that, once added together, gives the intensity modulation sought. To achieve this, several static MLC fields are used. Some quality assurance tests must be added to the static MLC quality assurance tests described in the previous chapter in order ensure that the MLC computer system is able to automatically place the leaves in sequence. On the other hand, in the continuous motion technique, the leaves are allowed to move in the presence of radiation, which is the ultimate level of dynamic treatment. The step and shoot method will tend toward the continuous motion method when the number of subfields is increased. However the dynamic technique is not a simple extension of static MLC and several tests must be performed before it can be implemented clinically. To finish, a simple extension to dynamic MLC, the dynamic beam delivery (DBD) toolbox is examined.

6.1 Positional reproducibility of the leaves using the step and shoot technique.

Intensity modulation using the step and shoot method corresponds to several segments composed of static MLC fields. As a consequence, once the reliability of the MLC system for static treatment has been established, only a simple set of tests is required to check that the MLC can be used for radiotherapy through the step and shoot technique[13]. In appendix A.2, two tests to verify the positional reproducibility of the leaves completely under computer control are described. The first test measures the reproducibility of the leaves as measures with the penumbra by exposing an array of diodes to a pair of leaves moving in succession many times between two positions. On the other hand, the second test is a visual examination of the junction between adjacent rectangles defined by a pair of leaves using film as an integrating dosimeter.

When the MLC in the step and shoot mode is used on a regular basis, the reproducibility of the leaves position should be tested frequently to avoid systematic errors in the placement of the leaves. In practice, small fields will be used to boost certain areas of the irradiated volume to achieve the desired dose distribution. Hence if the placement of the leaves under computer control is not always accurate, it could lead to a large error in dose deposition due to the utilization of relatively small fields. Moreover, frequent examination of the positional reproducibility of the leaves could be helpful to detect trends in the accuracy of the MLC system.

6.2 Dose linearity.

When the step and shoot technique is used to implement conformal radiotherapy, some subfields will be used to deliver very small doses, or monitor unit (MU) settings, compared to the MU setting normally employed for clinical treatment. However the calibration of the beam output is done with relatively large doses and the same characteristics measured at those large MUs are assumed to apply even when small MU settings are used. Non-linearity of linacs for small doses has been reported in the literature[14-20], suggesting that the use of very small MU for subfield should be performed with care.

6.2.1 Charge per monitor unit.

The charge accumulated, Q, in an ion chamber for a range of MU settings going from 1 to 300 MU was measured. The Farmer-type ion chamber was placed at d_{max} in a solid water phantom and exposed to 6 and 18 MV beams with the collimator defining a 10x10 cm^2 field. The dose to medium can be calculated using the following equation as described in AAPM Task Group 21[21]:

$$D_{med} = QN_{gas}\left(\bar{L}/\rho\right)_{gas}^{med} P_{ion}P_{repl}P_{wall}, \qquad (6.3)$$

where Q is the measured charge corrected for temperature and pressure, N_{gas} is the cavity calibration factor, $\left(\bar{L}/\rho\right)$ is the restricted stopping power ratio of medium to chamber gas, P_{ion} is a correction for ion recombination, P_{repl} is the replacement correction factor and P_{wall} is a correction for the chamber wall. All of these parameters are discussed in AAPM Task Group 21. All the parameters can be considered constant for a given machine and energy such that D_{med}/Q should be constant. Since only relative dose or accumulated charge are considered here, only charge Q as a function of MU has to be considered. Ideally, a curve of charge per MU as a function of MU would be constant.

6.2.2 Current as a function of time.

Using a high voltage power supply (model 648, Keithley, Cleveland, OH) and an electrometer (model 35617, Keithley, Cleveland, OH) interfaced with a PC, the current as a function of time for the Farmer-type ion chamber (0.6 cm^3, model PR-06C, Capintec, Ramsey, NJ) and a diode (p-type, Scanditronics, Uppsala, Sweden) was measured when exposed to the 6 MV beam. The dosimeters were placed at the isocenter with the proper buildup cap on. Once the current was stabilized, the beam was stopped for varying lengths of time before being turned back on. These measurements were repeated in a cobalt-60 beam, which is a continuous beam as opposed to the pulsed linac beam. The cobalt-60 measurements served the purpose of distinguishing a linear accelerator unstable output for few seconds from dosimeter non-linearity with dose or time.

Two kinds of dosimeters, ionization chambers and diodes, were used for the current measurements to compare their results. Again, this was done in order to be able to recognize a dose non-linearity of a dosimeter as opposed to linac instability. The two dosimeters were connected to the same electrometer system to minimize the source of variation between the measurements.

The current measurements as a function of time was integrated in order to be compared with the charge per MU results explained in 6.2.1. The integration was calculated assuming that each pair of points is connected by a straight line, and the error, however significant, was ignored in this calculation.

6.3 Special features of dynamic multileaf collimator (DMLC).

Considering the DMLC used for dynamic compensation, the dose delivered to a certain point is directly proportional to the leaf speed and the dose rate, which is inherently controlled by the MLC system. Speed and dose rate are selected by the MLC controller in order to have the shortest possible treatment time within the MLC system and linac limits and the user has no direct control over these parameters. In fact, the dose rate will be the user defined dose rate, which acts as a maximum, as long the maximum speed of the leaves is not exceeded. The specified dose as a function of the MLC subfield, defined by the user, uniquely defines the dose distribution regardless of the dose rate and the MLC speed, controlled by the MLC system.

The MLC system will place its leaves to the position corresponding to the current dose fraction when the DMLC file is loaded. Hence, if the accumulated dose has not been reset to zero from the previous treatment, the normalized dose will be 1, indicating that the intended dose has entirely been given, and the MLC will move to the last subfield of the loaded DMLC file. As soon as the accumulated dose is set to zero, the MLC will be positioned at the first field of the DMLC file. By extension, if the treatment is interrupted before it is completed, the partial treatment remaining can be delivered by turning the beam back on since the MLC field corresponding to the current dose fraction will be automatically loaded in order to complete the treatment. An IPSN interlock (Initial Position) will prevent the firing of the beam unless the leaves are positioned so as to correspond to the current dose fraction.

The MLC system guaranties that the leaves are within the tolerance of the prescribed position. The tolerance can be changed by the user within the range of 0.01 to 0.5 cm. The tolerance represents the maximum allowed error of the leaf position at isocenter. In the case that one or several leaves can not be kept within the tolerance of the prescribed position, the DSPN interlock (Dose Position) will interrupt the beam. In practice, this interlock should not appear, even when the tightest tolerance is selected. The overall treatment time may become quite long for a small tolerance; on the order of a minute.

6.4 Stability of the leaf speed.

The speed stability of the leaves was tested as described in test 1 of appendix A.3[22]. The test was performed for one pair of leaves at a time even though it is possible to test all the pairs of leaves at once using film. The speed stability of the leaves was examined relative to the opposing leaf of a pair. Consequently, the method proposed is not absolute since both leaves may have the same speed variation at a given point so that the resulting profile will be flat leading to the conclusion that the speed of the leaves was constant.

The method by which the MLC system selects the speed of the leaves and the dose rate has been considered in the design of this experiment. The MLC system will favor the dose rate given by the user, which acts as a ceiling dose rate, as long as the maximum speed of the leaves is not exceeded. Hence the ceiling dose rate chosen for this experiment has to be low enough to avoid the maximum speed of any leaf to be exceeded, and avoid a dose rate adjustment during the experiment. This observation is important since each pair of leaves was programmed to move at different speeds during the same exposition. As a result, not all leaves were moving at the same time such that the dose rate could be varying in the case that the ceiling dose rate was too high. Since the dose rate and the leaf speed are directly related, the dose rate changes when certain leaves move suddenly move fast. As a consequence, the speed of the already moving leaves must be compensated.

The maximum speed of the leaves is listed as 1.5 cm per second for the multileaf collimator used. However, the maximum speed of the leaves was observed to vary with respect to the selected ceiling dose rate. For this reason some rough measurements of maximum speed of the leaves, described in test 3 of appendix A.3, were conducted.

6.5 Effect of acceleration.

A test to verify the effect of acceleration and deceleration of the leaves during irradiation is introduced in test 2 of appendix A.3[22]. In test 1 discussed in section 6.4, attention to avoid acceleration of the leaves was mentioned. The same leaf patterns can be used for this experiment to have the leaves moving with a constant speed for a certain time. Deceleration and acceleration of the leaves is induced by interrupting the beam for a short period. The leaves are subject to acceleration when the beam is stopped since they were moving with a certain speed and they have to come to rest as quickly as possible due to the abrupt halt of the beam. The acceleration of the leaves might lead to a positional error. In principle, the MLC system should be able to keep track of the position of the leaves and the dose should be delivered only if the leaves are within the tolerance of their prescribed position. In fact, there is certainly some error introduced by interrupting the beam and this experiment measures its significance.

6.6 Positional accuracy of the leaves in the dynamic mode.

A test designed to verify the positional accuracy of the leaves during a dynamic treatment delivery is described in test 4 of appendix A.3[22]. The positional accuracy in dynamic treatment is very important due to the possibility of error propagation. For example, a positional error in a static field will only affect the edge of the field while the same error in a dynamic beam delivery could have an impact across the entire treatment field.

It is certainly conceivable to create an experiment that can determine the positional accuracy of the leaves while they are moving. For example, a calibrated video recording system could be used. However it would imply the use of special equipment that might not be readily available and might be too complicated to set up for a regular quality assurance test. Hence a simpler method that involves equipment used on a regular basis in the radiotherapy clinic was preferred. Test 4 described in appendix A.3 uses film and has been modified so that a visual inspection suffices to check the positional accuracy of all the leaves at once. The preparation time is minimal and the analysis is relatively simple; important qualities if the test is to be implemented in a regular quality assurance program. The visual test is good enough to detect an error that would require an adjustment while the original test could be used to detect trends with time in the leaves positional error.

The leakage of radiation at the edge of the leaves, due to their rounded design, has been exploited by having both leaves of a pair stopping for a moment at the same predetermined points, but at different times. A hot spot is left at the stopped position because of the increased radiation at the edges of the leaves. By observing the hot spots, it is possible to determine that the leaves, under computer control, have either stopped at the intended places, overtraveled, or stopped before the selected locations.

The disadvantage of this method is that it is not truly dynamic since it is the positions that the leaves stop at that are verified. It is a practical way of verifying that the MLC system is reliable in the dynamic mode.

6.7 Evaluation of dynamic beam delivery toolbox.

The dynamic beam delivery (DBD) toolbox available on the Clinac 2300 C/D provides the opportunity to change the position of the four jaws, the collimator angle, and the gantry angle under computer control. These axes can be moved with or without the presence of radiation. The treatment delivery is controlled by a file similar to an ST table used for the enhanced dynamic wedge. The position of the moving axes as a function of normalized accumulated MU's is listed following a strict syntax in a text file loaded on the accelerator console computer[23].

Even though the DBD toolbox can be used only in a service mode (*i.e.* not clinically), a series of tests has been conducted to verify the accurate motion of the axes using the step and shoot and continuous motion techniques. These tests are described in appendix B. When the DBD toolbox is available clinically, the verifications listed in this chapter could be part of a quality assurance program.

6.8 Verification of dynamic motion of jaws under DBD toolbox control.

The set of five tests presented in appendix B.1 were conducted in order to verify the accuracy of the jaw position and motion when under the control of the DBD toolbox[22]. These experiments are the same as those performed to examine the multileaf collimator, so that the details of the experiments are not repeated here. The range of motion is not the same for both pairs of jaws. At the isocenter, the y-jaws can be opened to 20 cm from the centerline and can overtravel the isocenter by 10 cm. On the other hand, the x-jaws are limited to an overtravel distance of 2 cm but can still be opened to 20 cm from the isocenter. Another constraint is added for the tests that required the jaws to be closed since they can not be placed closer than about 3 mm apart. The strategy employed was to ignore the small gap left and to make sure that the motion of the jaws is as if there was no gap. As a result, the jaws remained stationary for the time it would have taken to travel the first and last 3 mm. The results will be slightly influenced by this assumption at the edges, but it can be accounted for in the analysis.

6.9 Verification of dynamic rotation of collimator under DBD toolbox control.

Four tests to verify the accuracy of the collimator angle and the precision of its dynamic rotation when under the control of the DBD toolbox are described in some detail in appendix B.2[23]. Both the step and shoot and the continuous motion approaches were considered in the design of these quality assurance tests.

Contrary to previously described tests involving the jaws, the motion investigated is not a translation but a rotation. Unfortunately it is not simple to take a profile or any dose measurement along a circle, therefore special strategies were developed in order to implement quality assurance tests of the dynamic collimator rotation. The primary intention was to use existing measuring equipment. As a result, the array of diodes was positioned such that the irradiated area can be uniquely related to the collimator angle. This was implemented by having the jaws defining an asymmetric rectangular field with the line of dosimeters placed perpendicular to the y-jaw axes away from the central axis, as illustrated in figure B.2.1. As a result, the irradiated area on the linear diode array will change non-linearly with rotation of the collimator. The length of the rectangular field and the distance of the array of diodes from the isocenter has to be adjusted to produce a sufficient displacement of the irradiated area between the smallest and largest collimator angle. A film can also be used for this experiment instead of an array of diodes since similar results would be obtained.

Because of the non-linear relationship of the collimator speed and the motion of the irradiated area on the line of detectors, the measured profile will not be flat. In previous experiments to test the speed and the effect of acceleration in dynamic beam delivery, flat open beam profiles were compared with the profiles obtained with dynamic beam delivery. In this case, the profile obtained with dynamic beam delivery is associated with several other profiles obtained in a similar manner, giving an indirect verification of the reproducibility of the dynamic collimator rotation.

The speed of rotation of the collimator is slow enough to impose a practical limit to the change of angle for a given test, especially when the collimator angle varies between two positions as in test 1 of appendix B.2. In principle, these tests could have been done with angular variation of 180°, however the time to complete the experiment can be over 30 minutes. Hence the collimator angle was changed between 170° and 190°. When a file for dynamic treatment is loaded at the console of the linac, the accelerator computer calculates an approximate time of treatment that is taken, with a margin, as a limit of exposure time. This limiting time can be used to judge if the intended experiment is practical or not.

As was done with the MLC and the dynamic jaws, the accuracy of the position should be measured for the dynamic collimator rotation. The strategy used is to dynamically rotate the collimator without radiation for most of the treatment. Since there is no beam, by default the speed of rotation is at its maximum speed. Every 20°, the beam is turned on briefly exposing a film (Kodak TL) with a narrow asymmetric rectangular field resulting in a small dark line on the developed film every 20°. The intention is to have the beam present for a short period of time without altering the speed of rotation of the collimator. Hence, the beam is turned on for 2° arc giving a dose of 2 MU at a dose rate of 400 MU/min. As a result, the speed of rotation is limiting the process and not the dose delivery such that the collimator will rotate at its maximum speed with and without the presence of radiation in order to deliver the dose intensity in the least time possible. On the developed film, the position of the narrow dark lines can be measured with a protractor and compared to the intended position, given that the isocenter has been marked on the film.

6.10 Verification of dynamic rotation of gantry under DBD toolbox control.

In appendix B.3, four tests are described that verify the accuracy of the gantry rotation when the angle of the gantry is changed by the DBD toolbox[23]. These tests (as for the MLC, the jaws and the collimator rotation) examine the positional reproducibility, the ability to rotate the gantry with a constant speed, the effect of acceleration, and the positional accuracy. Because the linac used is isocentrically mounted, a detector placed at the isocenter will see little change when the angle of the gantry changes. But when the line of detectors is placed above the isocenter but still on the plane of the isocenter, as illustrated in figure B.3.1, the irradiated area can be related to the gantry angle by equation a.1 in appendix B.3. This approach gives an indirect way with which to measure the gantry angle using existing equipment such that the tests described in appendix B.3 could easily be part of a quality assurance program.

As with the dynamic rotation of the collimator, the profile measured with the gantry moving at a constant speed will not be flat due to the non-linear relationship between the speed of rotation and the motion of the irradiated area on the array of diodes. However, as before, an indirect measure of the reproducibility of the gantry angular velocity can be obtained. The effect of acceleration is investigated by the comparison of profiles obtained with and without interruptions in the dose delivery as explained in test 3 of appendix B.3.

To finish, as described in test 4 of appendix B.3, the positional accuracy of the gantry is measured using the same strategy as for the dynamic collimator rotation. The gantry is made to rotate at its maximum speed without radiation and the beam is turned on every 10° for 2° exposing a fast film to 2 MU increments. As for the dynamic rotation of the collimator, the speed of rotation of the gantry is kept at its maximum when the beam is turned on by selecting a high dose rate such that the process is always limited by the gantry rotation speed and not dose rate limitations. Once developed, a series of narrow lines can be seen on the film. The position of the lines relative to the central axis previously marked on the film can be related to the gantry angle by equation a.1 in appendix B.3. These angles should be the same as the intended gantry angle in the file used to control the dynamic beam delivery.

6.11 Summary.

In this chapter, tests to verify the MLC system used to create an intensity modulated field using the step and shoot and the continuous motion method have been described together with the axes that can be moved under the control of the DBD toolbox. The step and shoot technique is a relatively simple extension of the MLC used to replace custom shaped cerrobend blocks. The only real difference is the completely automated placement of the leaves. However the concern of the dose non-linearity at low MU settings has been introduced and the clinical implications are discussed in chapter 7. Additional tests required for the MLC system in the completely dynamic mode have also been described. The speed stability of the leaves and the effect of their acceleration is examined. For the last test on the MLC, a strategy to check the positional accuracy of the leaf during a dynamic beam delivery is introduced. Finally, tests done on the MLC have been repeated, with some modifications in certain cases, on the axes that can be controlled by the DBD toolbox (*i.e.* the four jaws, the collimator rotation, and the gantry rotation).

6.12 References.

1. S.V. Spirou, S.C. Chen, "Generation of arbitrary intensity profiles by dynamic jaws or multileaf collimators", Med. Phys. **21**(7), 1031-1041 (1994).

2. P. Källman, B. Lind, A. Eklöf, A. Brahme, "Shaping of arbitrary dose distributions by dynamic multileaf collimator", Phys. Med. Biol. **33** (11) 1191-1300 (1988).

3. C.X. Yu, M.J. Symons, M.N. Du, A.A. Martinez, J.W. Wong, "A method for implementing dynamic photon beam intensity modulation using independent jaws and a multileaf collimator", Phys. Med. Biol. **40**, 769-787 (1995).

4. R. Svensson, P. Källman, A. Brahme, "An analytical solution for the dynamic control of multileaf collimators", Phys. Med. Biol. **39** 37-41 (1994).

5. J. Stein, T. Bortfeld, B. Dörschel, W. Schlegel, "Dynamic X-ray compensation for conformal radiotherapy by means of multi-leaf collimator", Radiother. and Oncol. **32**, 163-173 (1994).

6. C.S. Chui, T. LoSasso, S. Spirou, "Dose calculation for photon beams with intensity modulation generated by dynamic jaw or multileaf collimations", Med. Phys. **21** (8), 1237-1244 (1994).

7. P. Xia, L.J. Verhey, "Multileaf collimator leaf sequencing algorithm for intensity modulated beams with multiple static segments", Med. Phys. **25** (8), 1424-1434 (1998).

8. E.E. Klein, D.A. Low, A.S. Meigooni, J.A. Purdy, "Dosimetry and clinical implementation of dynamic wedge", Int. J. Radiat. Oncol., Biol., Phys. **31**(3), 583-592 (1995).

9. D. P. Barry, *Dynamic Wedge Dosimetry on a Dual Energy Linear Accelerator*, M. Sc. Thesis, McGill University, Montreal, Canada, 1997.

10. T.C. Zhu, L. Ding. C.R. Liu, J.R. Palta, "Performance evaluation of a diode array for enhanced dynamic wedge dosimetry", Med. Phys. **24**(7) 1173-1180 (1997).

11. H.H. Liu, E.P. Lief, E.C. McCullough, "Measuring dose distribution for enhanced dynamic wedges using a multichamber detector array", Med. Phys. **27**(9), 1515-1519 (1997).

12. P.K. Kijewski, L.M. Chin, B.D. Bjarngard, "Wedge-shaped dose distributions by computer-controlled collimator motion", Med. Phys. **5**, 426-429 (1978).

13. A.V. Thompson,K.L. Lam, J.M. Balter, D.L. McShan, M.K. Martel, T.A. Weaver, B.A. Fraass, R.K Ten Haken, "Mechanical and dosimetric quality control for computer controlled radiotherapy treatment equipment", Med. Phys. **22**(5):563-6, (1995).

14. I.J. Das, K.R. Kase, V.M. Tello, "Dosimetric accuracy at low monitor unit settings", Br. J. Radiol. **64**, 808-811 (1991).

15. I.J. Indra, J.C. Harrington, S.F. Akber, A.F. Tomer, J.C. Murray, CW Cheng, "Dosimetric problems at low monitor unit settings for scanned and scattering foil electron beams", Med. Phys. **21**(6), 821-826 (1994).

16. R.J. Barish, R.C. Fleischman, Y.M. Pipman, "Teletherapy beam characteristics: The first second", Med. Phys. **14**(4), 657-661 (1987).

17. J.L. Humm, A.L. Larsson, E.P. Lief, "Dosimetric properties of a scanned beam microtron at low monitor unit settings: Importance for conformal therapy", Med. Phys. **23**(3), 329-335 (1996).

18. R. Rajapakshe, S. Shalev, "Output stability of a linear accelerator during the first three seconds", Med. Phys. **23**(4), 517-519 (1996).

19. M. Buchgeister, F. Nüsslin, "Startup performance of a traveling wave versus standing wave linear accelerator", Med. Phys. **25**(4), 493-495 (1998).

20. A. Curtin-Savard, *Dose delivery uncertainty in photon beam radiotherapy*, M. Sc. Thesis, McGill University, Montreal, Canada, 1995.

21. American Association of Physicists in Medicine. RTC Task Group 21. "A protocol for the determination of absorbed dose from high energy photon and electron beams". Med. Phys. **10**, 714 (1983).

22. CC Chui, S. Spirou, T. LoSasso, "Testing of dynamic multileaf collimator", Med. Phys. **23**(5), 635-641 (1996).

23. *Dynamic beam delivery (DBD) toolbox, Engineering reference manual*, Varian Associates, Palo Alto, California, version 5.1.00.

RESULTS AND DISCUSSION

Several quality assurance tests for the multileaf collimator and the dynamic beam delivery toolbox have been described in chapter 5 and 6 and in the appendices. The results and a discussion of these experiments are presented here.

7.1 Output factor.

As presented in section 5.1, measurements have been performed to verify that the output factor is accurately predicted by equation 5.1 when the MLC is used to replace custom cerrobend blocks. As a first step, the collimator factor (CF) has been measured for the 6 MV beam of the Clinac 2300 C/D for fields defined by the jaws, and is presented in figure 7.1. Each data point is the average of few readings, however the collected charge was very stable from one experiment to the next resulting in very small error bars that would fit within the data point.

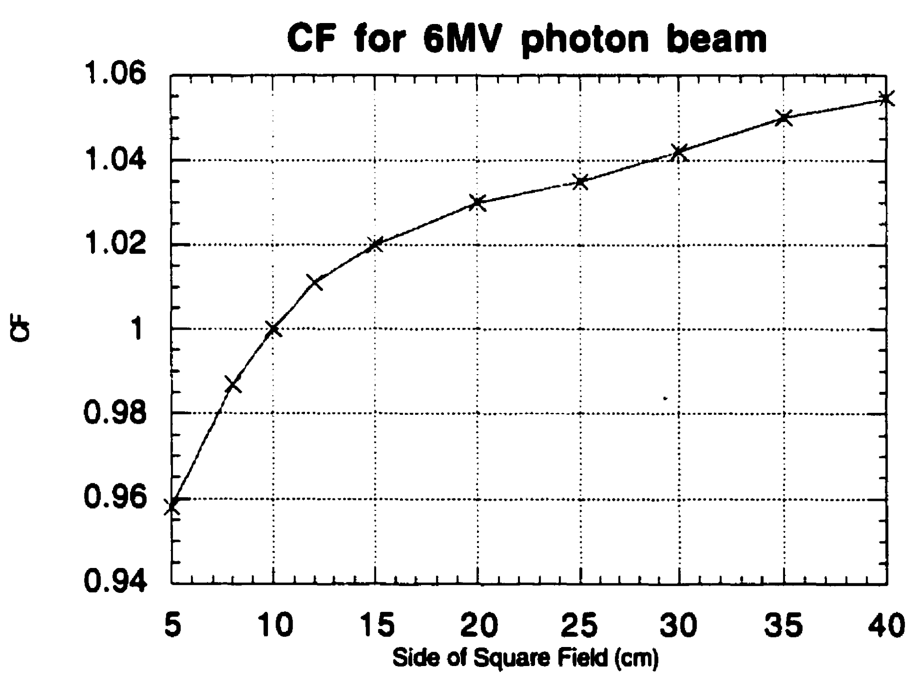

Figure 7.1 Collimator factor (CF) measured for the 6 MV beam of the Clinac 2300 C/D as a function of square field size as defined by the jaws.

The second step is the measurement of the relative dose factor (RDF) as a function of MLC field size for several fixed jaw settings. The results are presented in figure 7.2. As for fields shaped with custom blocks, the RDF for a given MLC field size depends on the jaw settings as shown in figure 7.2. Again the data points are the results of the average of a few stable measurements giving "invisible" error bars. Usually, RDF are 1.0 for a 10x10 cm^2 field, or 100 cm^2, by definition. However in figure 7.2, the area indicated is for the MLC field while the charge collected was normalized to 1.0 for a 10x10 cm^2 field defined by the jaws, explaining that the curves of figure 7.2 do not pass through 1 at 100 cm^2.

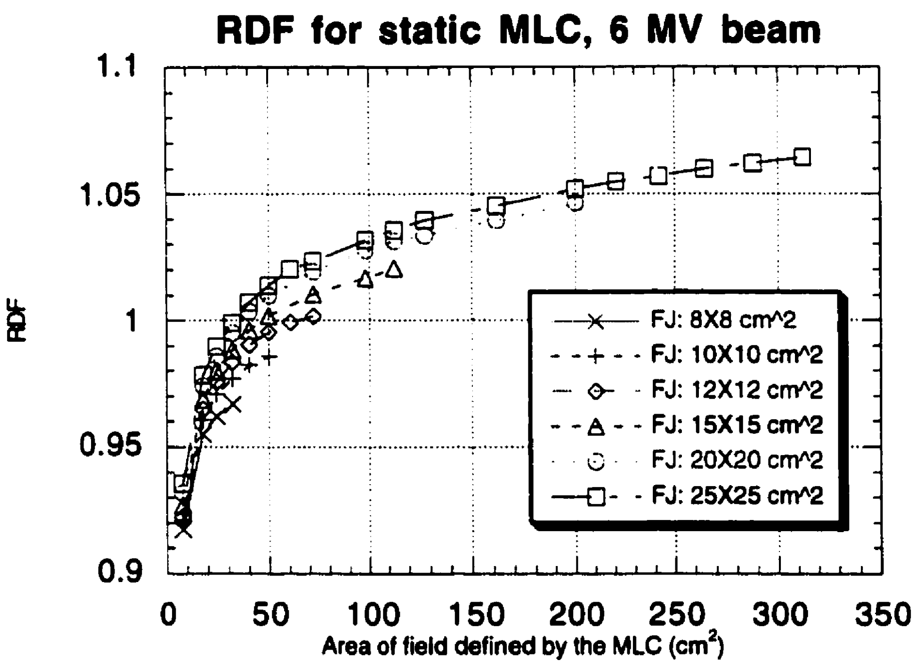

Figure 7.2 Relative dose factor (RDF) as a function of equivalent square field as defined by the MLC inside a fixed jaw positions ranging from 8x8 to 25x25 cm^2.

From the results presented in figure 7.1 and 7.2 and equation 5.1, the scatter factor (SF) of the MLC field can be calculated by dividing the RDF by the CF for a given field size. If the conventional method to calculate the output factor for blocked fields applies when the MLC is used to shape irregular fields, the calculated SF will be independent of the jaw setting and every resulting SF curve will be the same.

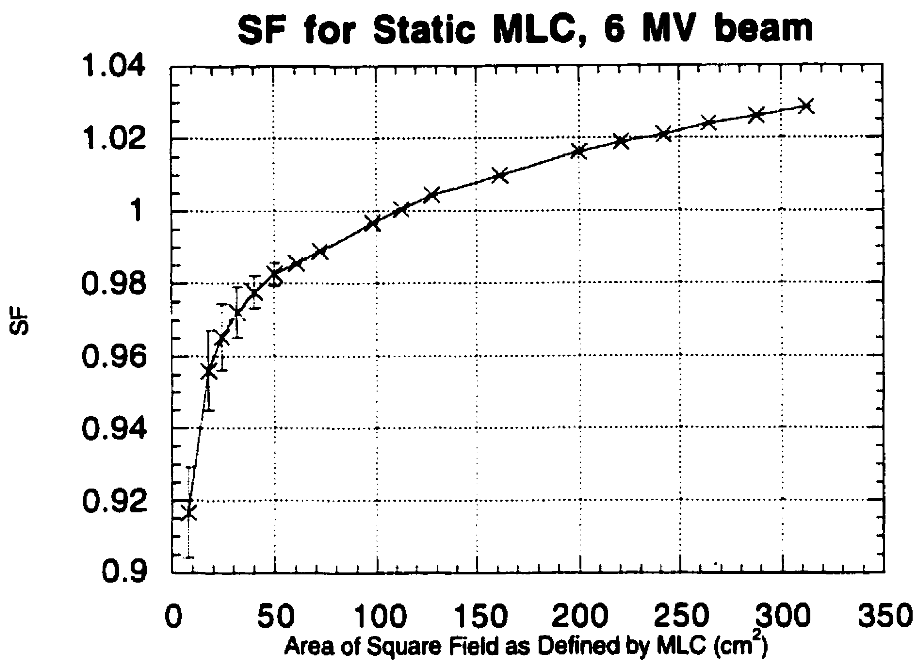

Figure 7.3 Scatter factor (SF) as a function of the field area defined by the MLC obtained using the results of figure 7.1 and 7.2 and equation 5.1. The error bars indicate the maximum discrepancies between SF obtained with different square field settings.

Figure 7.3 gives the resulting average SF curve. The error bars were obtained by taking the greatest discrepancy from the average value for a given area of a field. Hence error bars smaller than 2% indicate that equation 5.1 can be applied when the MLC system studied is used to replace custom blocks. Apart from the SF for the smallest field, which has a spread just above 2%, the SF's calculated are well within 2% confirming that the conventional method of calculating the output factor can be used with the MLC. However, very small MLC fields inside relatively large jaw settings must be used with caution. Similar results have been noted for the 18 MV beam.

7.2 Percentage depth dose.

The percentage depth dose (PDD) was measured for square field sizes as defined by the jaws and by the MLC (the jaws retracted at 25x30 cm2) for both the 6 and 18 MV photon energies. The goal was to verify that the PDD's used normally, involving the jaws, can still be used when the MLC is used to define the radiation field. Clinically, the two PDD's measured for a given field size need to be within 2% to be considered the same[1]. Figure 7.4 shows a series of graphs giving PDD's for a range of fields going from 4x4 to 24x24 cm^2 for the 6 MV beam. Each graph includes the curves obtained when the jaws and the MLC were defining the given field size. Figure 7.5 shows the PDD's for the 18 MV beam.

Small differences between the PDD's are expected because of the change in the scatter radiation component when the field is defined by another means. However it is expected that these changes will be insignificant for most clinical applications. From figure 7.4 and 7.5, it is observed that the curves involving the jaws and the MLC are most often within 1% of each other and never more than 2% apart. Greater discrepancies are obtained with the larger field sizes, confirming that the main difference is due to an increase in scatter radiation. The differences between the PDD's with the jaws and the MLC are less important with the higher photon energy as seen in figure 7.5.

Even though small differences are observable between the PDD's obtained with the jaws and the MLC, they are insignificant in practice such that the PDD usually used to calculate the dose delivered in a phantom can be used even when the MLC is shaping the field or part of the field.

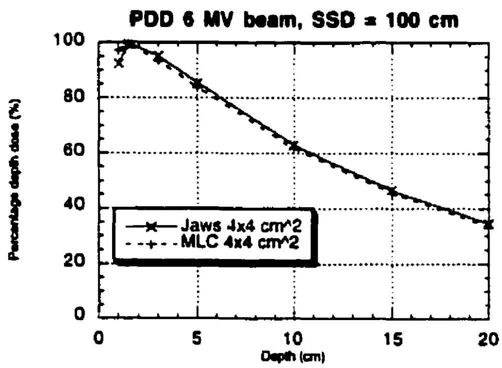

(a)

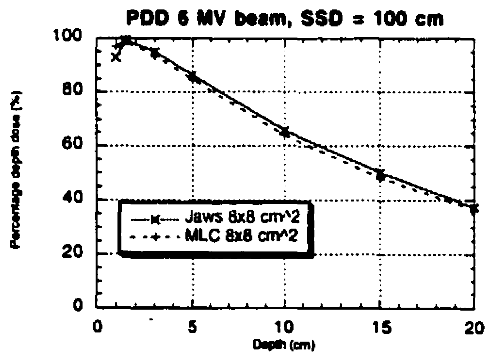

(b)

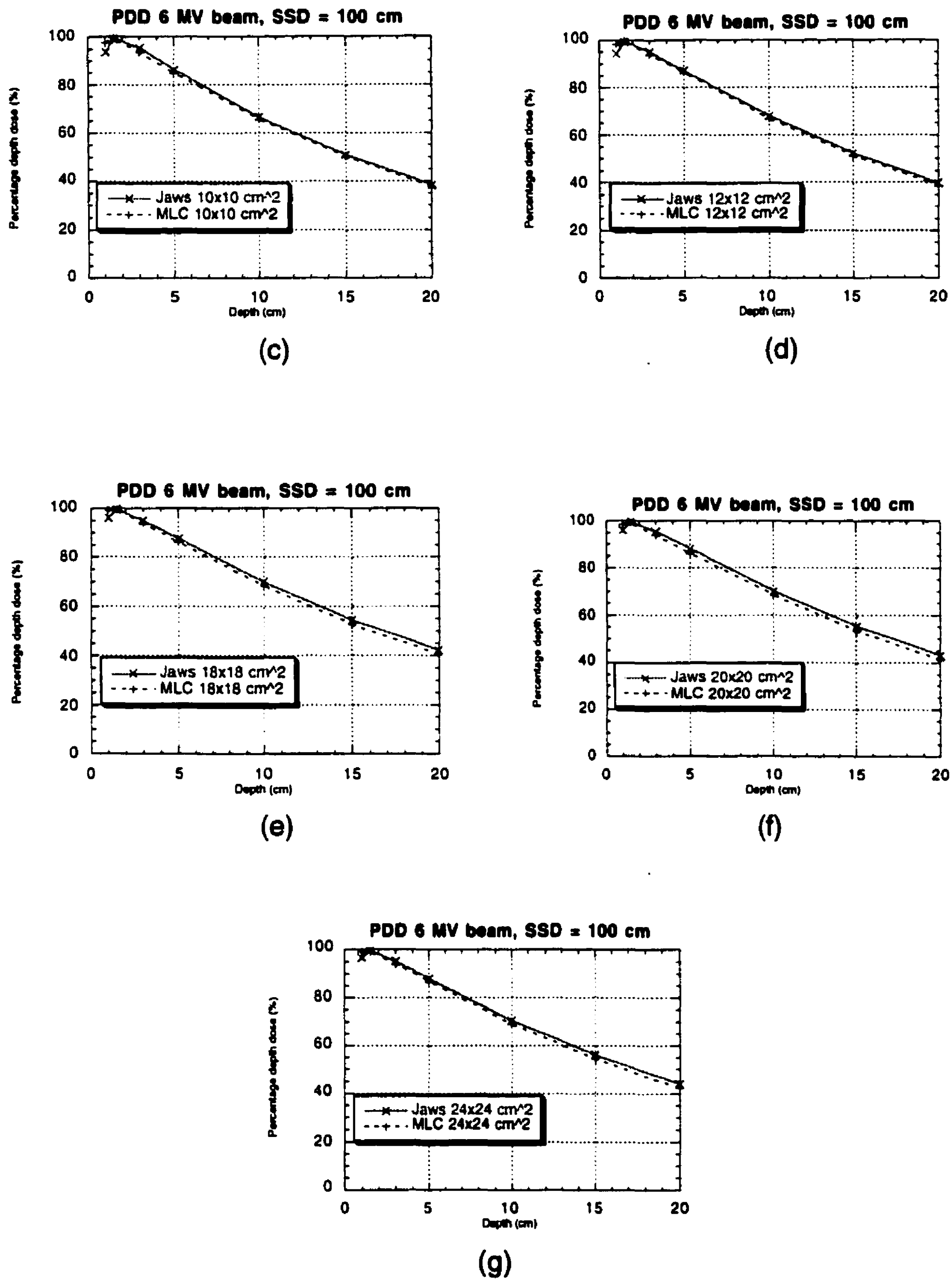

Figure 7.4 Percentage depth dose (PDD) curves for the 6 MV beam for radiation fields defined by the jaws and the MLC for a range of field sizes: (a) 4x4 cm^2, (b) 8x8 cm^2, (c) 10x10 cm^2, (d) 12x12 cm^2, (e) 18x18 cm^2, (f) 20x20 cm^2, (g) 24x24 cm^2.

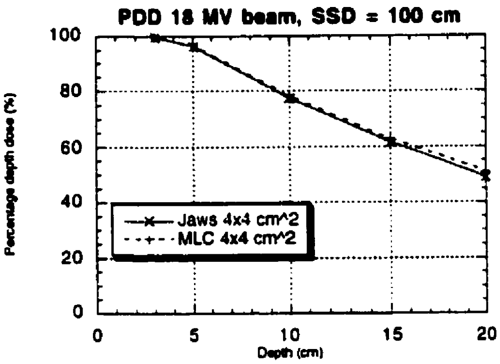
PDD 18 MV beam, SSD = 100 cm
Percentage depth dose (%)
Depth (cm)
Jaws 4x4 cm^2
MLC 4x4 cm^2

(a)

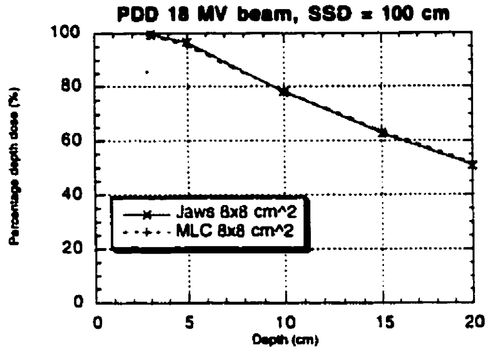
PDD 18 MV beam, SSD = 100 cm
Percentage depth dose (%)
Depth (cm)
Jaws 8x8 cm^2
MLC 8x8 cm^2

(b)

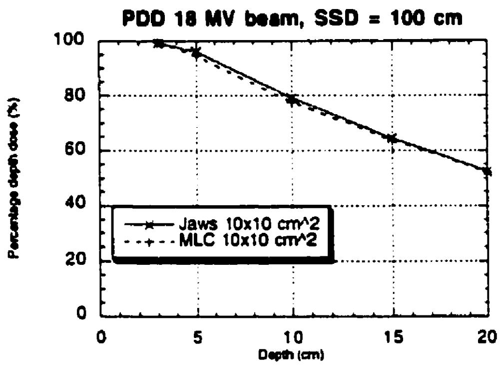
PDD 18 MV beam, SSD = 100 cm
Percentage depth dose (%)
Depth (cm)
Jaws 10x10 cm^2
MLC 10x10 cm^2

(c)

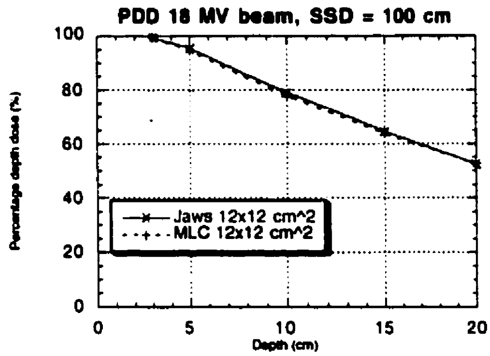
PDD 18 MV beam, SSD = 100 cm
Percentage depth dose (%)
Depth (cm)
Jaws 12x12 cm^2
MLC 12x12 cm^2

(d)

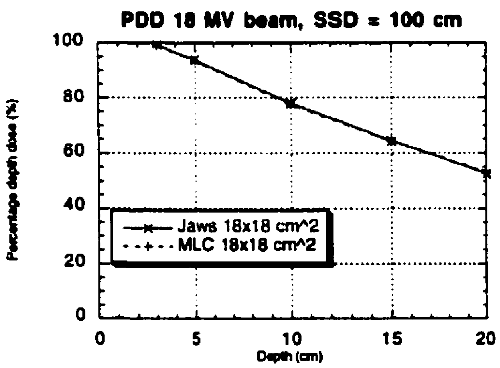
PDD 18 MV beam, SSD = 100 cm
Percentage depth dose (%)
Depth (cm)
Jaws 18x18 cm^2
MLC 18x18 cm^2

(e)

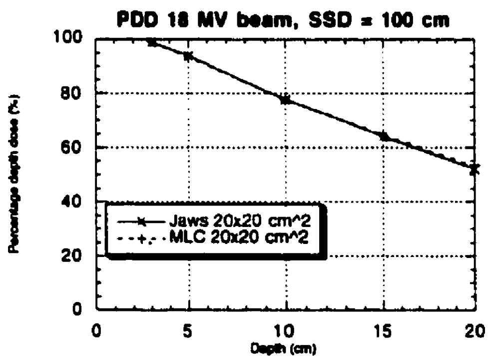
PDD 18 MV beam, SSD = 100 cm
Percentage depth dose (%)
Depth (cm)
Jaws 20x20 cm^2
MLC 20x20 cm^2

(f)

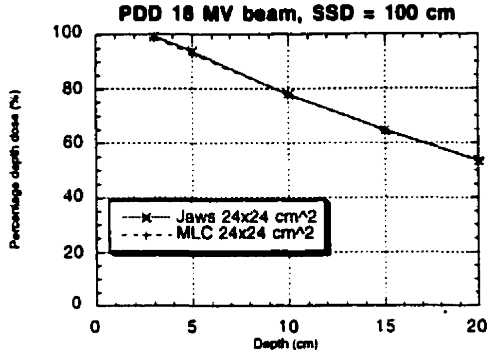

(g)

Figure 7.5 Percentage depth dose (PDD) curves for the 18 MV beam for radiation fields defined by the jaws and the MLC for a range of field sizes: (a) 4x4 cm^2, (b) 8x8 cm^2, (c) 10x10 cm^2, (d) 12x12 cm^2, (e) 18x18 cm^2, (f) 20x20 cm^2, (g) 24x24 cm^2.

7.3 Penumbra.

As described in section 5.3, the penumbra of the MLC has been compared to the penumbra of the secondary collimators as a function of field size[2-5]. In figure 7.6, the measured penumbra for the 6 MV beam are reported, while the results for the 18 MV beam are in figure 7.8.

From the measurements of the penumbra of the side of the leaves reported in figure 7.6 a and c, it can be seen that the penumbra for the MLC may be smaller than the penumbra of the jaws. Even though this observation has been reported in the literature[6], it is surprising since larger penumbra for the MLC is expected. Moreover the smaller penumbra for the MLC is only measured with the 6 MV beam. The smaller penumbra from the MLC could be due to the MLC being closer to the patient than the secondary collimators reducing the geometric penumbra.

Of particular interest is the difference between the penumbra of the MLC and the corresponding jaw. For the 6 MV beam, the mean difference for all field sizes is 0.96 mm larger for the MLC in the direction of motion of the leaves at the depth of dose maximum at the isocenter, as shown in figure 7.6b. For the side of the leaves at d_{max}, the mean difference measured between the penumbra of the

MLC and the jaws is 0.09 mm greater for the MLC, as shown in figure 7.6a. At a depth of 10 cm, the mean difference in the penumbra is 1.6 mm larger for the leaf end and 0.13 cm for the leaf side as compared to their corresponding jaws, as shown in figure 7.6 d and c respectively.

The mean differences in penumbra between the MLC and the secondary collimators have also been measured for the 18 MV beam. At the depth of dose maximum, on average the penumbra is larger for the MLC by 2.4 mm in the direction of motion of the leaves and larger by 1.5 mm from the side of the leaves. At the depth of 10 cm, the mean differences in penumbra grow to 2.7 mm at the leaves end and 2.1 mm at the leaves side. Other investigators have reported similar results[6].

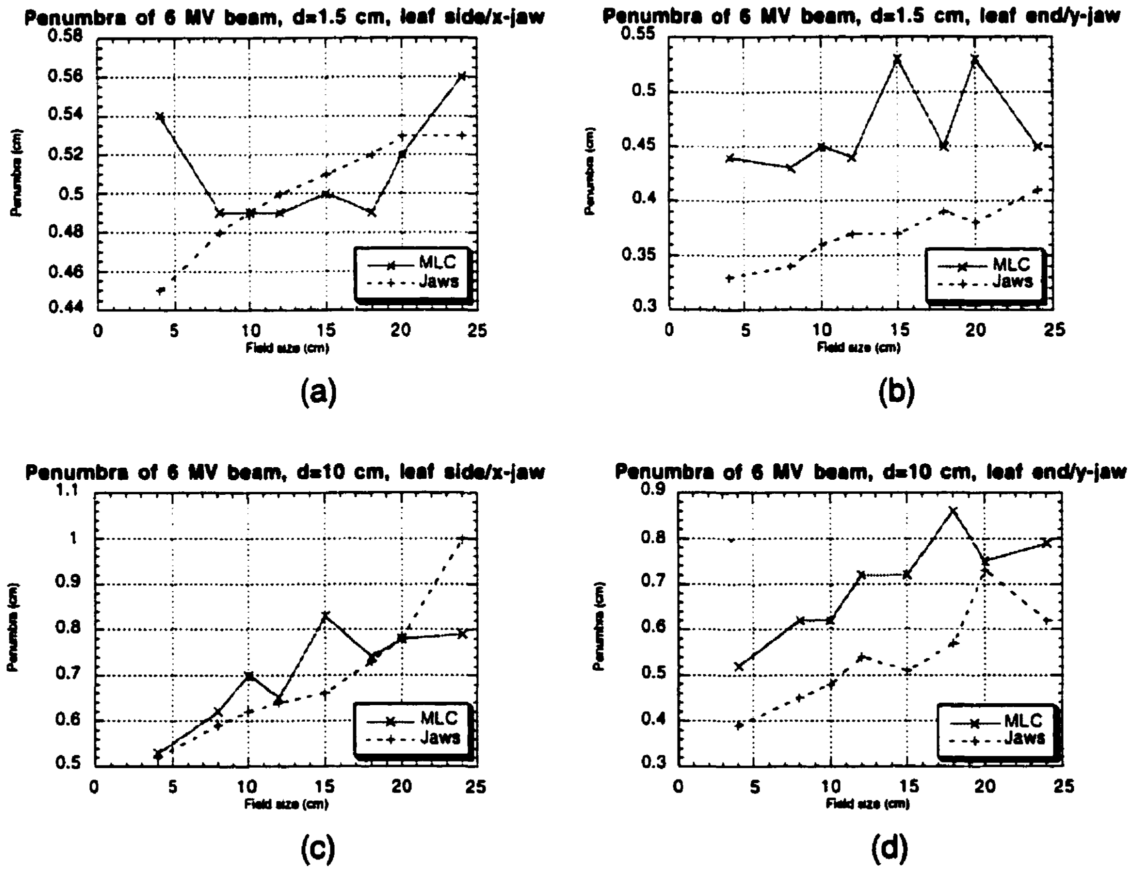

Figure 7.6 Penumbra of the MLC compared to the penumbra of the appropriate jaw exposed to the 6 MV beam as a function of field size.

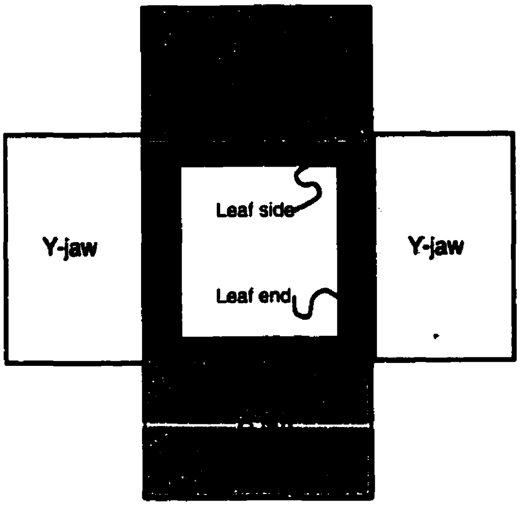

Figure 7.7 Diagram of the position of the MLC leaves relative to the secondary collimator.

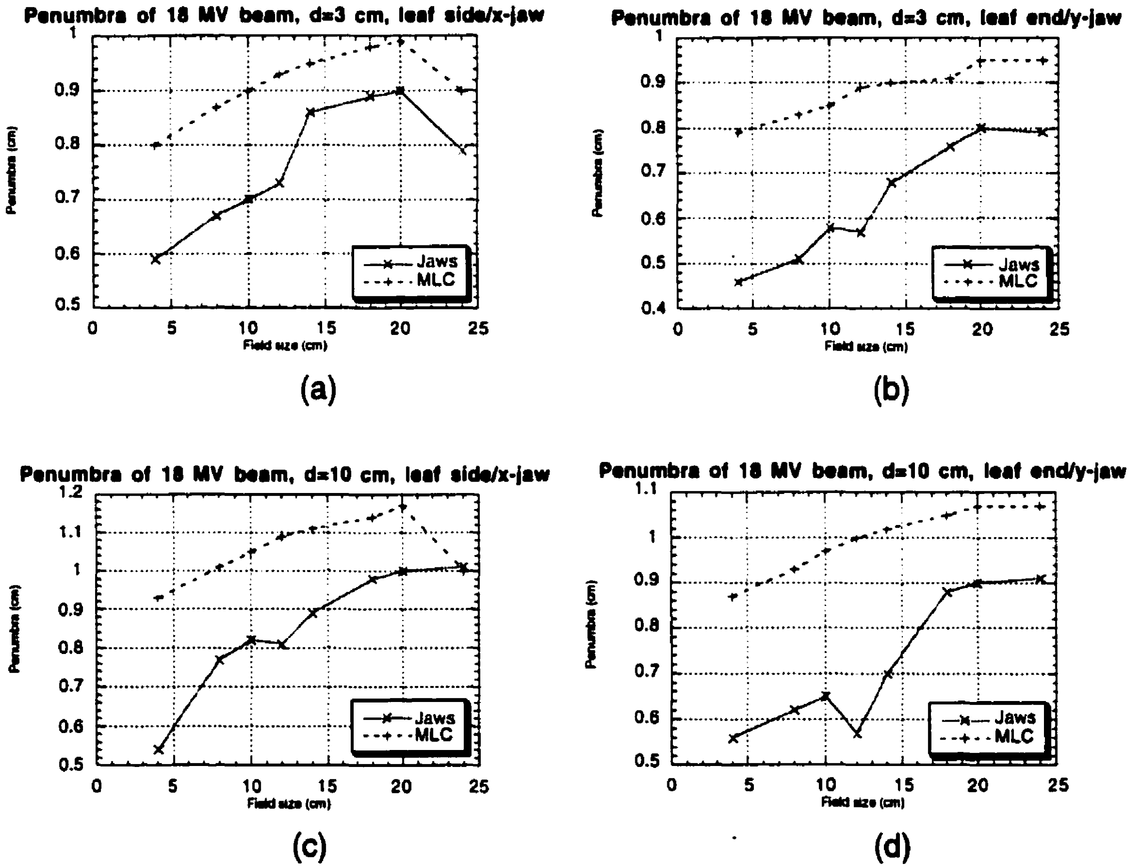

Figure 7.8 Penumbra of the MLC compared to the penumbra of the appropriate jaw exposed to the 18 MV beam as a function of field size.

A series of measurements has been conducted as illustrated in figure 5.2 to verify that the penumbra does not change as a function of the position of the leaf end with respect to the central axis. It was found that no clinically significant change in penumbra could be measured as a function of the leaf end position, as illustrated in figure 7.9.

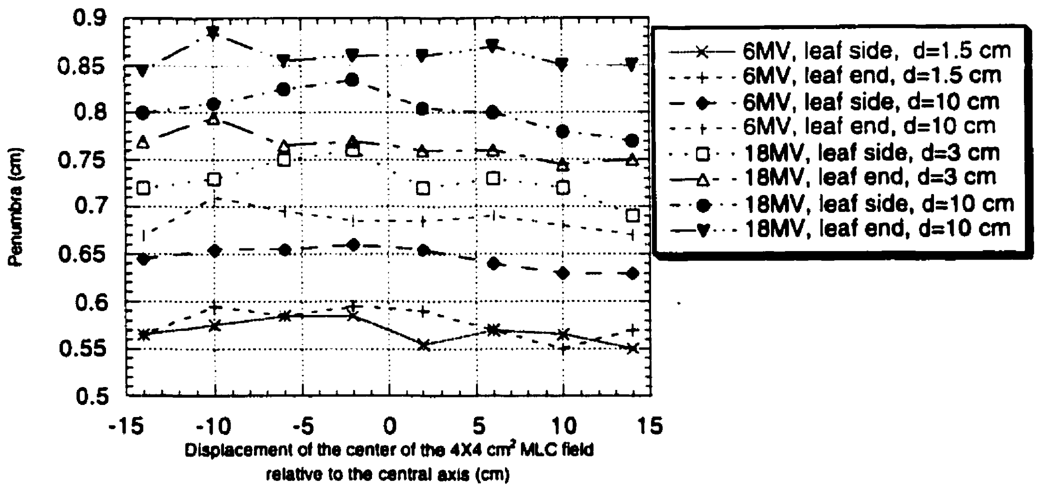

Figure 7.9 Penumbra of the leaf of the MLC when a 4x4 cm^2 MLC field is moved across the possible range of the MLC for the 6 and 18 MV beams at depths of d_{max} and 10 cm.

7.4 Radiation transmission.

The first test on the transmission of radiation through the MLC, consisting of a block of an increasing number of pairs of leaves around the beam central axis as illustrated in figure 5.3, can be used as an indication of the number of adjacent leaves needed to achieve the wanted level of radiation. As seen in figure 7.10, at least three leaves placed side by side are needed in order to bring the dose under the 10% level in the shielded region at the depth of dose maximum for the 6 MV beam. Similar results were seen with the 18 MV beam, but at the higher energy, four adjacent pairs of leaves were needed to bring the dose down to about 10% under the shielded region. The dose under the shielded region is mainly due to lateral transport of dose by scatter radiation when the block is narrow. On the other hand, for wider blocks the dose comes from radiation passing between and through the leaves leaving a constant radiation level as the blocked region gets larger.

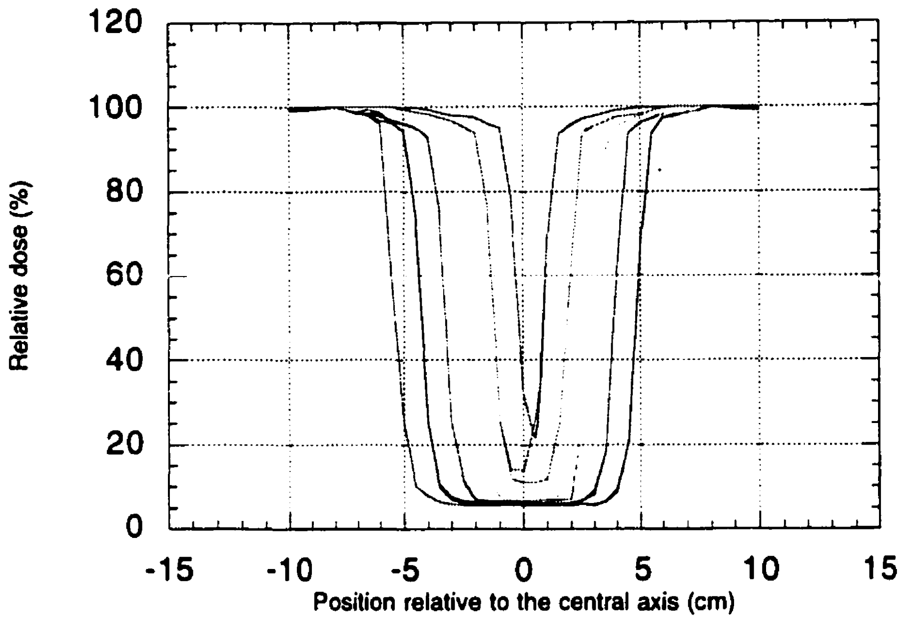

Figure 7.10 Superposition of profiles measured at d_{max} taken under an increasing number of pairs of leaves in an open beam around the beam central axis normalized to a point in the open beam.

The second test for the transmission of radiation through the MLC is meant to be compared with the transmission of the secondary collimators. A profile of an open region defined by the MLC always reveals a wider penumbra and more transmission of radiation than the same open area defined by the jaws. The measured transmission of the MLC with an open area of width 3 cm or more at the isocenter was up to 2.3% higher than the jaws only for both the 6 and 18 MV beams. The measurements were performed at the depth of dose maximum and 10 cm. Both depths lead to about the same surplus of transmission of radiation of the MLC. For open area 1 cm wide, the transmission of radiation through the MLC was measured to be up to 4.6% higher than the jaws for the 6 MV beam and 3.8% higher for the 18 MV beam. The 2 cm gap has an intermediate excess of transmission for the MLC just below 3% for both beam energies.

Other authors[6] have reported a MLC transmission approximately 3% higher as compared with the conventional collimators. This is greater than the measurements done here that indicate 2% more transmission for the MLC. The same authors state transmission for the 18 MV x-rays between 5% and 3.5%

and between 4% and 2.5% for the 6 MV beam which agrees very well with the data collected for the present study.

The last test on the transmission of radiation through the MLC consisted of taking a profile under one pair of leaves in an open beam for the whole range of leaf positions. Each profile was normalized to its maximum dose across the profile. The results are presented in figure 7.11 as a function of the leaf number where the small leaf number is nearer the edge of the field and leaf number 13 is just beside the central axis. The other half of the field gave similar results.

From figure 7.11, it is easily seen that the dose under one pair of leaves is greater toward the central axis or the right of the graph. The dose under one pair of leaves decreases rapidly for leaves close to the beam edge due to the decrease of side scatter, and the fact that they are farther from the source.

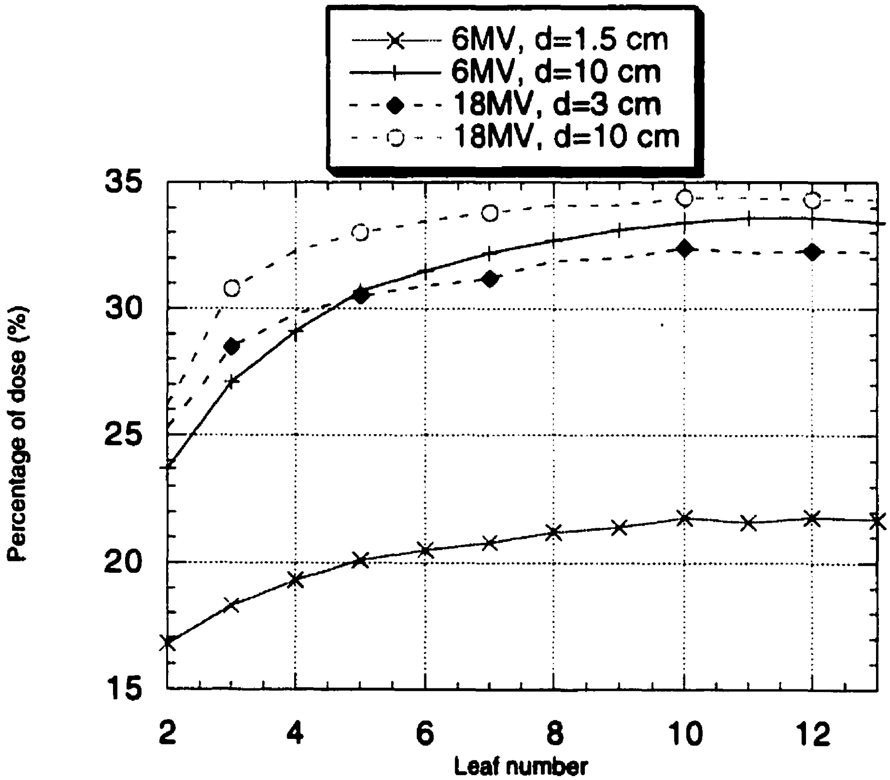

Figure 7.11 Normalized dose under one pair of leaves as a function of the position of the pair of leaves in an open beam. Leaf number 13 corresponds to the leaf just beside the central axis, while leaf number 2 is at the edge of the field.

7.5 Mechanical alignment of the MLC.

As stated in section 5.5, six tests have been conducted to check the mechanical accuracy of the MLC system[7]. The first two; accuracy of leaf position and leaf calibration, are designed to be done regularly to check that the leaf position is within a predetermined tolerance of 0.5 mm for test 1 and 1 mm for test 2 of appendix A.1. For the MLC examined, all leaves were within the margin of the prescribed position for both tests.

For test 3 of appendix A.1, the light field check of the leaf carriage skew relative to the x-jaws, the two carriages have been tested and different, but acceptable, results were observed. When carriage A was tested, a fine but constant line of light could be observed between the leaves and the conventional collimator. However the line was much less than a millimeter wide, causing no problem. For carriage B, no line of light could be seen, but with very careful observation, light passing at the corners of the leaves could be noticed for all leaves confirming good alignment of this MLC carriage.

The film taken for test 4 explained in appendix A.1 is shown in figure 7.12. This test, as for test 3 above, checks the carriage skew but relative to the y-jaw. Figure 7.12 can be correlated to figure A.1.2. The line AB and CD have been measured with a ruler on the film and they were well within 1 mm indicating that carriage B is well aligned with the y-jaws. The same measurements have been done on the film for carriage A confirming that it is not skewed relative to the y-jaws.

Figure 7.12 Film taken for test A.1.4 to check the skew of the MLC relative to the secondary collimator using the radiation field. Line AB and CD should be within 1 mm.

Test 5 and 6 verify the collimator rotation and the MLC carriage sag, both using a star pattern test as can be seen in the irradiated films in figure 7.13 for test 5 and figure 7.14 for test 6. Both tests are explained in appendix A.1. The two star patterns revealed no problem with the MLC assembly since the lines of the star pattern intercept at a single well defined point for both tests. In figure 7.14, the fading strips illustrate that the film was exposed edge-on, measuring the attenuation of the x-ray beam.

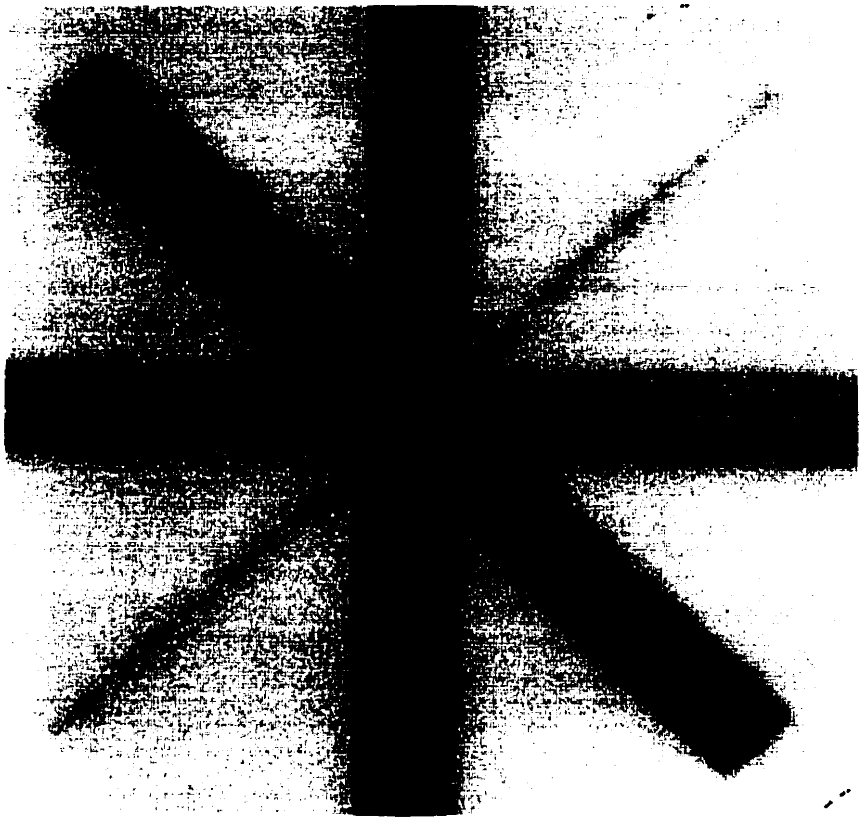

Figure 7.13 Film irradiated for test A.1.5 showing the star pattern used to verify the radiation field center when the collimator is rotated.

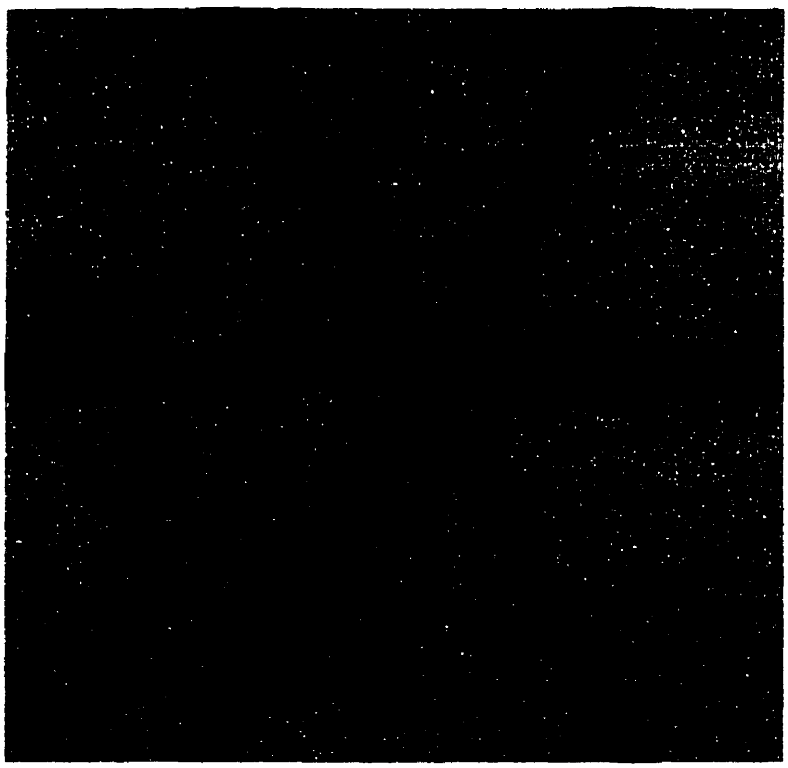

Figure 7.14 Film for test A.1.6 showing another star pattern used to assess the MLC carriage sag when the gantry is rotated.

Results and discussion

7.6 Positional reproducibility of the MLC using the step and shoot technique.

Chapter 6.1 describes two tests conducted to verify the positional reproducibility of the MLC when the step and shoot technique is used. For the first test, the MLC is driven back and forth between two positions 10 times and compared to the same dose delivered to the two positions for a single irradiation. As can be seen from figure 7.15, the two resulting profiles measured with the array of diodes are very similar confirming that the positional reproducibility of the MLC is excellent. In fact, no significant difference was measured in the penumbra of the two profiles. After making sure that the two profiles were normalized at the same point, the percentage dose difference for each measured point was calculated and was never greater than 0.3%. It is a remarkably small difference since it is well smaller than the accepted stability of the diodes of around 1%.

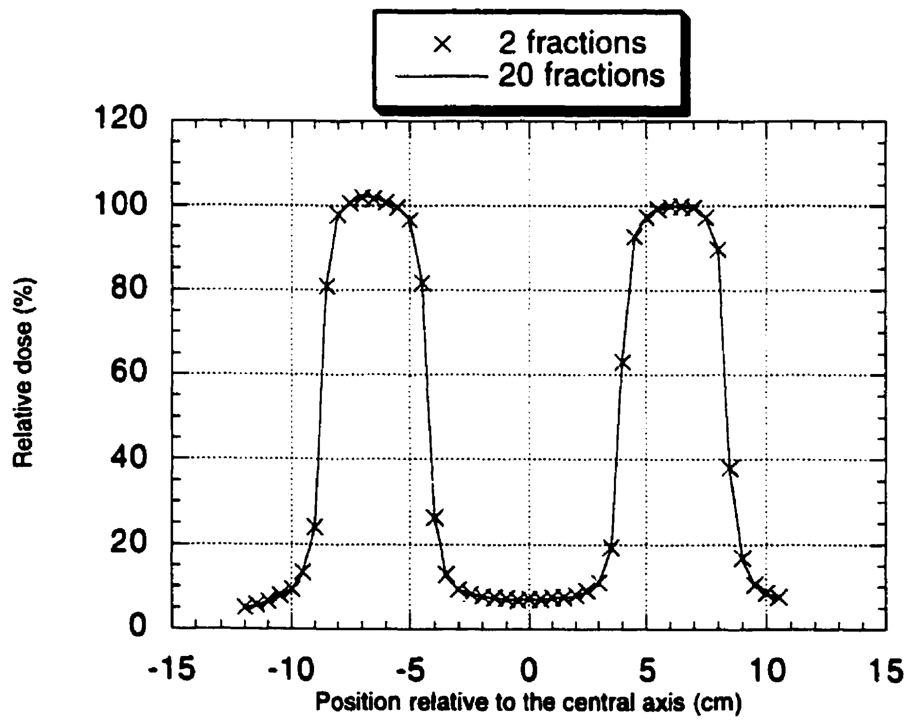

Figure 7.15 Superposition of the two profiles acquired for test 1 of appendix A.2; the positional reproducibility of the MLC (a), showing an almost identical dose deposition for the 20 fractions versus the 2 fractions dose delivery.

For the second test of appendix A.2 (the positional reproducibility of the MLC), the profile measured by the linear diode array is shown in figure 7.16. From test 1 discussed above, the position of the leaves was almost certainly good, but the junctions of the fields can be clearly seen in figure 7.16. While test 1 gave a nearly perfect result, test 2 suggests that the MLC system must be used with caution in the step and shoot technique since junctions with dose close to 10% higher than the dose in the middle of the field were observed. Taking into consideration that the linear diode array has only one diode every 5 mm, the real extent of the hot spots could have been missed. In order to appreciate the junctions when the step and shoot technique is used, a film irradiated with this technique is compared to a film exposed using a continuous motion of the leaves in figure 7.17.

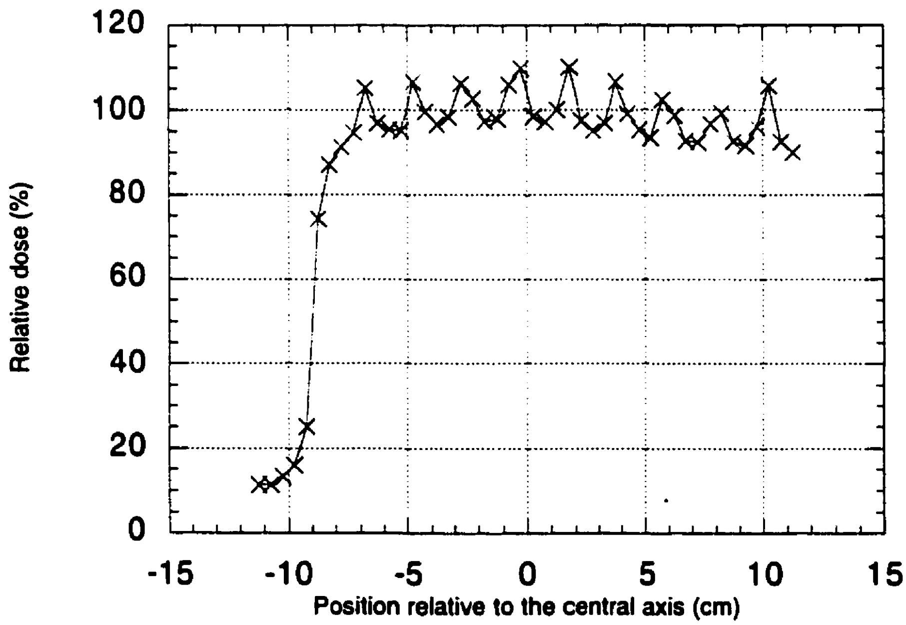

Figure 7.16 Resulting profile as measured by the linear diode array for test 2 of appendix A.2, positional reproducibility of the MLC (b), where the junctions of the fields are clearly seen.

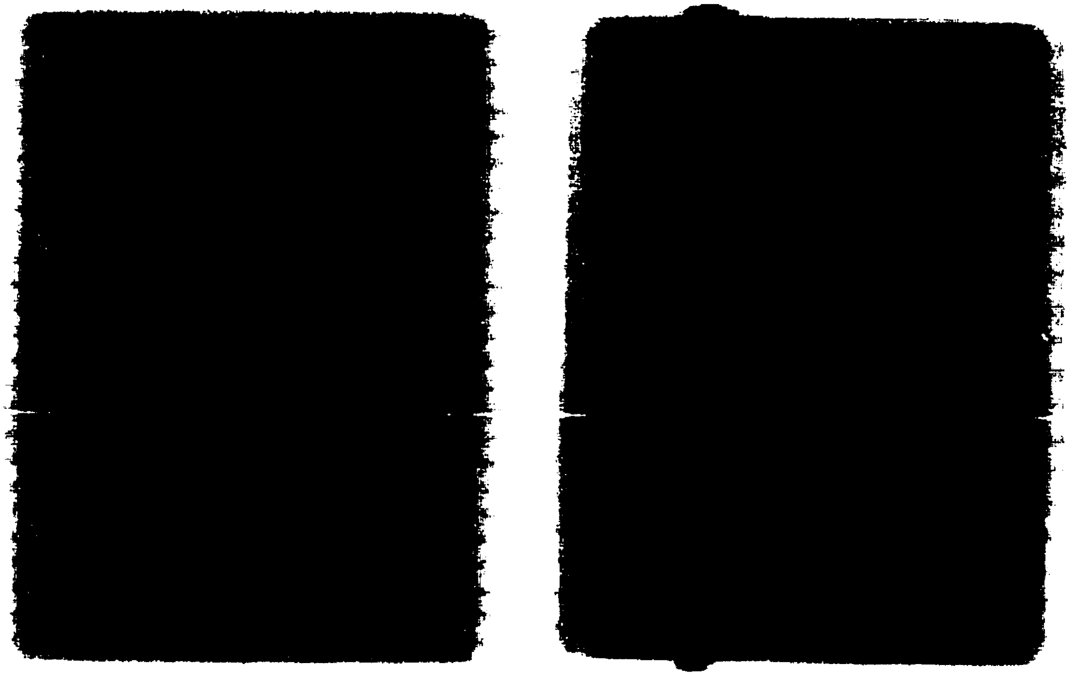

(a) (b)

Figure 7.17 Comparison of a film exposed to a small MLC rectangle in the step and shoot mode in (a) and in the dynamic mode in (b).

7.7 Dose linearity.

The dose linearity of the Clinac 2300 C/D has been first verified by comparing the dose accumulated in an ion chamber with 10 fractions of 1 MU with the dose collected for only one fraction of 10 MU. Because the two readings were significantly different (over 3%) it was concluded that the linac may not be sufficiently linear and further investigations were initiated. As described in section 6.2, the charge per MU was the first experiment conducted[8-10]. The results of charge per MU as a function of MU setting for three different dose rates are shown in figure 7.18 for the 6 MV beam and in figure 7.19 for the 18 MV beam. Both energies gave very similar results except that the 18 MV data are not as smooth as the data for the 6 MV beam.

In practice, when the data are within 2% of each other, they are considered to be the same. Hence from figure 7.18 and 7.19, only extremely small MU settings, less than 3 MU, are of real concern. However, for MU settings below 10 MU, the curve is above 1.00 sufficiently to become significant, such as the case where a few fields exposing a patient for less than 10 MU are used, due to the accumulation of systematic errors.

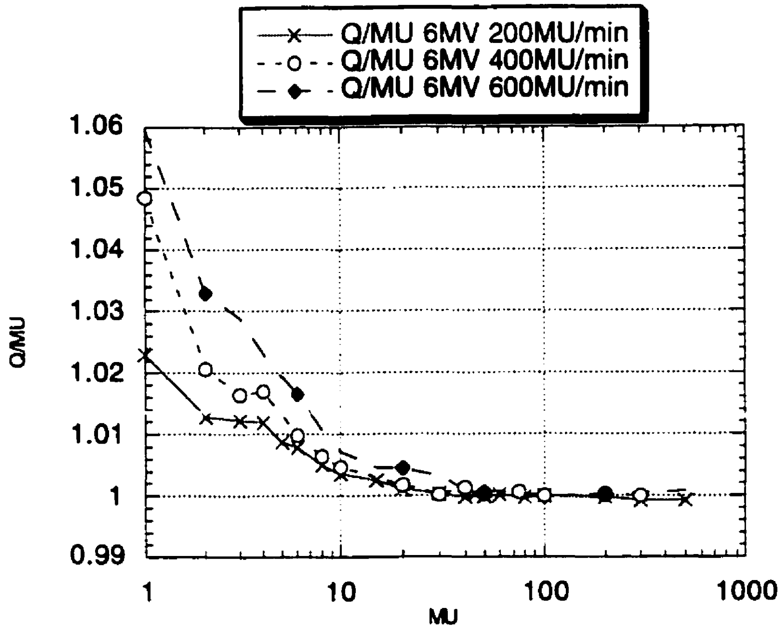

Figure 7.18 Collected charge with an ionization chamber exposed to the 6 MV beam per monitor unit (MU) normalized to 1 at 100 MU as a function of MU for 3 dose rates; 200, 400, and 600 MU/min.

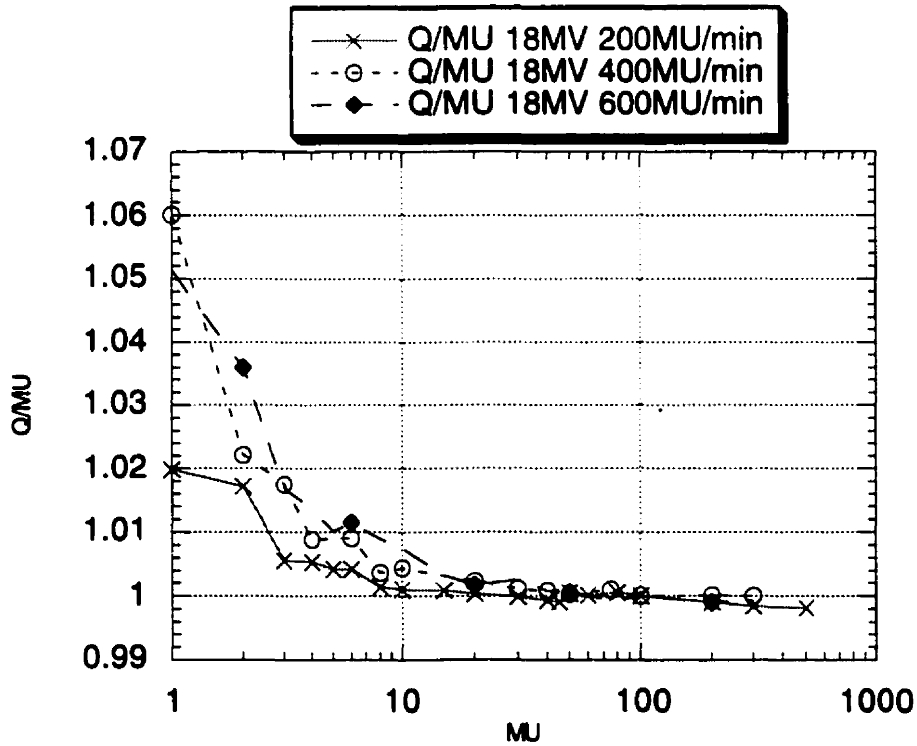

Figure 7.19 Collected charge with an ionization chamber exposed to the 18 MV beam per monitor unit (MU) normalized to 1 at 100 MU as a function of MU for 3 dose rates; 200, 400, and 600 MU/min.

Because there were some concerns about the integrity of the results measured with the ionization chamber, it was not appropriate to conclude that the results shown in figure 7.18 and 7.19 was due to the linac being unstable for the first few seconds. As a result, the same measurements performed with the Clinac 2300 C/D have been repeated with the same detector exposed to a cobalt-60 beam. This experimental set-up has no instability due to the fact that the continuous beam comes from a radioactive source which is always "on" as opposed to a linear accelerator pulsed beam.

The charge collected per unit time when the ion chamber is exposed to the cobalt beam is reported in figure 7.20. As for the curves obtained with the linac beams, the charge per minute is not linear as expected indicating a non-linearity problem with the ion chamber. This finding could explain the non-linearity observed in figure 7.18 and 7.19, but it does not exclude the linear accelerator instability when the beam is turned on as concluded by several investigators[10-12].

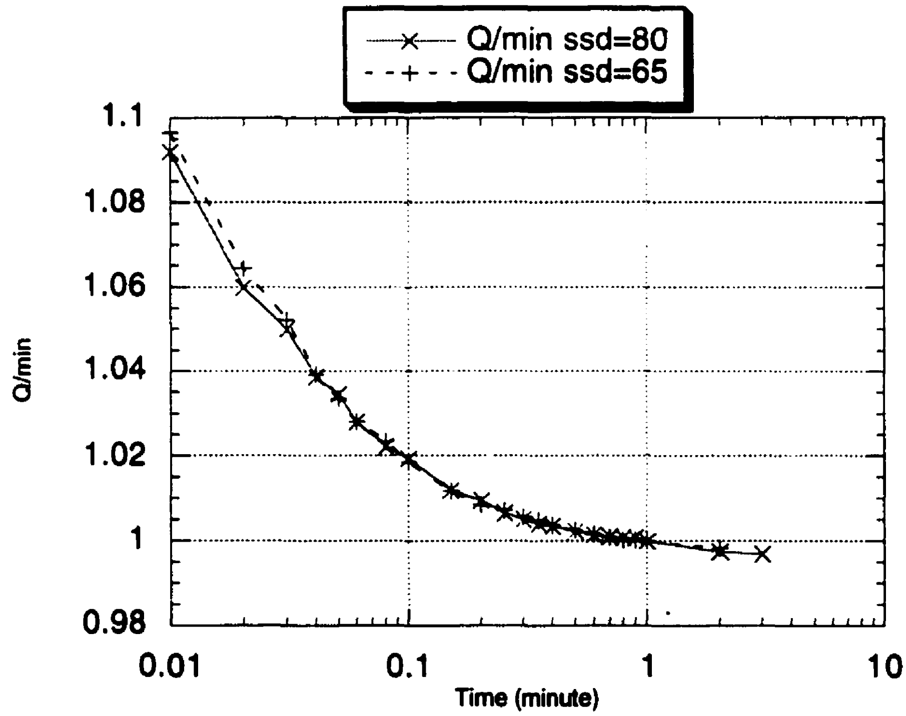

Figure 7.20 Collected charge with an ionization chamber exposed to a cobalt-60 beam per minute normalized to 1 at 1 minute as a function of time for 2 dose rates.

By exposing the ion chamber to the 6 MV beam, an example of the relative current, defined as being 100 for the average current of the steady state signal, as a function of time is reported in figure 7.21. It is clear that when the beam comes on, the measured output is higher than the stable current, when the beam has been on for a relatively long time. These higher currents are not only measured for the first exposure, but every time the beam is interrupted and turned back on, regardless of the period of time without radiation. The current is between 2% and 3% higher for the first few seconds and usually stabilized after around 10 seconds of irradiation. Usually the current in the chamber is more important when the beam has just been turned on after a longer period without radiation than when the beam was off for a short period. Measurements have been performed for other dose rates showing that the time to stabilize the current depends on the dose rate, suggesting that the chamber might need a certain dose to have a stable output.

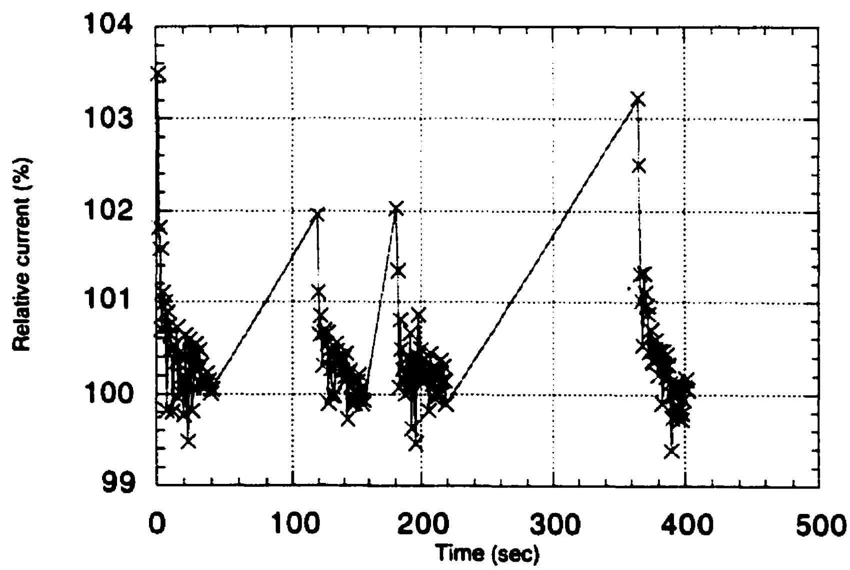

Figure 7.21 Current measured with an ionization chamber as a function of time when exposed to the 6 MV beam interrupted 3 times with a dose rate of 400 MU/min.

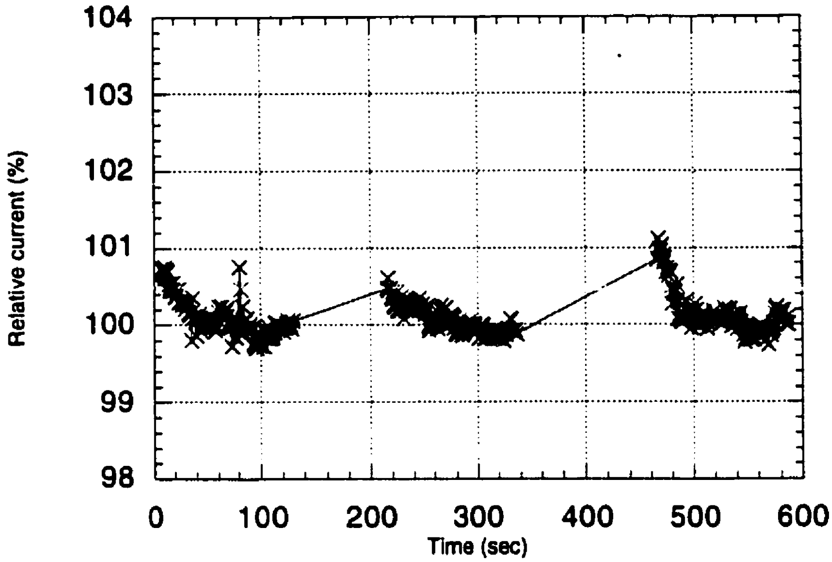

Figure 7.22 Current measured with the ionization chamber as a function of time when exposed to the cobalt beam and interrupted 3 times.

As for the charge per MU curves, the current as a function of time has been measured with the ion chamber in the cobalt beam. The resulting curve is shown in figure 7.22 establishing very similar behavior then when the chamber is exposed to a linac beam. It seems that the time to produce a stable current in the chamber is longer when the radiation is from the cobalt-60 source, possibly related to the dose rate effect observed in the pulsed beam from the linear accelerator. A difference between the measurements in the pulsed beam and the cobalt beam is when the beam is stopped for a short period. In the cobalt beam, when the beam is resumed after a short stop, the current is not higher than the stable current, while the effect was still observed in the linac beam and for relatively long cobalt beam pauses. Since the source travels with a relatively fast speed the current read in the ion chamber is due to a chamber effect and not a source-transit effect.

Because several measurements have been done with an array of diodes for this project, the current as a function of time has been evaluated using a single diode instead of the ionization chamber using the same electrometer. The diode was first exposed to the cobalt beam and the current as a function of time is shown in figure 7.23. This graph shows noisier data than with the ion chamber, but it does not have the higher current effect observed with the chamber. This is true for both short and long pauses of irradiation of the diode indicating that the current is always stable immediately after the beam comes on. Thus the higher current effect observed in the linac beam is due at least in part to the non-linearity of the ion chamber for the first few seconds of exposure.

Curves of accumulated charge per MU have been measured with the linear diode array. The results showed that the array of diodes probably need a small amount of radiation time to start measuring the dose. As a result, the linear diode array was of no use to clarify the dose non-linearity at small MU settings. As with the results of the findings with the cobalt beam, the diode was used to measure the current as a function of time for the 6 MV beam. The current in the diode exposed to the linac beam is very similar to the curves obtained with the ion chamber. This signal is believed to be a measure of the real output of the linac, supported by previous readings collected in the cobalt beam. However, the higher current effect is less important with the diode than with the ion chamber, confirming that the chamber has some non-linear effect. In fact, it was observed that the current curve of the ion chamber tends to be closer to the diode readings when the chamber has already been exposed to a significant dose (more than 1000 MU) and when the chamber has been connected to the high voltage source for a long time without changing the bias voltage (more than one hour).

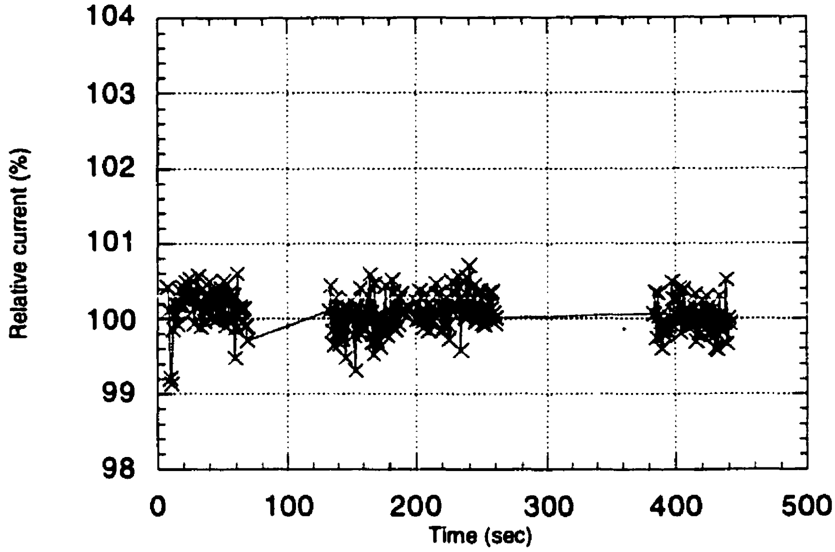

Figure 7.23 Current measured with a single diode as a function of time when exposed to a cobalt-60 beam interrupted 3 times.

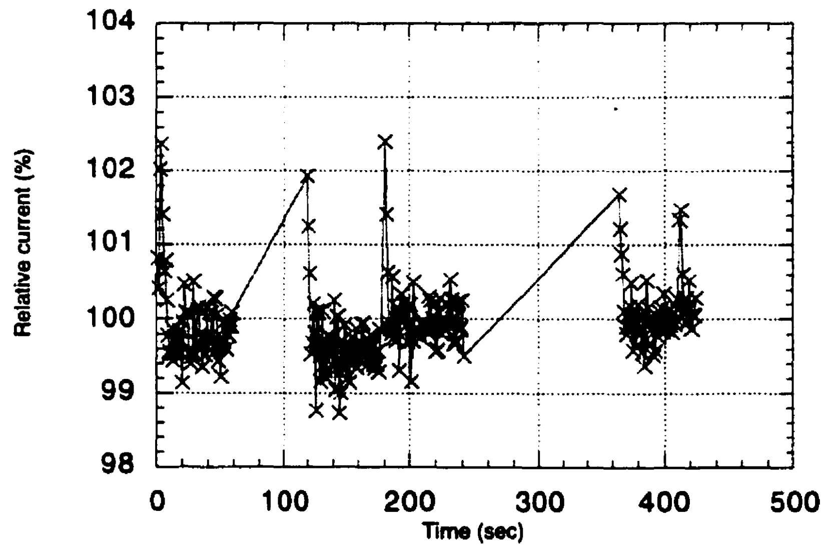

Figure 7.24 Current measured with a single diode as a function of time when exposed to the 6 MV beam at a dose rate of 400 MU/min interrupted 3 times.

The percentage error for the accumulated dose of 100 MU in the 6 MV beam calculated from the integration of the current curves of figure 7.21 and 7.24 is at least 0.3% from the diode reading which is believed to be the real output of the accelerator. From the current readings done with the ion chamber, error in the order of 0.5% has been calculated for an accumulated dose of 100 MU. For doses of less than 5 MU, the error on the dose is believed to be at least 1% when a diode or a stable, "hot", ion chamber is used, but the error can be double for a "cold" ion chamber.

In conclusion, the linac-output has been shown to be non-linear at small MU settings, due in part to the linac instability for the first few second of irradiation as found by other investigators in the past[10-12]. The non-linearity was shown to be due also to the non-linear response of the ionization chamber, especially when it has not been previously exposed to significant dose and connected to the high voltage supply for a long period. Some concerns about the ion chambers used by the linac to monitor its beam can be mentioned since they are the primary input used by the linac to adjust and measure its radiation output. If these ion chambers are unstable for the first few seconds of irradiation, the consequences on the accelerator output are immediate. In consequence, fields with MU settings less than 10 MU should be avoided especially when several low MU fields are to be used in a treatment.

7.8 Stability of the leaf speed.

The stability of the speed of the MLC was examined as described in section 6.4[13]. Typical results are given in figure 7.25 where the profile acquired under the constantly moving pair of leaves using the array of diodes is overlaid on the profile acquired in the same manner but for an open beam. From figure 7.25, the two profiles are almost identical, indicating that the leaves were both moving with a constant speed. In figure 7.26, a zoom of the plateau of figure 7.25 is shown. The curves look noisy, but are identical, the fluctuations being due to the variation of response from one diode to the next which can be in the order of 1%. The slope of the profiles has been eliminated by the adjustment of the linac during routine maintenance.

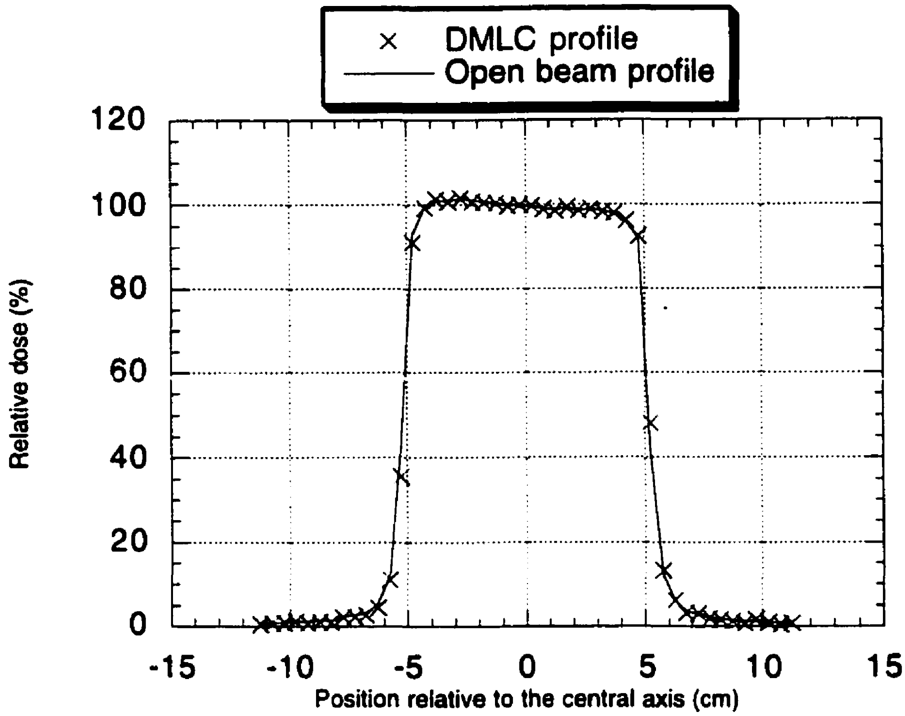

Figure 7.25 Superposition of profiles taken under one pair of leaves moving at a constant speed but with a time lag between the two leaves (DMLC) and a profile under the same pair of leaves in an open field.

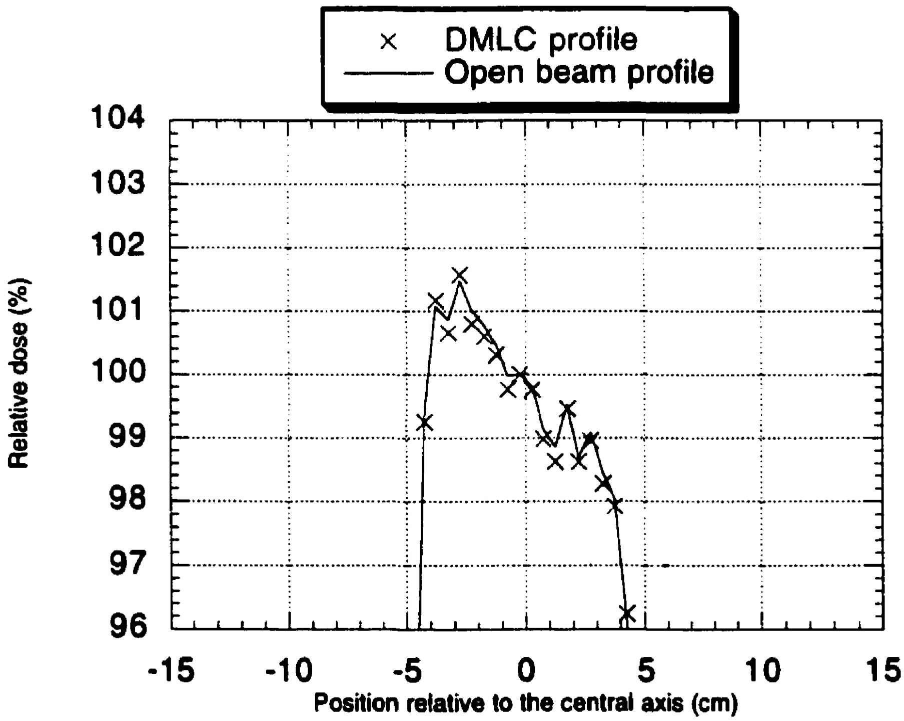

Figure 7.26 Zoom of the superposition of profiles taken under one pair of leaves moving at a constant speed but with a time lag between the two leaves (DMLC) and a profile under the same pair of leaves in an open field.

In figure 7.27, another superposition of profiles for the same test, but another pair of leaves, is presented showing an imperfect overlay of the DMLC profile in the dose fall-off region. Although this feature has been observed for a few profiles, the more common situation was an almost perfect superposition shown in figure 7.25. In fact, the higher dose in the tails of the profile for the dynamic beam delivery appears when slower leaf speeds are tested. This surplus of dose can be up to 5% over the open beam profile tail. This increase in dose at the edge of the field is believed to be due to the proximity of the closing leaf of a pair for a relatively long period of time as the gap closes slowly. Consequently, more radiation is scattered on the front of the closing leaf increasing the dose at the tails of the profile as seen in figure 7.27[14].

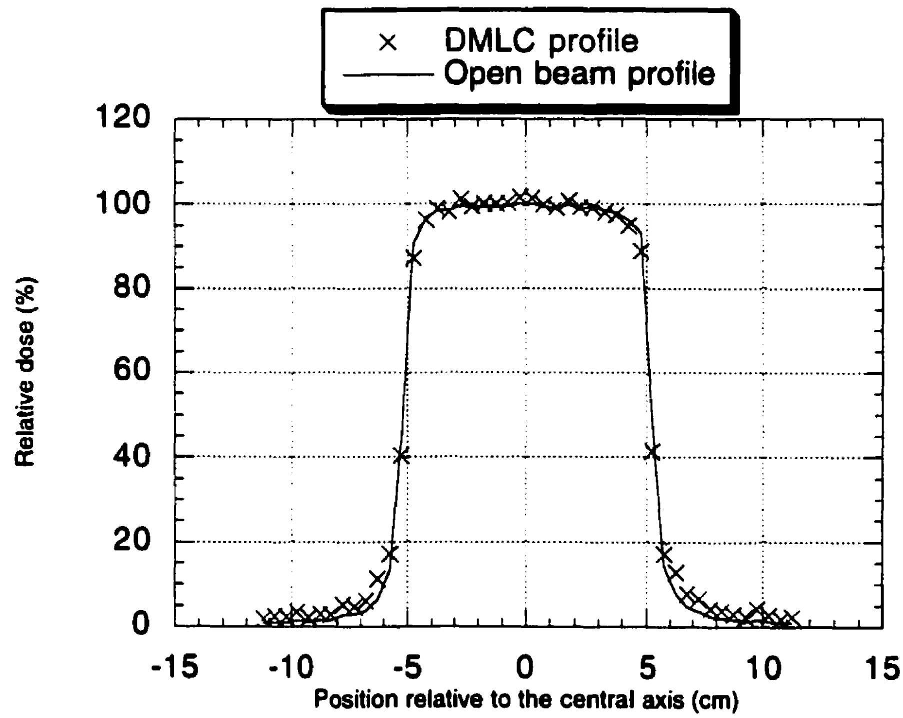

Figure 7.27 Inexact superposition of profiles taken under one pair of leaves moving at a constant speed but with a time lag between the two leaves (DMLC) and a profile under the same pair of leaves in an open field showing a problem in the dynamic dose delivery.

In conclusion, when profiles measured for the same dynamic MLC motion are compared, their flat regions are within 0.2%, which is remarkably good. The DMLC profiles are usually well within 1% of the appropriate open field profile which is also good. However when the leaves were moving slowly, the profile may be up to 5% above the open beam profile in the fall-off region. Hence, no leaf speed stability problem has been measured for a variety of leaf speeds although very slow leaf speed, or low maximum dose rate, should be avoided if possible due to the increased in scatter radiation from the front of the slowly closing leaf. If low MU settings are used, high dose rate should be avoided as mentioned before. In the case of treatment with DMLC involving small MU settings, an average dose rate should be used as a compromise between the two effects.

7.9 Effect of acceleration.

The effect of the acceleration of the leaves on the resulting dose profile has been investigated as described in section 6.5. An example of the superposition of an open beam profile and a profile measured with the acceleration of the leaves is shown in figure 7.28. The figure is similar to the figure presented for the verification of the speed stability of the leaves in section 7.8 and the same comments apply for the noisy appearance and the slope of the profiles.

In fact, the analysis of the profiles involving acceleration reveals results very similar to those obtained for constant speed as expected if the acceleration of the leaves is insignificant or well compensated by the MLC system. The departure of the DMLC profiles from the open beam profiles is inferior to 1% as for the speed stability profiles. However the average difference between the DMLC profiles and the open beam profiles is greater for the tests involving acceleration than the constant speed tests by 0.1% to 0.4%, which is acceptable. Hence, an acceleration effect has been measured but the MLC system is reliable enough to keep it small such that it can be ignored.

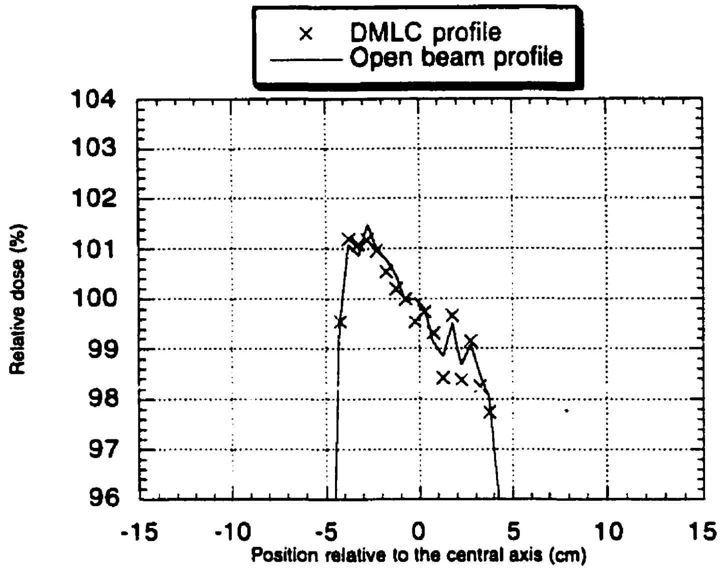

Figure 7.28 Zoom of the superposition of profiles taken under one pair of leaves moving at a constant speed but with a time lag between the two leaves with interruptions of the beam (DMLC) inducing acceleration and a profile under the same pair of leaves in an open field to test the effect of acceleration of the leaves.

7.10 Maximum speed of the leaves.

The maximum speed of the leaves of the MLC system studied has been estimated has described in section 6.4. Even though the maximum speed of the leaves is stated to be 1.5 cm/sec, the maximum speed measured was around 1.3 cm/sec. The maximum speed of the leaves varies according to the selected dose rate. A maximum speed just above 1 cm/sec has been measured for an MLC file that would require a speed above the specified 1.5 cm/sec limit. However the effect of the limited maximum speed is insignificant although it leads to longer treatment times.

7.11 Positional accuracy of the leaves in the dynamic mode.

In section 6.6, two tests on film are described that verify the positional accuracy of the MLC when it is used in the dynamic mode. The two films are presented in figure 7.29 and 7.30. The film in figure 7.29 has been analyzed with a scanning densitometer to determined the position, the height and the width of the peak of radiation deposited where both leaves of a pair stopped. The position of the peak was determined after the profile was correctly aligned using the fact that the profile was symmetrical relative to the central axis. This position has been measured to be at most 0.6 mm from the prescribed position, but it was often closer. It was noted that the position of the film relative to the isocenter can significantly alter the results such that attention to have the film at the level of the isocenter is important. The width and the height of the peak has been compared with the adjacent peaks and no significant difference was observed indicating that both leaves of the observed pair stopped at the same position. Hence the positional accuracy of the leaves of the MLC is within the acceptable limit of 1 mm and probably much better.

Figure 7.30 is a modified test of the experiment reported above in order to examine the positional accuracy of the leaves visually, avoiding the involvement of the scanning densitometer. This test can detect a 1 mm error in leaf position as proved by the three intentionally introduced 1 mm errors in figure 7.30. One error illustrated is a leaf that over travels, another error is a leaf under traveling and the last error illustrated is both leaves stopping at a position 1 mm beside the proper place. This test takes only a few minutes of irradiation of the film and once developed, the positional accuracy of all leaves can be checked in a minute or so such that this test could be done on a regular basis, every week for example, to assure that the MLC stays well calibrated.

Figure 7.29 Resulting film that has been analyzed using a scanning densitometer to test the positional accuracy of the leaves of the MLC when it is used in the dynamic mode. The narrow dark lines are where both leaves of a pair stopped for a certain period of beam on time. The position of the line and the height of the peak is used to determine that both leaves stopped at the prescribed position.

Figure 7.30 Resulting film used to visually test the positional accuracy of the leaves of the MLC used in the dynamic mode. Three 1 mm position errors have been introduced to check that the test was sensitive enough to detect a 1 mm leaf positional error.

7.12 Verification of the dynamic motion of the jaws under the DBD toolbox control.

As described in section 6.8, five tests performed on the MLC have been repeated for the jaws controlled by the DBD toolbox. The results for the tests on the jaws are very similar to the set of results presented for the MLC in section 7.6 to 7.11, hence they will only be summarized in this section.

For the positional reproducibility of the MLC, the jaws used for the step and shoot technique can be placed very accurately by the computer controlled linac. In fact, as for the MLC, no difference in the penumbra was measured and the mean difference between the open beam profile and the dynamic profile is 0.3%.

The precision of the placement of the jaws under the control of the DBD toolbox across the range of motion has been tested by exposing a film to adjacent rectangles. As for the MLC test presented in figure 7.17, the junctions between the rectangles defined by the jaws can be clearly identified. The junctions were appearing regularly and they all had the same height indicating that both jaws were placed accurately throughout the range of the jaws.

The speed stability of the y-jaws has been tested as for the MLC and the results are of the same magnitude of those displayed in figure 7.25. Because the jaws can not be placed closer than about 3 mm apart, the edges of the dynamic profile will be different from the open field. Hence, as mentioned before, the comparison of the dynamic and open beam profiles has been done only in the fully exposed region, avoiding the edges of the profiles. Once this is done, the two profiles are very close, less than 0.4% apart on average and never more than 1%, such that the speed of the jaws is obviously stable. The x-jaws have not been tested because the distance they can over travel the central axis is limited to 2 cm while the y-jaws can cross the isocenter by 10 cm.

The effect of the acceleration of the y-jaws has been investigated and the profile measured was very close to the constant speed profile with small differences of less than 0.4%. In fact a small drop in dose can be observed where the jaw was when the beam stopped. Hence the DBD toolbox is able to deliver the required dose intensity even in the presence of acceleration of the jaws.

The positional accuracy of the jaws under the control of the DBD toolbox has been tested in a manner similar to that of the MLC. The resulting film, with hot spots where the jaws stopped for a given amount of beam on time, is not shown here but it has been analyzed with a scanning densitometer. Once the positions of the hot spots were corrected by considering that the profile was symmetric relative to the central axis, they were within 0.02 cm of the prescribed position which is much better than the 0.05 cm expected. Also the width and the height of the hot spots were all very similar indicating that both jaws stopped almost exactly at the right place for all stopping points. Hence the DBD toolbox is able to place the jaws very accurately in the dynamic mode.

7.13 Verification of the dynamic rotation of the collimator under the DBD toolbox control.

As described in section 6.9, four tests were conducted to verify the dynamic rotation of the collimator when it is under the control of the dynamic toolbox. The first test is to check the positional reproducibility of the collimator angle when the step and shoot strategy is used. Results similar to these presented for the positional reproducibility of the MLC in figure 7.15 are shown in figure 7.32. The two fully exposed sections are close together since a small angle variation of the collimator had to be used to keep the time to complete the experiment reasonable. As a consequence, the dose at the central axis is significant although it was never fully exposed. However, even for the dose at the central axis, which was in the penumbra, both sets of readings are almost exactly the same. All points are within 0.9% and often much closer confirming that the positional reproducibility of the collimator angle is very good.

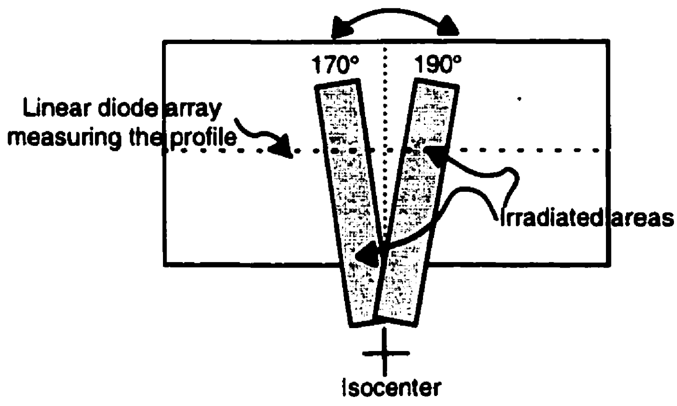

Figure 7.31 Diagram illustrating how the profile of figure 7.32 was created.

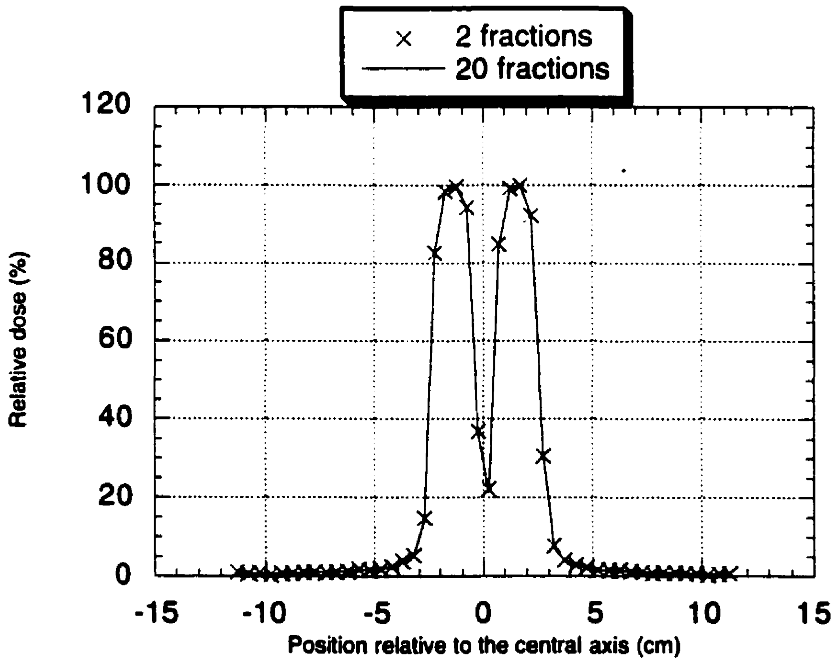

Figure 7.32 Superposition of the two profiles acquired to test the positional reproducibility of the collimator angle under the control of the DBD toolbox, showing almost identical dose deposition for the 20 fractions and the 2 fractions dose delivery.

The speed stability of the collimator rotation has been verified indirectly as described in section 6.9 and the result is shown in figure 7.33. As discussed before, since the profiles were measured on a straight line instead of on an arc of a circle, the profiles have a maximum at the central axis. Figure 7.33 has two local maximum near the edges of the profiles. These are due to an error in the creation of the file governing the motion of the jaws and the collimator. The intention was to compensate for the fact that the jaws can not be put closer than about 3 mm apart before the collimator starts to rotate to have more uniform profiles. The attempt failed but there is no consequence on the primary goal of the experiment, that is to verify that the collimator can be dynamically rotated with a constant speed since the meaningful central part of figure 7.33 shows very good results. The three profiles are almost always within 0.1% of each other and no points are more than 1% apart. Even though this experiment does not prove directly that the collimator was rotating with a constant speed, it shows that the three runs were delivered exactly the same way, and probably with a constant speed.

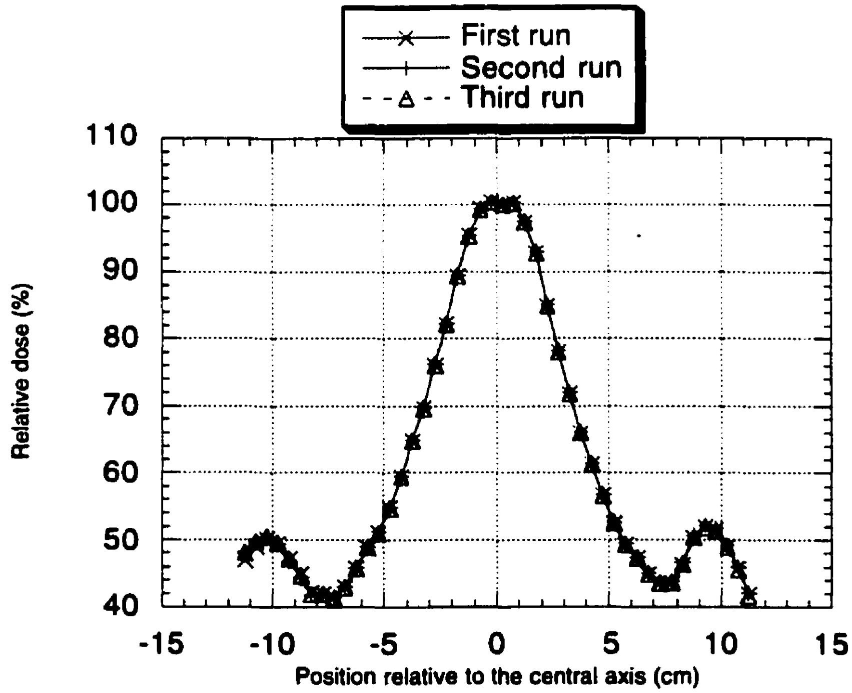

Figure 7.33 Overlay of three runs with a narrow rectangle dynamically rotated while irradiating a straight array of diodes to verify the rotation speed stability of the collimator under the control of the DBD toolbox.

As for the other axes that can be moved dynamically, the effect of acceleration has been investigated for the rotation of the collimator. The departure of the profile delivered with a constant speed and profiles involving acceleration was never greater than 1.3% which is acceptable since it is below 2%. Hence, the DBD toolbox is able to deliver the desired dose intensity when the collimator is dynamically rotated even in the presence of change in speed of rotation.

The positional accuracy of the collimator angle has been verified using the film presented in figure 7.34. The angle from the middle of each trace to the central axis marked on the film was measured with a protractor. As a result, the precision of this test is very dependent on the precision of the marking of the central axis. In fact, in figure 7.34, the position of the central axis marked is seen to be inaccurate due to the angle read and its position in the middle of the dose trace. This error was probably introduced when sheets of solid water were put on top of the film after the central axis had been marked. Moreover the position of the center of each trace on the film is mostly done by eye introducing an uncertainty of the order of 0.5 mm. All traces were within 1 degree of their intended angle which is good when an overall uncertainly of the order of 0.5° is taken into account.

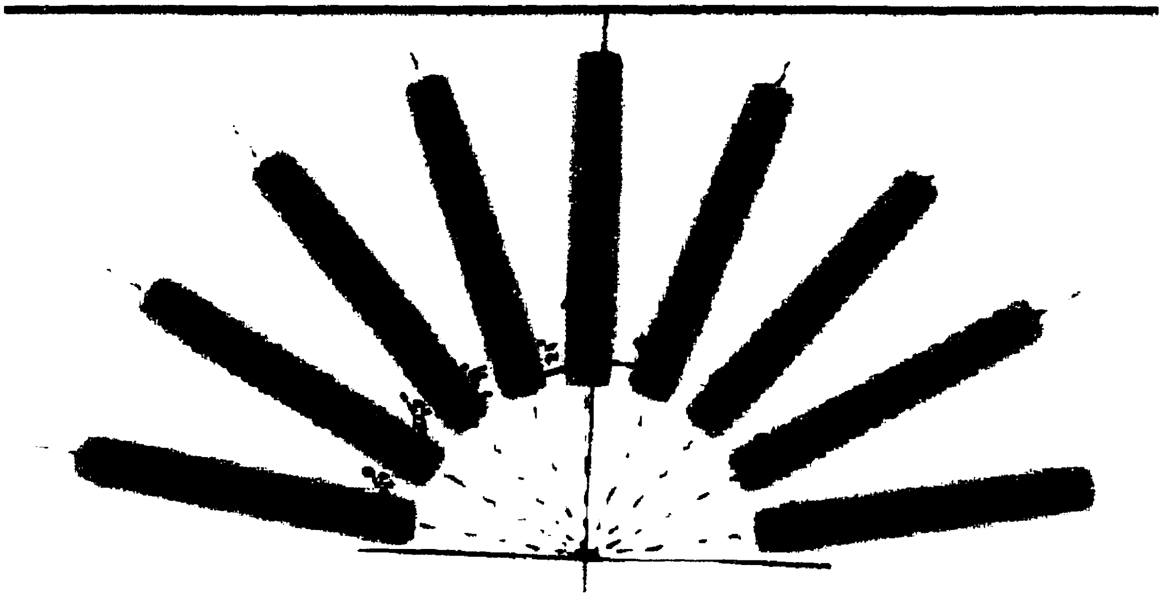

Figure 7.34 Resulting film of the test of the positional accuracy of the collimator angle when under control of the DBD toolbox.

7.14 Verification of the dynamic rotation of the gantry under the control of the DBD toolbox.

The dynamic rotation of the gantry has been assessed through four tests described in section 6.10. The gantry rotation is the last axes to be tested that can be moved dynamically and it is the only one that will require special care as explained in the present section.

The dose deposition delivered at two different gantry angles using the step and shoot strategy in two and 20 fractions has been compared. The first remark is relative to the way the dose was delivered. It was clearly heard and seen that when the gantry was automatically rotating to the next angle at which dose had to be given, a small amount of dose was given when the gantry first passed the desired angle, but since the linac was unable to stop the gantry at this position, the beam was interrupted. When the gantry angle is outside the tolerance of the intended position, the beam is automatically turned off. As the gantry experienced this oscillation and moved back to the right position, the beam was turned back on by the DBD toolbox, and the rest of the dose was delivered.

The dynamic rotation of the gantry puts in evidence the role of the DBD toolbox and its tolerance. The DBD toolbox is guaranteeing that dose will be given only if the axes are within the tolerance of the desired position, and this explains the good results reported above for every axes tested.

The profiles measured to check the positional reproducibility of the gantry angle were within 1.3% of each other, which is a larger interval than for the other axes tested, but it is still within the limit of 2%. The penumbras of all profiles are identical, minimizing the differences between the profiles since the penumbras indicate a sharp edge even for dose delivered in several fractions. The profiles for the same number of fractions showed variations of the order of 0.6%, which is relatively large, but clinically acceptable.

The speed stability of the dynamic gantry rotation has been measured indirectly by comparing four profiles acquired running the same dynamic file which yields dynamic rotation of the gantry with a constant speed. Although the profiles are within 0.6% of each other on average, some dose measurements at certain positions are over 3.5% apart, and with almost 10% of the points more than 2% apart. More profiles were measured with the gantry rotating at a slower speed and all of their points of measurement were within 0.5% of each other and often much closer, which is very good. Hence the DBD toolbox is able to rotate the gantry with a constant speed when the speed is slower and speeds close to the maximum should be avoided to obtain reliable dose deposition.

The effect of acceleration in the dynamic rotation of the gantry has been investigated. The gantry was rotating at its maximum speed and the beam was interrupted stopping the rotation of the gantry. Because of its weight, the gantry was not able to stop right away. The DBD toolbox was able to bring the gantry back to the position where the beam stopped relatively quickly and no radiation was delivered before the gantry was inside the tolerance of the current prescribed position. As a result, only a few reading points were more than 2% apart, and never more than 2.5% apart. Hence the acceleration of the rotation of the gantry does not seem to be a problem keeping in mind the results for the gantry rotating with a constant speed. As noted before, the speed of rotation should be kept below the maximum speed in order to reduce the fluctuations of the dose delivery.

As for the collimator, the accuracy of the gantry angle when changed by the DBD toolbox has been checked indirectly on a fast film as shown in figure 7.36. The position of the stripes left on the developed film is measured and related to the angle of the gantry by equation a.1 in appendix B.3. The traces on the film were all within 0.13 cm of the intended position, or the gantry was within 0.75° of the position declared in the governing computer file. Due to the results reported for the speed constancy of the rotation of the gantry above and the uncertainty of this experiment to test the positional accuracy, mainly limited by the position of the central axis marked on the film, the measured accuracy is good. Hence the DBD toolbox is seen to be able to position the gantry accurately, even in the dynamic mode.

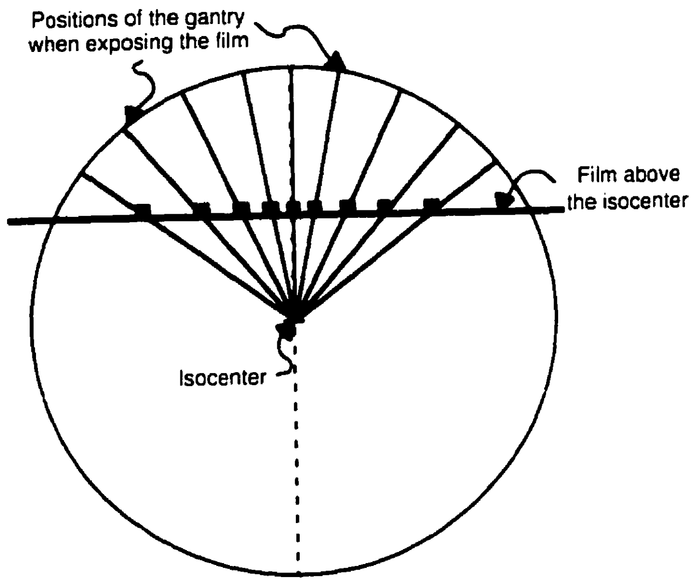

(a)

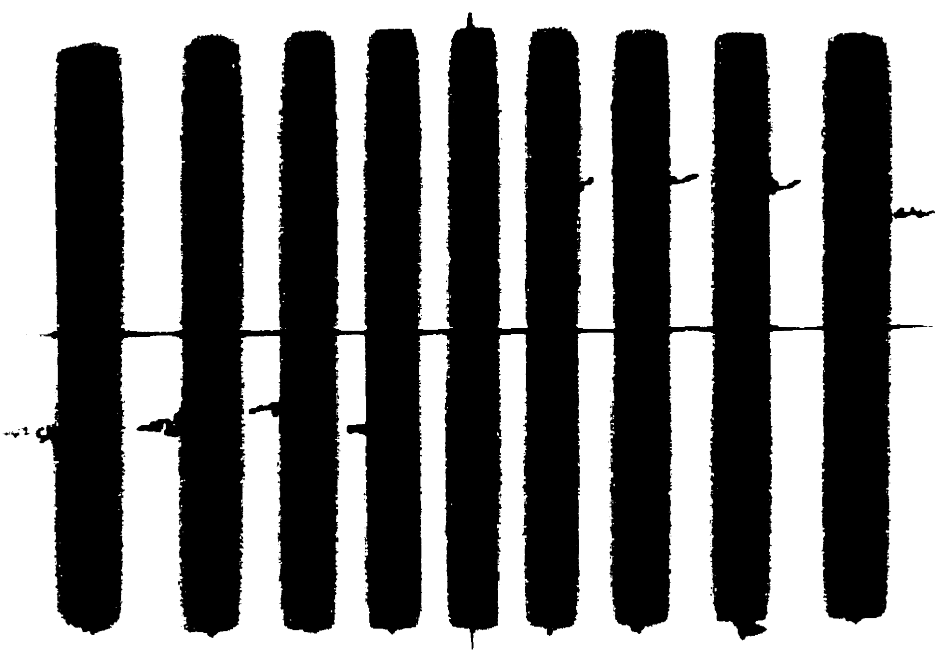

(b)

Figure 7.35 In (a), a diagram explaining how the film presented in (b) has been produced in order to verify the positional accuracy of the gantry angle when under control of the DBD toolbox.

7.15 Summary.

This chapter refers to an extensive set of experiments conducted to assure the reliability of the dynamic dose delivery capability of the Clinac 2300C/D. The tests showed that the internal mechanisms of the accelerator are sufficient to assure the delivery of the dose intensity. One minor exception was the dynamic rotation of the gantry. Due to its great weight, the gantry should be restricted to speeds of rotation below its maximum capability to ensure the stability of the dose delivery.

7.16 References.

1. G.J. Kutcher, L. Coia, M. Gillin, W.F. Hanson, S. Leibel, R.J. Morton, J.R. Palta, J.A. Purdy, L.E. Reinstein, G.K. Svensson, M. Weller, L. Wingfield, "Comprehensive QA for radiation oncology: Report of AAPM Radiation Therapy Commitee Task Group 40", Med. Phys. **21**(4), 581-617 (1994).

2. C.H. Sibata, H.C. Mota, A.S. Beddar, P.D. Higgins, K.H. Shin, "Influence of detector size in photon beam profile measurements", Phys. Med. Biol. **36**(5), 621-631 (1991).

3. D.J. Dawson, N.J. Schroeder, J.D. Hoya, "Penumbral measurements in water for high-energy x rays", Med. Phys. **13**(1), 101-104 (1986).

4. P. Metcalfe, T. Kron, A. Elliott, T. Wong, P. Hoban, "Dosimetry of 6-MV x-ray beam penumbra", Med. Phys. **20**(5), 1439-1445 (1993).

5. D.J Dawson, J.M. Harper, A.C. Akinradewo, "Analysis of physical parameters associated with the measurement of high-energy x-ray penumbra", Med. Phys. **11**(4), 491-497 (1984).

6. A.L. Boyer, T.G. Ochran, C.E. Nyerick, T.J. Waldron, C.J. Huntzinger, "Clinical dosimetry for implementation of a multileaf collimator", Med. Phys. **19**(5), 1255-61 (1992).

7. C.D. Mubata, P. Childs, A.M. Bidmead, "A quality assurance procedure for the Varian multi-leaf collimator", Physics in Medicine & Biology. **42**(2), 423-31, (1997).

8. T.C. Zhu, L. Ding. C.R. Liu, J.R. Palta, "Performance evaluation of a diode array for enhanced dynamic wedge dosimetry", Med. Phys. **24**(7) 1173-1180 (1997).

9. R. Watts, "Evaluation of a diode detector array for use as a linear accelerator QC device", Med. Phys. **25**(2), 247-250 (1998).

10. I.J. Das, K.R. Kase, V.M. Tello, "Dosimetric accuracy at low monitor unit settings", Br. J. Radiol. **64**, 808-811 (1991).

11. R. Rajapakshe, S. Shalev, "Output stability of a linear accelerator during the first three seconds", Med. Phys. **23**(4), 517-519 (1996).

12. R.J. Barish, R.C. Fleischman, Y.M. Pipman, "Teletherapy beam characteristics: The first second", Med. Phys. **14**(4), 657-661 (1987).

13. CC Chui, S. Spirou, T. LoSasso, "Testing of dynamic multileaf collimator", Med. Phys. **23**(5), 635-641 (1996).

14. X. Wang, S. Spirou, T. LoSasso, J. Stein, C.S. Chui, B. Mohan, "Dosimetric verification of intensity-modulated fields", Med. Phys. **23**(3), 317-27 (1996).

CONCLUSIONS

8.1 Summary.

The present generation of linear accelerators are controlled by computers giving the possibility of dynamic beam delivery, implying that one or several components of the linac can be moved during irradiation. Consequently, dose intensity modulation may be created in order to implement conformal radiotherapy. The goal of this conformal approach is to maximize the dose to the tumor while avoiding the irradiation of surrounding healthy tissue. The work presented here was intended to verify that dynamically enabled linacs can be used with confidence for the implementation of dynamic radiotherapy treatment by verifying the accuracy and the stability of the motions of the movable axes.

The collection of possible axes that can be controlled by the linac has been tested. The most encompassing set of experiments was performed on the multileaf collimator. Its importance comes from the fact that the dynamic MLC (DMLC) has been proven to be capable of delivering any arbitrary dose intensity, within the inherent limitations of the leaf width. There are two techniques used to implement dynamic beam delivery, the step and shoot, and the continuously moving method. Tests verifying that the MLC can be used with both methods with an accuracy and a stability acceptable clinically have been presented, and indicate that the MLC can be used to implement conformal radiotherapy. Many of the tests reported could be part of an ongoing quality assurance program to verify that the MLC system meets the high standards required for dynamic treatment at all times.

The dynamic beam delivery (DBD) toolbox can translate the jaws while the beam is on, as well as dynamically rotate the collimator and the gantry. The same tests conducted for the DMLC have been adapted to verify the operation of the DBD toolbox. The jaws can be displaced very accurately under the control of the DBD toolbox at all available speeds for the entire range of possible positions.

Verification of the dynamic rotation of the collimator and the gantry has been indirectly inferred in order to use existing measuring equipment instead of developing methods involving new equipment or long procedures that would be cumbersome to implement as part of a quality assurance program. Even though the dynamic rotation of the collimator is not as precise as the dynamic translation of the MLC and the jaws, it is within tolerable limits so as to be used clinically. The dose intensity as measured with the rotating collimator was found to be constant and within the expected tolerance.

The dynamic rotation of the gantry is cause for some concern. When the speed of rotation was close to the maximum speed, an instability was detected. As a result, it is recommended to implement dynamic beam delivery with the gantry limited to relatively slow speeds of rotation where the stability is excellent.

In general the linac's computer is able to deliver dynamic treatments reliably due to its internal checks that guaranty that no dose will be given if one of the moving axes is not within an adjustable tight tolerance. In the case that this requirement can not be met, dedicated interlocks stop the beam and terminate the dynamic delivery sequence.

The dose linearity of the Clinac 2300 C/D at low monitor unit (MU) settings has been investigated. In the literature, it was found that linacs are usually unstable for the first few seconds of irradiation. The Clinac 2300 C/D did show a dose instability when the beam was turned on, but further investigations showed a non-linearity in the ionization chamber as well. The instability of the ion chamber has been observed to be less important when the chamber has been exposed to a large dose (over 1000 MU) and when it was maintained at the same bias voltage for over an hour. When the ion chamber was replaced by a diode, it was shown not to be subject to non-linearity for the first few seconds of irradiation, however the diode has a noisier output. As a result of this set of measurements, it is recommended not to use fields for less than 10 MU to avoid the accumulation of systematic errors due to potential linac instability when the beam is turned on.

8.2 Future work.

The work presented in this document provides the confidence necessary prior to clinical implementation of dynamic radiotherapy. Research is now being done on delivering dynamic MLC treatments such that it is likely this will be a modality that will be widely available within the next few years. The current state of understanding of the dynamic motion of the other axes of the linac is not as complete. For example, the precise dosimetry of the dynamic axes has to be known in order to be able to predict the dose deposition essential for treatment planning. Also, efficient computer algorithms for treatment planning systems will have to be developed and tested before the DBD toolbox is used.

The DBD toolbox is not enabled in the clinical mode, and could be currently used only to position the gantry, the collimator, and the jaws for the next field in a dynamic treatment plan. In this case, efficient protocols must be created to have DMLC and possibly several other moving axes in a single file governing a complete dynamic treatment plan. Future work will be required to develop tests to verify that the linac can accurately move several axes at the same time while delivering therapeutic doses of radiation. The implementation of a complete dynamic treatment plan should result in significant time savings such that conformal radiotherapy would be easily and safely achievable.

Appendix A.1: quality assurance (QA) tests for static multileaf collimator (MLC).

Test 1: accuracy of leaf position using the light field.

An arbitrary MLC pattern, but involving all the leaves is created and a template is printed out. The gantry and the collimator angle are set at 0°. The MLC file is loaded on the computer and executed. The shadow of each leaf is compared with the template placed at SSD 100 cm. The leaf shadow should match the template within 0.5 mm.

Test 2: leaf calibration.

An MLC file is created in which the leaf carriage travels from -16 cm to 16 cm in increments of 4 cm. The minus sign indicates distances traveled across the central axis. The gantry and the collimator angle are set at 0°. At each position, the actual distance with respect to the light field cross-wire is checked at SSD 100 cm. The difference between the actual leaf positions and the set values must not exceed 1 mm.

Test 3: light field check of the leaf carriage skew.

This test is performed to check that the MLC leaf carriage is aligned with the opposite jaw. The gantry and the collimator angle are set at 0°. All leaves are driven 1 cm across the central axis. The opposing jaw is moved to the 1 cm position as shown in figure A.1.1. This test will be done for both leaf carriages. If the carriage is well aligned, only the light transmitted at the corners of each leaf should be visible at 100 cm SSD. In the case of a skewed carriage, more light will appear at one end of the carriage creating a triangle of light.

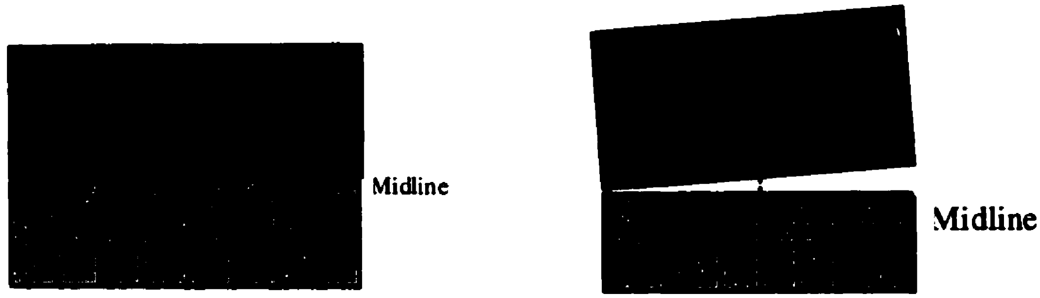

(a) (b)

FIGURE A.1.1. Diagram representing the position of the MLC and the x-jaw in the determination of the skew of the MLC assembly with respect to the main collimators using the light field. Shown in (a) is the expected pattern and shown in (b) is the result of a misaligned MLC.

Test 4: radiation check of the leaf carriage skew.

The gantry and the collimator are set at 0°. A film with sufficient buildup and backscatter material is placed at SSD 100 cm. As shown in figure A.1.2, the leaves are driven to positions 7.0 cm, except leaves A4 and B23 which are set to -6.5 cm. The y-jaws are set to 25.5 cm and the x-jaws are set to 15 cm. With a ball-pen, the position of the y-jaws, both carriages, and the light field center are marked on the film which is exposed to about 50 MU with the 6 MV beam. Once the film has been developed, the skew of the two carriages is determined by measuring the distances between points A and B, and C and D, as shown in figure A.1.2. This is to check the skew of the y2-jaw. The two distances obtained should not be different by more than 1.0 mm. The same measurements will be done for the y1-jaw and the B23 leaf to check the skew of the y1-jaw.

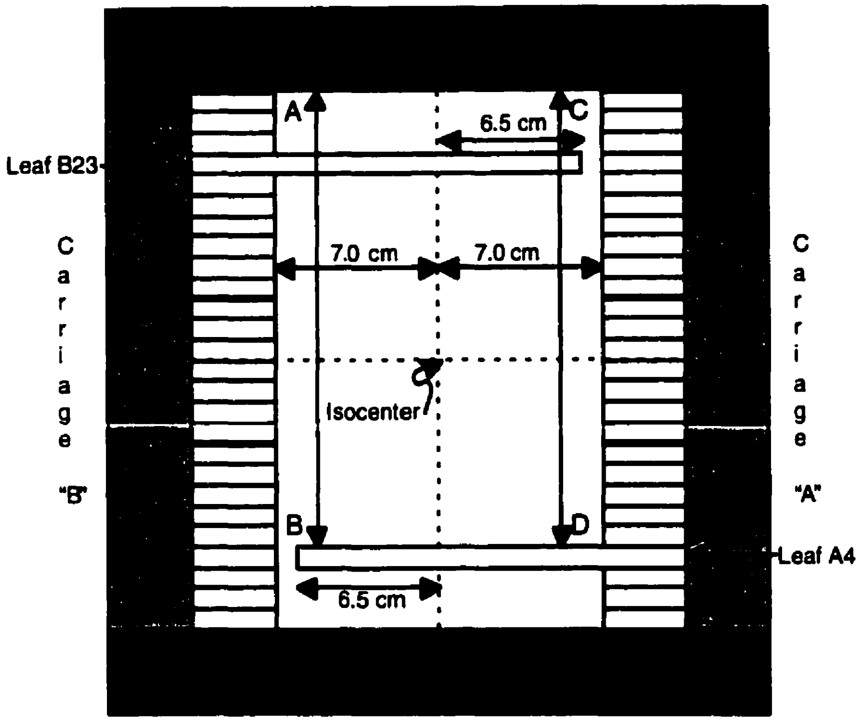

FIGURE A.1.2. Geometric set-up for the measurement of the MLC skew with respect to the secondary jaws using the radiation field.

Test 5: MLC field radiation center.

The gantry is set at 0° and a film is placed at SSD 100 cm with sufficient buildup and backscatter material. Verification is made that the shadow of the cross-wire is describing a circle of less than 1.0 mm about the isocenter when the collimator is rotated from 270° to 90°. The center is marked on the film with a ball-pen. The jaws are opened to 20 cm and all leaves of the MLC are closed except leaves 13 and 14, the central leaves, on either carriages which are set to 10 cm as illustrated in figure A.1.3. Two pairs of leaves are opened since the central axis passes between the two leaf edges. The collimator is successively rotated to 315°, 0°, and 90° and the film is exposed at each position to about 40 MU. On the developed film, the spoke shots are split with very thin lines. These lines should intersect within a circle of radius 1.0 mm.

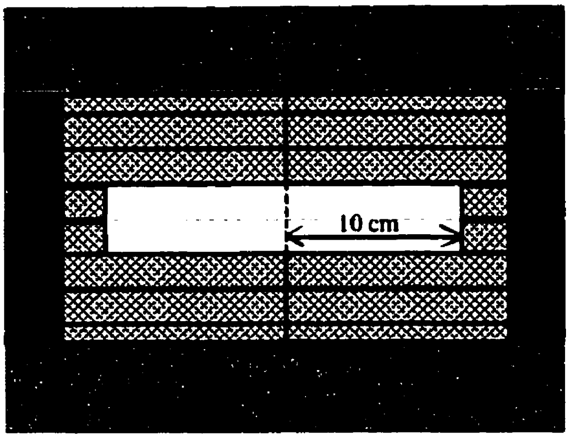

FIGURE A.1.3. MLC configuration to determine the radiation field center.

Test 6: MLC carriage sag.

A film is placed edge-on with its center close to the isocenter such that the radiation will pass through the film lengthwise as the gantry is rotated. Material should be placed around the film to ensure sufficient dose buildup. All MLC leaves are set to 0.5 cm with the main jaws 1.0 cm behind the leaf edges as shown in figure A.1.4. The film is exposed to about 40 MU with gantry angles of 60°, 120°, and 270°. The lines through the middle of the radiation spokes should intersect with a radius of less than 1.0 mm.

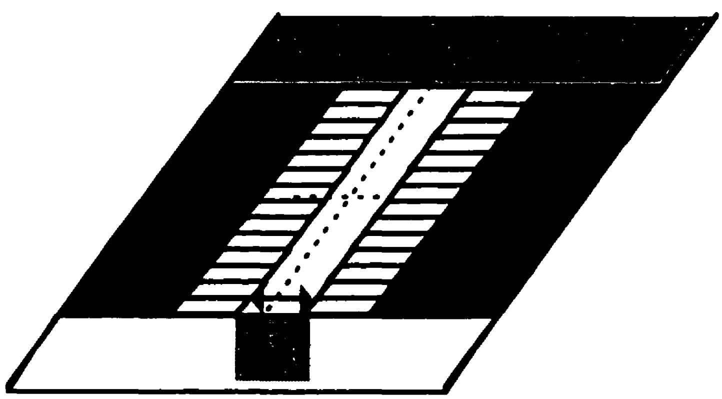

FIGURE A.1.4. The leaf configuration used to test the MLC carriage sag.

Appendix A.2: quality assurance (QA) tests for step and shoot multileaf collimator (MLC).

Test 1: positional reproducibility of the MLC (a).

The linear diode array is placed at SSD 100 cm on the couch of the linear accelerator with sufficient buildup material. The line of diodes is positioned directly under one pair of leaves, parallel to the motion of the leaves. The jaws of the linear accelerator are opened to define a rectangular field of 25x23 cm^2, and the MLC is used to define a narrow rectangle of 4x26 cm^2 centered 6 cm to the left of the centerline. 10 MU will be delivered with this field with the 6 MV beam and a dose-rate of 400 MU/min. The center of the field will then be moved 6 cm to the right of the beam centerline and 10 MU delivered again. The field will continue to be moved alternatively from the left to the right of the beam centerline while delivering 10 MU at each position until a total of 200 MU is delivered. The data collection is then stopped and the file saved. The same process is repeated for a selection of leaf pairs.

The profiles obtained will be compared to the corresponding profile of the same total dose delivered in only two large fractions of 100 MU, one on each side of the beam centerline.

The two profiles for each pair of leaves are compared. If the positional reproducibility of the MLC leaves is good, the two profiles, characterized by their penumbra, will be the same as in figure A.2.1a. A wider penumbra on the first profile compared to the second profile will indicate poor positional reproducibility of the MLC leaves as in figure A.2.1b.

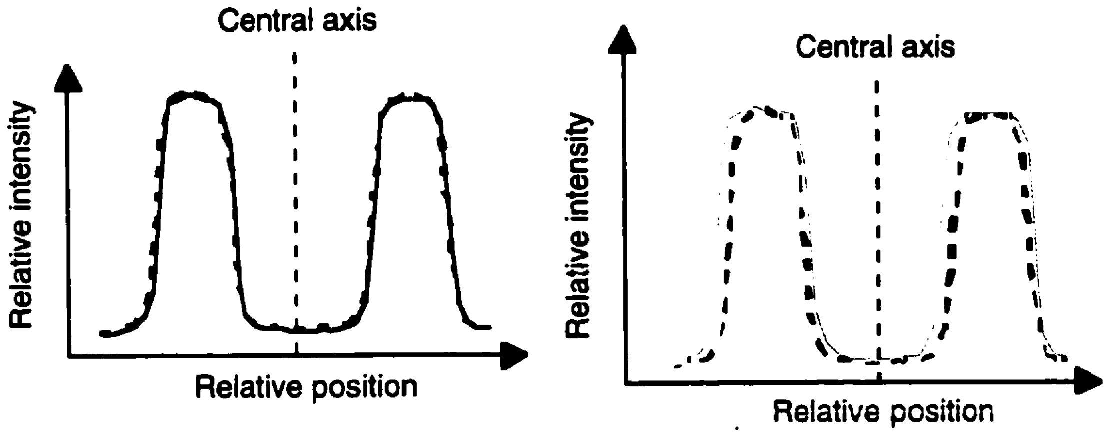

(a) (b)

FIGURE A.2.1. Resulting overlaid profiles when testing the positional reproducibility. The solid line profile represents the dose delivered in many fractions while the dashed line indicates two fractions. In (a), the acceptable result, two identical profiles are seen where as in (b), the result in the case of poor positional reproducibility giving a wider profile in solid as compared to the dashed profile is shown.

Test 2: positional reproducibility of the MLC leaves (b).

The linear diode array is placed at SSD 100 cm on the couch of the linear accelerator with sufficient buildup material. The line of diodes is positioned directly under one pair of leaves, parallel to the motion of the leaves. The jaws of the linear accelerator are maximally opened. The multileaf collimator is used to define a narrow rectangle of 2x26 cm^2, 10 cm to the left of the beam centerline. A dose of 40 MU will be delivered with this field with a 6 MV beam at a dose rate of 400 MU/min. The center of the field will then be moved 2 cm to the right and another 40 MU will be delivered. The field will continue to be moved 2 cm to the right while delivering 40 MU at each position until the center of the field reaches 10 cm to the right of beam centerline. The profile will be examined to check the accurate positioning of the MLC leaves by producing a regular pattern. This test is also performed with film for a visual record of the pattern left by the MLC motion.

Appendix A.3: quality assurance (QA) tests for dynamic multileaf collimator (MLC).

Test 1: stability of leaf speed.

To test the stability of the leaf speed, a pair of opposed leaves are configured to move with a constant speed from 5 cm to the left to 5 cm to the right of the beam centerline. Adjacent pairs of leaves will be programmed to move at different, but constant speeds. The motion of the leaves are illustrated in two different ways in figure A.3.1. The leaves of a pair start at the same point and move with the same speed, but with a time lag between the two, corresponding to the amount of dose delivered under this particular pair of leaves. The jaws will be maximally opened with the collimator and gantry angle at 0°. For each pair of opposed leaves, the profile will be flat since every point will see the same dose. The linear diode array is placed under a pair of leaves parallel to the motion of the multileaf collimator with sufficient buildup material. The linear diode array is exposed to a total of 100 MU at a dose rate of 200 MU/min using the 6 MV beam. A profile is recorded for every pair of leaves. These profiles are compared with the corresponding open field profile for each pair of leaves. If both leaves of a pair are moving with constant speed, the open beam and dynamic profiles will be the same.

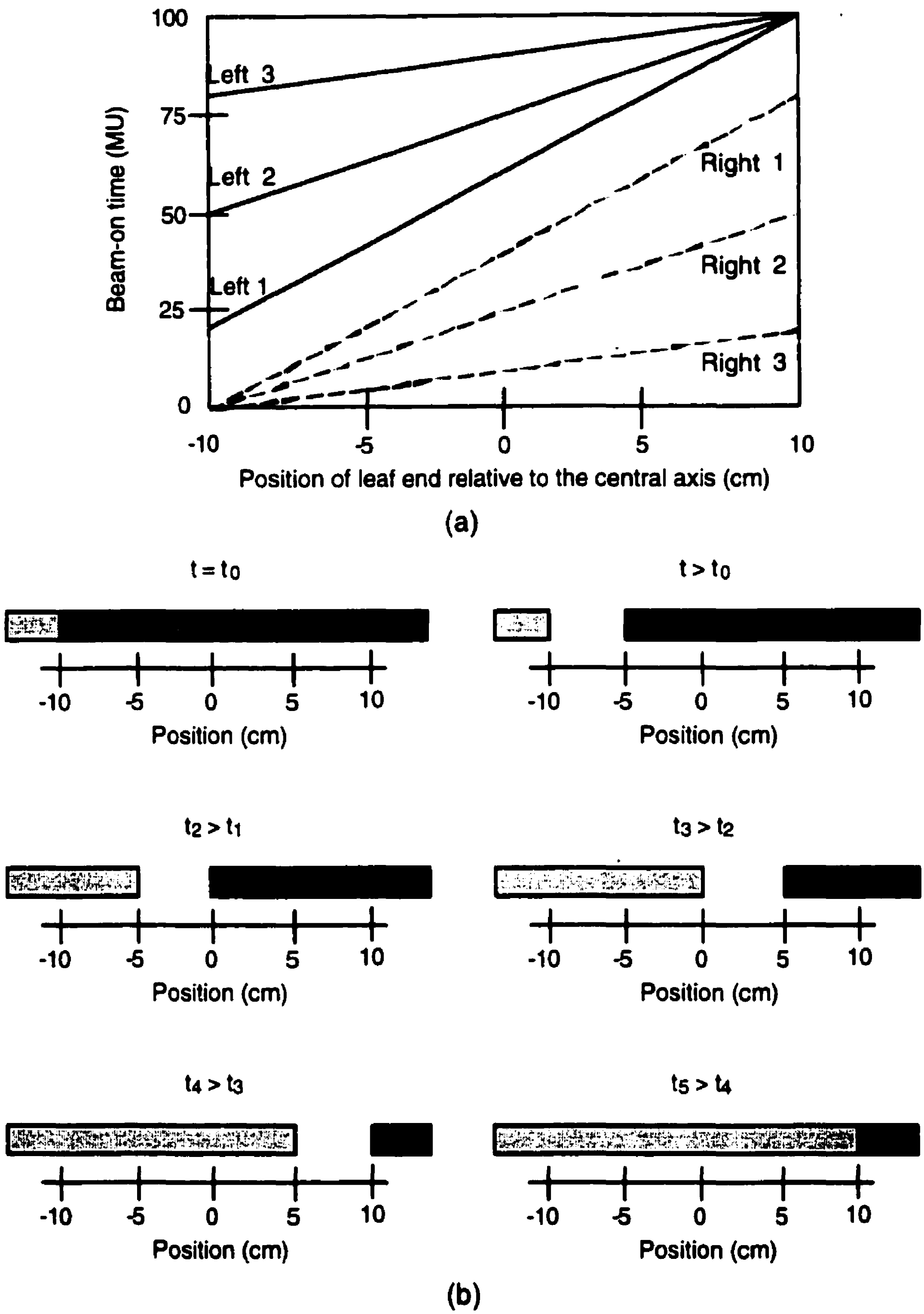

FIGURE A.3.1. In (a), the patterns of leaf motion to produce uniform intensity profiles by constant leaf speed are shown for three pairs of leaves: Leaf pair-1 moves at the lowest speed and leaf pair-3 moves at the highest speed. In (b), a sample of the position of each leaf of a pair is illustrated at several different times to produce the wanted profile in the determination of leaf speed stability.

Test 2: effect of acceleration.

The same MLC motion patterns as used in test A.3.1 are repeated, but this time the beam is turned off 3 to 5 times during the delivery of the beam. For each pair of leaves tested, the profile recorded by the linear diode array, placed as in test A.3.1, is compared with the corresponding open field profile. If the acceleration of the leaves does not change the intensity of dose delivered, the two profiles will be exactly the same.

Test 3: maximum speed of the leaves.

The maximum speed of a leaf can be estimated when a known leaf motion is programmed with a constant speed, as in test A.3.1. From the created file that defines the motion of the leaves, the number of MU per cm is known. Hence by selecting a maximum dose rate well above the dose rate that can be achieved by the linear accelerator when delivering the dynamic file, and by noting the maximum dose rate at which this known pattern was delivered, the maximum leaf speed can be calculated. The speed is given by the maximum dose rate observed divided by the number of MU per cm demanded. The maximum speed will vary as the dose rate demanded is changed. Hence calculated values of maximum speed should be compared to previously calculated values for the same test performed under the same conditions.

Test 4: positional accuracy of the multileaf collimator.

To test the positional accuracy and calibration of the leaves, the left and right leaves are made to travel according to the same pattern but with a time-lag between them as illustrated in figure A.3.2. Each leaf moves at a constant speed until it reaches a preselected point where the leaf stops for a fixed duration of beam-on time, then it resumes its motion again. Both leaves of a pair will stop at the same position but at a different time of exposure. Due to the rounded ends of the leaf, a hot spot will be present at the location of the pause in motion. If, however, the left leaf under-travels or the right leaf over-travels, there will be an observable, more noticeable, hot spot. Conversely, if the left leaf over-travels or the right leaf under-travels, there will be an overlap, leading to a relative cold spot.

A film is placed at SSD of 100 cm with sufficient buildup and backscatter material. The jaws are set to 25.6x11.6 cm^2 and a dose-rate of 200 MU/min and the 6 MV photon beam is used. Both leaves of a pair are programmed to travel a total of 10 cm, with 5 cm on each side of the central line. Both leaves go through exactly the same motion, but with a time lag between them, stopping at the same position. The total dose is selected such that a dose of 40 MU is given to the film at all points, which is proportional to the time lag between the motion of the leaves of a pair. Each pair of leaves are programmed to stop at different positions to test the positional accuracy of more points.

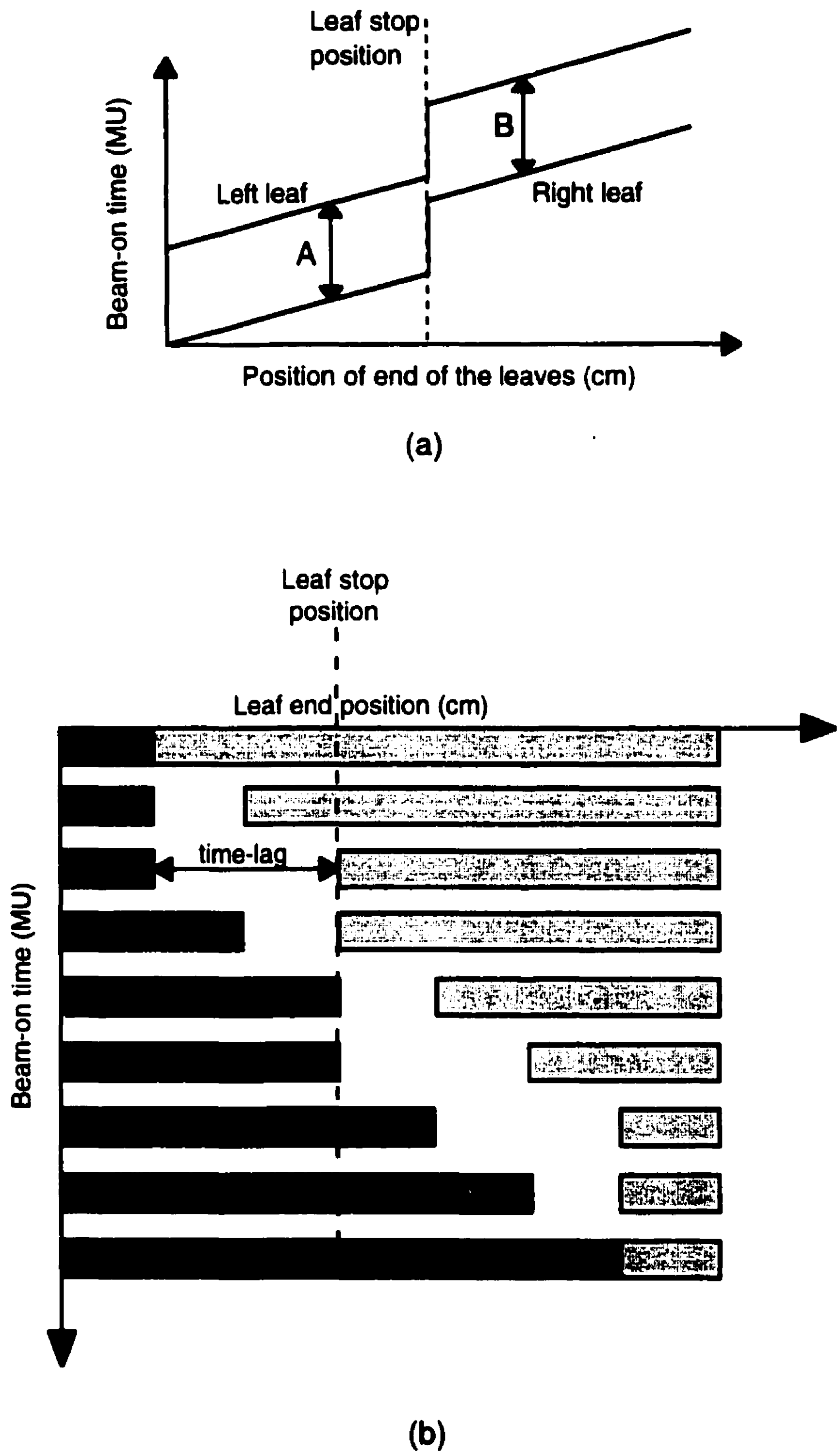

FIGURE A.3.2. (a) and (b) are two ways to represent the motion as a function of beam-on time to test the positional accuracy of the MLC. The right leaf travels at a constant speed until it reaches a preselected position, where it stops for a duration of beam-on time, before it resumes its motion. The left leaf follows the exact same pattern, but with a time-lag, producing a hot spot at the leaf stop position.

In figure A.3.2 (a), when A is equal to B, the intensity of the profile will be uniform for the whole motion of the leaves except at the position where they are stopped as explained above.

This test can be modified to check to positional accuracy visually on a film. Each leaf of a pair are made to stop with a one millimeter gap between the two leaves to accentuate the hot spot. All pairs are made to stop at the same regular intervals such that a steady pattern is created and a one millimeter error in position can be easily observed.

Appendix B.1: quality assurance (QA) tests for dynamic motion of the jaws using the dynamic beam delivery (DBD) toolbox.

Test 1: positional reproducibility of the jaws under DBD toolbox control (a).

The same approach as in test A.2.1 for step and shoot MLC is used. The linear diode array is placed parallel to the jaw motion at SSD 100 cm with sufficient buildup material. The y-jaws are programmed to define a 4 cm wide rectangle with the center 6 cm to the left of the beam centerline. The x-jaws are set at 20 cm. A dose of 10 MU with the 6 MV beam and a dose rate of 400 MU/min is delivered, after which the center of the rectangle is moved 6 cm to the right of the beam centerline with the beam off. Fractions of 10 MU are delivered on each side of the isocenter until a total of 200 MU is accumulated. The second part of this test consists of exposing the linear diode array to the same total dose of 200 MU, but in only two fractions, one on each side of the beam centerline. The penumbras of the two tests are compared and no change in the penumbra should be observed. The same tests are done with the x-jaws, but with the center of the rectangle 3 cm beside the beam centerline, due to the limit of overlap of the x-jaws.

Test 2: positional reproducibility test of jaws under DBD toolbox control (b).

The same test as for A.2.2 for step and shoot MLC is performed. The linear diode array is placed on the linear accelerator couch at SSD 100 cm with sufficient buildup material. The x-jaws are set at 20 cm while the y-jaws are programmed to create a 4 cm wide rectangle with its center starting at 12 cm to the left of the beam centerline. A dose of 40 MU is delivered with the 6 MV beam at a dose rate of 400 MU/min. The rectangle is moved with the beam off to 4 cm to the right of the previous position, and another 40 MU is delivered. The movement of the rectangle is repeated until the center of the rectangle is 12 cm to the right of the beam centerline. This test can also be performed with film to see the junctions of adjacent rectangles.

Test 3: stability of jaw speed.

As in test A.3.1 for dynamic MLC, the stability of the speed of the y-jaws is checked by instructing the y-jaws to move at constant speeds from 9 cm to the left to 9 cm to the right of the beam centerline. They are programmed to move with the same speed, but with a time lag between the two, corresponding to the dose delivered at any point. The profile will not be flat at the beginning and the end due to the constraint that the jaws cannot be closer than about 3 mm, however it will be flat in the middle. The x-jaws will be maximally opened. The linear diode array is placed parallel to the motion of the jaws with sufficient buildup material. The detectors are exposed to a 6 MV beam at a dose rate of 400 MU/min. Another profile will be recorded for an open field. If both jaws move with constant speed, the open and dynamic profiles will be the same, excluding the edges of the profiles from the analysis.

Test 4: effect of acceleration on the delivery of dose with jaw motion controlled by the DBD toolbox.

The same jaw motion pattern as used in test B.1.3 is repeated, but this time the beam is turned off 3 to 5 times during the delivery of the dose. The profile recorded by the linear diode array, placed as in test B.1.3, is compared with the corresponding open field profile. If the acceleration of the jaws does not change the intensity of dose delivered, the two profiles will be exactly the same.

Test 5: positional accuracy of the jaws when under the control of the DBD toolbox.

To test the positional accuracy and calibration of the y-jaws, the left and right jaws are made to travel according to the same pattern but with a time-lag between them. Each jaw moves at a constant speed until it reaches a preselected point, where it stops for a fixed duration of beam-on time, then it resumes its motion again. Due to an increased radiation scatter component near the jaw, a hot spot will be present at the location of the pause in motion. If, however, the left jaw under-travels or the right jaw over-travels, there will be an observable, more noticeable, hot spot. Conversely as before, if the left jaw over-travels or the right jaw under-travels, there will be an overlap, leading to a cold spot.

A film is placed at an SSD of 100 cm with sufficient buildup and backscatter material. A dose-rate of 200 MU/min and beam energy of 6 MV are selected. The jaws are programmed to stop several times while traveling from 10 cm to the left to 10 cm to the right of the beam centerline. However at the start and the end of the motion, the jaws will be separated by at least about 3 mm due to the linear accelerator constraint. The total dose is chosen to give around 40 MU at every point on the film. The film should be analyzed with a densitometer with particular interest in the magnitude and the location of the hot spots.

Appendix B.2: quality assurance (QA) tests for dynamic rotation of the collimator using the dynamic beam delivery (DBD) toolbox.

Test 1: positional reproducibility of the collimator angle.

The jaws are set to describe a narrow rectangle. The x-jaws are set to 2 cm while the y1-jaw is at -5 cm (5 cm over the isocenter) and the y2-jaw is set at 13 cm. The linear diode array, with sufficient buildup material, is placed at SSD 100 cm perpendicular to the x-jaw axes when the collimator angle is placed at 180°. It is displaced from the isocenter toward the y2-jaw in order to see the light field from the rectangle going at least 5 cm on each side of the isocenter when the collimator angle swings from 170° to 190°. The linear accelerator is programmed to deliver 4 MU with the collimator angle at 170° after which the beam is turned off and the collimator angle is changed to 190° where another 4 MU is delivered. The collimator is moved between 170° and 190° until a total of 80 MU is given to the linear diode array.

The profile obtained is compared to the profile measured by delivering 2 times 40 MU, one fraction with the collimator angle at 170° and the other at 190°. The two profiles must have the same penumbra in order to confirm that the positional reproducibility of the collimator angle is accurate when rotated under control of the DBD toolbox.

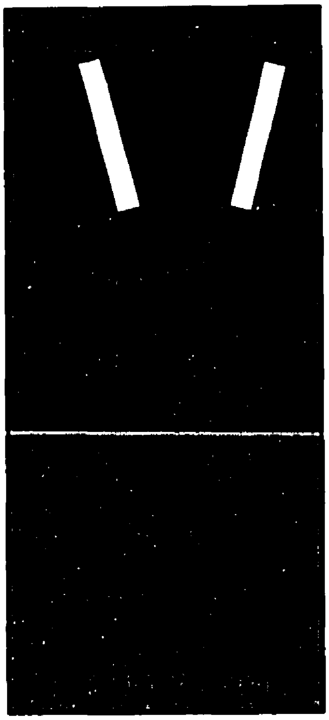

FIGURE B.2.1. Diagram of the set-up used to test the positional reproducibility of the collimator rotation. The linear diode array and its exposed regions are illustrated relative to the treatment couch placed at 180°. The position of the isocenter is also shown to illustrate that the jaws define a narrow rectangle off-axis.

Test 2: verification of constant rotation speed of the collimator under the DBD toolbox control.

This test verifies that the DBD toolbox is able to rotate the collimator with a constant speed. A profile taken on a line will not give a flat profile, on the other hand, there is no easy way to take a profile along the radius of a circle. Hence a profile taken on a line can be obtained over many trials and compared to check the reproducibility.

The linear accelerator is programmed to rotate the collimator dynamically from 100° to 260° with the beam on. The linear diode array is placed as in test B.2.1, perpendicular to the x-jaws and beside the isocenter in order to see the rectangle going from 10 cm to the left to 10 cm to the right of the center of the linear diode array for a total change of position of 20 cm. The x-jaws are set at 2 cm, except at the beginning and the end of the exposition where they are placed about 3 mm apart. The y1-jaw is set at -2 cm, where the minus sign means a position past the isocenter. The y2-jaw is set at 13 cm. The total dose is set to have around 40 MU at every point exposed.

Test 3: effect of acceleration on collimator rotation when under the control of the DBD toolbox.

The exact same test as in test B.2.2 is performed except that the beam is turned off every 20 MU. The recorded profile is compared to one of the profiles obtained in test B.2.2. The two profiles should be practically identical if the DBD toolbox is able to compensate for leaf acceleration.

Test 4: positional accuracy of the collimator with dynamic rotation under the control of the DBD toolbox.

The collimator is dynamically rotated with a constant speed with the beam off. Every 20°, the beam is turned on briefly for 2°, exposing a fast film to about 2 MU. A fast film is placed at SSD 100 cm with sufficient buildup and backscatter material. The film is exposed to a 6 MV beam at a dose rate of 400 MU/min. The x-jaws are opened to 1 cm and the y1-jaw is set at -5 cm while the y2-jaw is set at 13 cm. The gantry angle is fixed at the nominal 0° position. The central axis is marked with a ball-pen on the film and the film can be analyzed, with a protractor, to check that the beam was delivered at the appropriate collimator angles.

Appendix B.3: quality assurance (QA) tests for dynamic rotation of the gantry using the dynamic beam delivery (DBD) toolbox.

Test 1: positional reproducibility of the gantry when under control of the DBD toolbox.

This test employs the classic step and shoot technique. The linear accelerator is programmed to expose a narrow rectangle of 2x15 cm^2 with a fixed gantry angle of 200°, for 10 MU at 400 MU/min with a 6 MV beam. The collimator angle is fixed at 180°. The beam is turned off and the gantry is programmed to automatically go to 160° where another 10 MU is given. The gantry oscillates between these two angles until a total dose of 200 MU is achieved. The linear diode array is placed at SSD 90 cm, 10 cm above the isocenter, perpendicular to the x-jaws. With the detector above the isocenter, the change of angle of the gantry will result in the displacement of the irradiated area on the linear diode array as illustrated in figure B.3.1.

The profile obtained will be compared with a profile measured by exposing the linear diode array, set-up the same way, to only one fraction for each of the two gantry angles, for a total of 200 MU and the positional reproducibility can be evaluated.

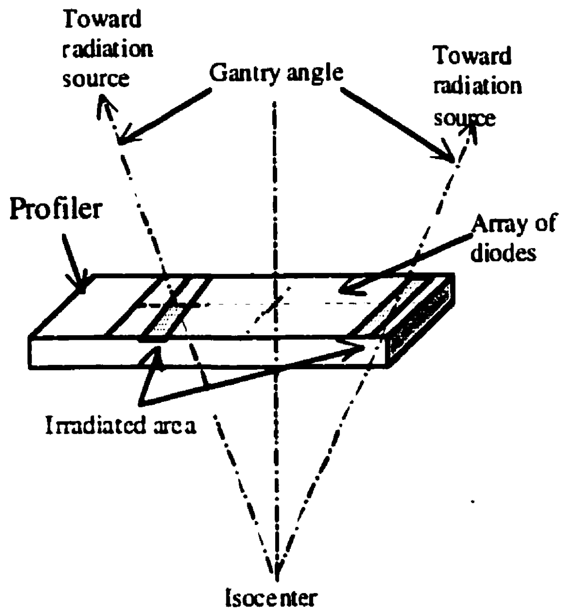

FIGURE B.3.1. Schematic diagram displaying the set-up used to test the positional reproducibility of the gantry. The linear diode array is placed on the treatment couch above the isocenter. As the gantry is rotated, the narrow rectangle defined by the jaws travels on the linear diode array giving a positional dependence on the linear diode array as a function of gantry angle.

Test 2: verification of constant rotation speed of the gantry under the DBD toolbox control.

The linear diode array, with sufficient buildup material, is placed as in B.3.1 (SSD 90 cm), which is 10 cm above the isocenter, with the line of diodes parallel to the y-jaws. The gantry is programmed to rotate with a constant speed and the beam on, from 140° to 220°. A total dose of 50 MU is delivered with the jaws defining a rectangle of 2x15 cm^2 and the collimator at 180° with a 6 MV beam. The dose rate is set at 400 MU/min such that the gantry rotation speed is maximum. Several profiles of the same test are compared to evaluate the reproducibility.

Test 3: effect of acceleration when gantry rotation is controlled by the DBD toolbox.

Test B.3.2 is performed again with the beam turned off every 20 MU. The profile obtained this way is compared with a profile from test B.3.2. The two profiles should be identical if the acceleration has no appreciable effect.

Test 4: positional accuracy of the gantry with dynamic rotation under the control of the DBD toolbox.

With a film placed at SSD 90 cm and sufficient buildup and backscatter material, the jaws define a narrow rectangle of 1x15 cm^2, and the gantry is programmed to go from 139° to 221° with a constant speed without beam. Every 10° the beam is turned on for 2°. For example, the beam is turned on at 139° until 141° is reached and the beam stays off until 149°. The dose rate is set to 400 MU/min with a 6 MV beam. The central axis is marked on the film with a ball-pen. On the developed film, a series of narrow lines appear. Their positions are compared with the predicted position given by the following relationship:

$$x = L \times \tan\theta \qquad \text{(a.1)}$$

where x is the distance of the line from the central axis, L is the distance of the film from the isocenter, and θ is the gantry angle from normal. If the gantry angle is accurate under the control of the DBD toolbox, the predicted and measured line position will be the same.

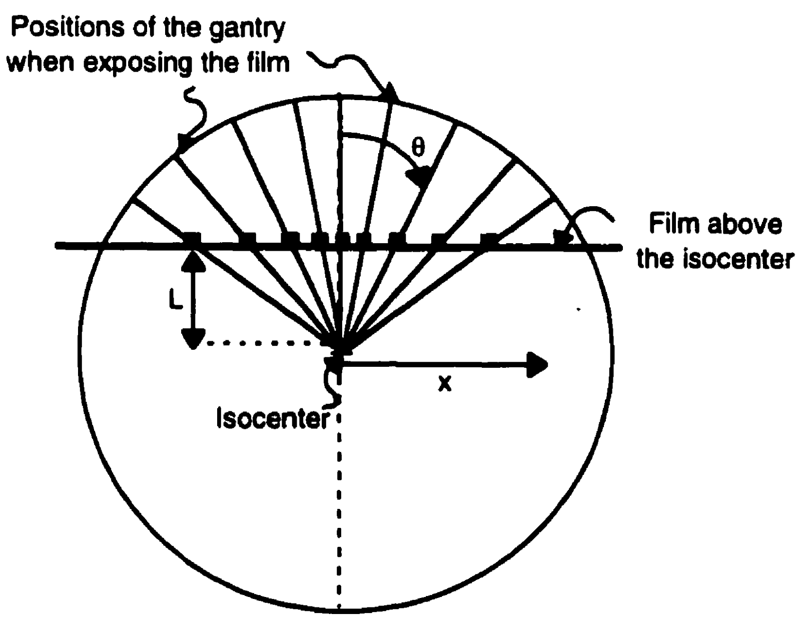

Figure B.3.2 Diagram illustrating the relationship between the variables of equation (a.1) used to measure the positional accuracy of the gantry with dynamic rotation under the control of the DBD toolbox.

LIST OF FIGURES

BIBLIOGRAPHY

American Association of Physicists in Medicine. RTC Task Group 21. "A protocol for the determination of absorbed dose from high energy photon and electron beams". Med. Phys. **10**, 714 (1983)..p. 50

Attix, F. H., Introduction to Radiological Physics and Radiation Dosimetry, John Wiley & Sons, Inc., New York, U.S.A. (1986)....................................p. 4, 21, 22, 24

Barish, R.J., R.C. Fleischman, Y.M. Pipman, "Teletherapy beam characteristics: The first second", Med. Phys. **14**(4), 657-661 (1987)............................p. 50, 82, 87

Barry, D. P., *Dynamic Wedge Dosimetry on a Dual Energy Linear Accelerator*, M. Sc. Thesis, McGill University, Montreal, Canada, 1997 ....p. 14, 22, 49

Boyer, A.L., "Basic Application of a Multileaf Collimator", in Teletherapy Present and Future, Proceedings of the 1996 Summer School of the American Association of Physicists in Medicine, edited by J. Palta and R. Mackie (Medical Physics Publishing, Madison, WI (1996)....................................p. 29, 30, 31, 34, 39

Boyer, A.L., T.G. Ochran, C.E. Nyerick, T.J. Waldron, C.J. Huntzinger, "Clinical dosimetry for implementation of a multileaf collimator", Med. Phys. **19**(5), 1255-1261 (1992)..p. 29, 39, 40, 42, 44, 49, 69, 70, 73

Boyer, A.L., S. Li, "Geometric analysis of light-field position of a multileaf collimator with curved ends", Med. Phys. **24**(5), 757-762 (1997)............p. 32, 33

Buchgeister, M., Nüsslin, F., "Startup performance of a traveling wave versus standing wave linear accelerator", Med. Phys. **25**(4), 493-495 (1998)...........p. 50

Chui, C.S., LoSasso, T., Spirou, S., "Dose calculation for photon beams with intensity modulation generated by dynamic jaw or multileaf collimations", Med. Phys. **21** (8), 1237-1244 (1994)..p. 49

Chui, CC, S. Spirou, T. LoSasso, "Testing of dynamic multileaf collimator", Med. Phys. **23**(5), 635-641 (1996).. p. 53, 54, 56, 87

Clinac 2300 C/D maintenance manual, Varian Associates, Palo Alto, California (1992)..p. 14

Curtin-Savard A., *Dose delivery uncertainty in photon beam radiotherapy*, M. Sc. Thesis, McGill University, Montreal, Canada, 1995......................................p. 50

Das, I.J., G.E. Desobry, S.W. McNeeley, E.C. Cheng, T.E. Schultheiss, "Beam characteristics of a retrofitted double-focused multileaf collimator", Med. Phys. **25** (9) (1998)...p. 29, 31

Das, I.J., K.R. Kase, V.M. Tello, "Dosimetric accuracy at low monitor unit settings", Br. J. Radiol. **64**, 808-811 (1991).................................... p. 50, 80, 82, 87

Dawson, D.J, Harper, J.M., Akinradewo, A.C., "Analysis of physical parameters associated with the measurement of high-energy x-ray penumbra", Med. Phys. **11**(4), 491-497 (1984)... p. 69

Dawson, D.J., Schroeder, N.J., Hoya, J.D. , "Penumbral measurements in water for high-energy x rays", Med. Phys. **13**(1), 101-104 (1986)..............................p. 69

Day, M. J. and Aird, E. G. A., "Central axis depth dose data for use in radiotherapy: 1996," Br. J. Radiol. **25**, 138–151 (1996)................................... p. 10

DMLC Implementation Guide, Varian Associates, Palo Alto, California (1997)..p. 36

Dynamic beam delivery (DBD) toolbox, Engineering reference manual, Varian Associates, Palo Alto, California, version 5.1.00.................................. p. 55, 56, 58

Gager, L.D., A.E. Wright, P.R. Almond, "Silicon diode detectors used in radiological physics measurements. Part I: Development of an energy compensating shield", Med. Phys. **4**(6), 494-498 (1977)..................................p. 24

Galvin, J.M., A.R. Smith, B. Larry, "Characterization of a Multileaf Collimator System", Int. J. Radiation Oncology Biol. Phys., Vol. **25**, 181-192 (1993). .... p. 30, 42

Galvin, J.M., A.R. Smith, R.D. Moeller, R.L. Goodman, W.D. Powlis, J. Rubenstein, L.J. Solin, B. Michael, M. Needham, C.J. Huntzinger, M.M. Kligerman, "Evaluation of Multileaf Collimator Design for a Photon Beam", Int. J. Radiation Oncology Biol. Phys., Vol **23**, 789-801 (1992)........ p. 30

Humm, J.L., Larsson, A.L., Lief, E.P., "Dosimetric properties of a scanned beam microtron at low monitor unit settings: Importance for conformal therapy", Med. Phys. **23**(3), 329-335 (1996)........ p. 50

Huq, M.S., Y. Yu, Z.P. Chen, N. Suntharalingam, "Dosimetric characteristics of a commercial multileaf collimator", Med. Phys. **22**(2):241-7 (1995)........ p. 44

Indra, I.J., Harrington, J.C., Akber, S.F., Tomer, A.F., Murray, J.C., Cheng, CW, "Dosimetric problems at low monitor unit settings for scanned and scattering foil electron beams", Med. Phys. **21**(6), 821-826 (1994)........ p. 50

Johns, H. E., J. R. Cunningham, The Physics of Radiology, 4th edition, Charles C. Thomas, Springfield, Illinois, U.S.A. (1983)........ p. 4, 5, 10, 21

Källman, P., Lind, B., Eklöf, A., Brahme, A., "Shaping of arbitrary dose distributions by dynamic multileaf collimator", Phys. Med. Biol. **33** (11) 1191-1300 (1988)........ p. 49

Khan, F. M., The Physics of Radiation Therapy, 2nd edition, Williams & Wilkins, Maryland, U.S.A. (1994)........ p. 4, 7, 21, 22, 25

Kijewski P.K., L.M. Chin, B.D. Bjarngard, "Wedge-shaped dose distributions by computer-controlled collimator motion", Med. Phys. **5**, 426-429 (1978)........ p. 49

Klein, E.E., Low, D.A., Meigooni, A.S., Purdy, J.A., "Dosimetry and clinical implementation of dynamic wedge", Int. J. Radiat. Oncol., Biol., Phys. **31**(3), 583-592 (1995)........p. 49

Klein, E.E., W.B. Harms, D.A. Low, V. Willcut, J.A. Purdy, "Clinical implementation of a commercial multileaf collimator: dosimetry, networking, simulation, and quality assurance", International Journal of Radiation Oncology, Biology, Physics. **33**(5), 1195-1208 (1995)........p. 30, 44

Kutcher, G.J., L. Coia, M. Gillin, W.F. Hanson, S. Leibel, R.J. Morton, J.R. Palta, J.A. Purdy, L.E. Reinstein, G.K. Svensson, M. Weller, L. Wingfield, "Comprehensive QA for radiation oncology: Report of AAPM Radiation Therapy Commitee Task Group 40", Med. Phys. **21**(4), 581-617 (1994)........p. 66

Liu, H.H., Lief, E.P., McCullough, E.C., "Measuring dose distribution for enhanced dynamic wedges using a multichamber detector array", Med. Phys. **27**(9), 1515-1519 (1997)........p. 49

Metcalfe, P., Kron, T., Elliott, A., Wong, T., Hoban, P., "Dosimetry of 6-MV x-ray beam penumbra", Med. Phys. **20**(5), 1439-1445 (1993)........p. 69

Mubata, C.D., P. Childs, A.M. Bidmead, "A quality assurance procedure for the Varian multi-leaf collimator", Physics in Medicine & Biology. **42**(2), 423-31, (1997)........p. 46, 75

Palta, J.R., D.K. Yeung, V. Frouhar, "Dosimetric considerations for a multileaf collimator system", Med. Phys. **23**(7), 1219-24 (1996)........p. 39, 42

Profiler Model 1170 Operating Instructions, Oct. 1996, Sun Nuclear Corp., Melbourne, FL........p. 24

Rajapakshe, R., S. Shalev, "Output stability of a linear accelerator during the first three seconds", Med. Phys. **23**(4), 517-519 (1996)........p. 50, 82, 87

Santvoort, J.P.C. van, B.J.M. Heijmen, "Dynamic multileaf collimator without 'tongue-and-groove' underdosage effects", Med. Biol. **41**, 2091-2105 (1996). ....p. 30

Sibata, C.H. , Mota, H.C., Beddar, A.S., Higgins, P.D., Shin, K.H., "Influence of detector size in photon beam profile measurements", Phys. Med. Biol. **36**(5), 621-631 (1991)....................p. 69

Spirou, S.V., Chen, S.C., "Generation of arbitrary intensity profiles by dynamic jaws or multileaf collimators", Med. Phys. **21**(7), 1031-1041 (1994)....................p. 49

Sun, J., Y. Zhu, "Study of dosimetric penumbra due to multileaf collimation on a medical linear accelerator", Int. J. Radiat. Oncol., Biol., Phys. **32**(5),1409-1417 (1995)....................p. 42

Stein, J., Bortfeld, T., Dörschel, B., Schlegel, W., "Dynamic X-ray compensation for conformal radiotherapy by means of multi-leaf collimator", Radiother. and Oncol. **32**, 163-173 (1994)....................p. 49

Svensson, R., Källman, P., Brahme, A., "An analytical solution for the dynamic control of multileaf collimators", Phys. Med. Biol. **39** 37-41 (1994)....................p. 49

Thompson, A.V.,Lam, K.L., Balter, J.M., McShan, D.L., Martel, M.K., Weaver, T.A., Fraass, B.A., Ten Haken, R.K, "Mechanical and dosimetric quality control for computer controlled radiotherapy treatment equipment", Med. Phys. **22**(5):563-6, (1995)....................p. 49

Wang, X., S. Spirou, T. LoSasso, J. Stein, C.S. Chui, B. Mohan, "Dosimetric verification of intensity-modulated fields", Med. Phys. **23**(3), 317-27 (1996)....................p. 89

Watts, R., "Evaluation of a diode detector array for use as a linear accelerator QC device", Med. Phys. **25**(2), 247-250 (1998)....................p. 24, 80

Wilkins, D., X.A. Li, J. Cygler, L. Gerig, "The effect of dose rate dependence of p-type silicon detectors on linac relative dosimetry", Med. Phys. 24(6), 879-881 (1997)..p. 24

Wright, A.E., L.D. Gager, "Silicon diode detectors used in radiological physics measurements. Part II: Measurement of dosimetry data for high-energy photons", Med. Phys. 4(6), 499-502 (1977)..p. 24

Xia, P., Verhey, L.J., "Multileaf collimator leaf sequencing algorithm for intensity modulated beams with multiple static segments", Med. Phys. **25** (8), 1424-1434 (1998)..p. 49

Yu, C.X., Symons, M.J., Du, M.N., Martinez, A.A., Wong, J.W., "A method for implementing dynamic photon beam intensity modulation using independent jaws and a multileaf collimator", Phys. Med. Biol. **40**, 769-787 (1995)........... p. 49

Zhu, T.C., L. Ding. C.R. Liu, J.R. Palta, "Performance evaluation of a diode array for enhanced dynamic wedge dosimetry", Med. Phys. **24**(7) 1173-1180 (1997). ....p. 24, 49, 80